UNIVERSITÀ DEGLI STUDI DI PADOVA

UNIVERSITA' DEGLI STUDI DI PADOVA

Dipartimento di Ingegneria Industriale DII

Corso di Laurea Magistrale in Ingegneria dell'Energia Elettrica

Studies on the reactive power demand in DEMO and mitigation strategies

Relatore: Prof. Paolo Bettini

Correlatori: Dott. Ing. Alberto Ferro

Laureando: Francesco Lunardon

ANNO ACCADEMICO 2017/2018

Table of Contents

Summary

In the framework of controlled thermonuclear fusion research, the European DEMO is a fusion reactor prototype which will investigate on the feasibility of electrical energy production from nuclear fusion reactions operating with a self-sustained closed fuel-cycle. According to the European Fusion Development Agreement (EFDA) and now EUROfusion (the 'European Consortium for the Development of Fusion Energy), DEMO is the subject of the last phase of the "Roadmap to the realisation of fusion energy" and its final design will depend on the results of ITER experiment, now under construction at Cadarache, in France.

DEMO and ITER will be both magnetic confinement devices, in which the plasma, heated up to temperatures of millions of Celsius degrees, is kept away from vessel walls using magnetic fields produced by current flowing in superconducting coils. In ITER, and typically in all the tokamaks, coils are supplied by thyristor-based converters resulting in a huge request of reactive power, especially when low voltage is required by the load. In ITER, the reactive power demand reaches a peak value of about 1000 MVAR during pulse operation. To comply with the limits on harmonic distortion and reactive power absorption from the grid, a Reactive Power Compensation and Harmonic Filtering (RPC&HF) system is adopted, based on Thyristor Controlled Reactors (TCR) and tuned filters as Fixed Capacitors (FC), with a rated power of 750 MVAR.

This thesis aims to investigate about the reactive power requested by DEMO Coil Power Supply System (CPSS), assuming to adopt the same converter technology used for ITER, and to start a first feasibility study of an innovative approach based on Active Front End (AFE) converter technology.

To estimate the reactive power demand at ac side of the DEMO thyristor converters, two analytical models have been created by the Author, using Simulink®. The first model implements a current sharing and a sequential control algorithm similar to those adopted in ITER CPSS. The second model implements a bypass logic control instead of sequential control for series-connected units, to evaluate the reactive power reduction achievable with the same converter technology. The results achieved with the two models have been compared in the phases of plasma breakdown, ramp-up and ramp-down of an operational scenario.

The second topic of this thesis is the investigation of a more advanced converter technology, the AFE. The author selected a possible AFE converter topology and then realized a Simulink® model to represent an entire DEMO base converter realized with this technology. The topology, the design criteria and the model are described in this thesis. A set of simulations have been carried out to quantify the currents on the power switches, then the number of parallel static switches per valve has been determined through thermal calculations. Different switching frequencies have been tested, to verify the impact on the number of components and dynamic performance. The capability of the AFE converter to follow the voltage references in the same phases of plasma scenario mentioned above has been verified.

Finally, the traditional solution and that based on AFE technology have been compared, focusing on the reactive power demand but also on the area occupancy and number of components, which play a crucial role in the CPSS design, reliability and cost.

This thesis is organized as follows.

The first chapter is a brief introduction to nuclear fusion reaction and confinement methods with a focus on magnetic confinement devices.

In the second chapter, ITER experiment is introduced, with particular attention on the CPSS and the base converter design.

In the third chapter, DEMO experiment and the analytical models for reactive power calculation are presented. All the control algorithms implemented in the models are described and reported. The results achieved with the sequential control model and bypass logic control model are compared in the last section.

The fourth chapter describes the proposed AFE converter topology, the design criteria and its Simulink® model. A comparison between the reactive power demand of the two different converter solutions is presented in the final section.

In the fifth chapter, an estimation of the sizes of the base converters realized with the two technologies is attempted, considering also the huge RPC&HF system required for the thyristor-based converters.

Sommario

Nell'ambito della ricerca sulla fusione termonucleare controllata, European DEMO è un prototipo di reattore che ha come scopo studiare la fattibilità della produzione di energia elettrica da reazioni di fusione nucleare operando con un ciclo del combustibile chiuso e autoalimentato. Secondo l'European Fusion Development Agreement (EFDA) e ora EUROfusion ('European Consortium for the Development of Fusion Energy'), DEMO è il soggetto dell'ultima fase della "Roadmap to the realisation of fusion energy" e la sua progettazione finale dipenderà dai risultati dell'esperimento ITER, ora in costruzione a Cadarache, in Francia.

DEMO e ITER saranno entrambi dispositivi a confinamento magnetico, nei quali il plasma, portato a temperature di milioni di gradi Celsius, è mantenuto a distanza dalle pareti del vessel usando campi magnetici derivanti dalle correnti che scorrono nei magneti superconduttori. In ITER, e tipicamente in tutti i tokamak, le bobine sono alimentate da convertitori a tiristori che richiedono una grande quantità di potenza reattiva, soprattutto quando il carico richiede una tensione bassa. La richiesta di potenza reattiva di ITER raggiunge picchi di circa 1000 MVAR durante la generazione dell'impulso. Per rispettare i limiti sulla distorsione armonica e sull'assorbimento di potenza reattiva dalla rete, è previsto un sistema di compensazione della potenza reattiva e di filtraggio delle armoniche (RPC&HF), con una potenza nominale di 750 MVAR.

Lo scopo di questa tesi è studiare la richiesta di potenza reattiva del Coil Power Supply System (CPSS) di DEMO supponendo di utilizzare la stessa tecnologia adottata in ITER, e iniziare un primo studio di fattibilità di una nuova soluzione basata sulla tecnologia Active Front End (AFE) per i convertitori.

Per stimare la potenza reattiva richiesta lato alternata dai convertitori a tiristori di DEMO, sono stati creati dall'Autore due modelli analitici, usando Simulink®. Il primo modello implementa un algoritmo di distribuzione della corrente e un algoritmo per il controllo sequenziale dei convertitori simile a quello adottato nel CPSS di ITER. Il secondo modello implementa una logica di bypass invece di quella sequenziale per le unità connesse in serie, al fine di calcolare la riduzione di potenza reattiva raggiungibile utilizzando la stessa tipologia di convertitori. I risultati ottenuti con i due modelli sono stati comparati nelle fasi di plasma breakdown, ramp-up e ramp-down di uno scenario operativo.

Il secondo argomento di questa tesi è lo studio di una tecnologia più avanzata per i convertitori, la tecnologia AFE. L'Autore ha scelto una possibile struttura di convertitore AFE e poi ha realizzato un modello Simulink® per rappresentare un intero convertitore di DEMO con questa tecnologia. La topologia, i criteri di progettazione e il modello sono descritti in questa tesi. Sono state eseguite una serie di simulazioni per quantificare la corrente sugli interruttori, poi è stato determinato il numero di interruttori statici in parallelo per valvola tramite un'analisi termica. Vengono considerate diverse frequenze di commutazione, per verificare l'impatto di queste sul numero di componenti e la performance dinamica. La capacità del convertitore AFE di seguire il riferimento di tensione nelle stesse fasi dello scenario di plasma menzionate in precedenza è stata verificata.

Infine, la soluzione tradizionale e quella basata su tecnologia AFE sono state comparate, concentrandosi sulla domanda di potenza reattiva ma anche sull'area occupata e sul numero di componenti, fattori che coprono un ruolo fondamentale nella progettazione del CPSS, nell'affidabilità e nei costi.

Questa tesi è organizzata come segue.

Il primo capitolo è una breve introduzione alla reazione di fusione nucleare e ai metodi di confinamento con un approfondimento sui dispositivi a confinamento magnetico.

Nel secondo capitolo è introdotto l'esperimento ITER, con particolare attenzione sul CPSS e sulla struttura dei convertitori.

Nel terzo capitolo vengono presentati l'esperimento DEMO e i modelli analitici per il calcolo della potenza reattiva. Tutti gli algoritmi di controllo implementati sono descritti e riportati. I risultati ottenuti con il controllo sequenziale e con la logica di bypass sono confrontati nell'ultima sezione.

Il quarto capitolo descrive la struttura proposta del convertitore AFE, i criteri di progettazione e il modello Simulink®. Viene eseguito, nel paragrafo finale, un confronto della richiesta di potenza reattiva con le due soluzioni di convertitore presentate.

Nel quinto capitolo viene proposta una stima delle dimensioni del convertitore considerando le due differenti tecnologie, tenendo in considerazione il grande sistema RPC&HF richiesto nella soluzione basata su convertitori a tiristori.

1 Introduction

The increasing global energy demand caused by global population growth and industrial development is becoming a big environmental and political issue. Today the energy requirement is mainly satisfied by fossil fuels, resulting in rising of greenhouse effect and pollution. Therefore, a sustainable and much lower pollutant energy production is needed. Controlled nuclear fusion has some valuable properties as an energy source because it is intrinsically safe, has virtually inexhaustible resources and it produces no air pollution or greenhouse gases during normal operation. The primary sources of radioactive by-products are neutron-activated materials (materials made radioactive by neutron bombardment), which can be minimized by careful material selection. A fusion power reactor will produce mostly low-level and short-term radioactive waste, in contrast to most fission by-products, which require special storage and handling for thousands of years.

1.1 Nuclear Fusion

The nuclear fusion is the process by which the nuclei of two light atoms are fused together to form a heavier nucleus, energy is a product of the reaction.

For particles energy from 10 to 100 KeV the most common reaction is:

$$D + T = {}^{4}He\ (3.52\ MeV) + n\ (14.1\ MeV) \tag{1.1}$$

In a fusion reaction, a Deuterium nucleus and a Tritium nucleus (which are Hydrogen isotopes) combine to form an α-particle and a very energetic neutron (Figure 1). Deuterium and Tritium must be heated at very high temperature, in the order of 20 keV (which correspond to about $200 \cdot 10^6$ K), to achieve a sufficiently high probability that their kinetic energy overcomes the Coulomb repulsion.

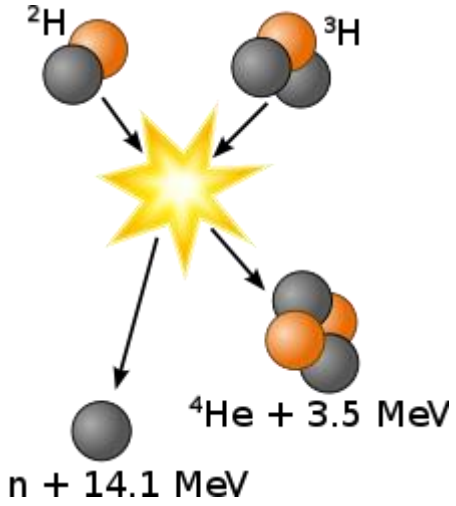

Figure 1 – D-T fusion reaction.

The primary challenge of nuclear fusion is to confine the heated plasma (an ionized gas of Deuterium and Tritium) to sustain fusion reactions. There are two ways to confine the plasma, considering that no materials are able to withstand these temperatures:

- Inertial confinement: the plasma is produced by the implosion of small amount of fuel (frozen Deuterium and Tritium), triggered by a powerful and well-focused set of laser beams. The fuel

remains compressed thanks to their inertia for a short period of time (in the order of ns) before exploding, sufficient to produce a certain number of fusion reactions.

- Magnetic confinement: the plasma is confined by magnetic fields which kept the plasma away from the walls of the reactor vacuum vessel. This confinement is possible due to the fact that the plasma is an ionized gas (i.e. made by charged particles), then it interacts with externally generated magnetic fields.

1.2 Tokamak

The most promising magnetic confinement devices are the tokamaks (Figure 2), which have the shape of a torus. The magnetic system includes toroidal field coils and poloidal field coils. The combined effect of electric current flowing in the toroidal and poloidal field coils and in the plasma is to produce helical magnetic field lines that provide a path for the plasma charged particles. In the tokamaks, the toroidal field is the dominant confining field and it is typically on the order of few Tesla.

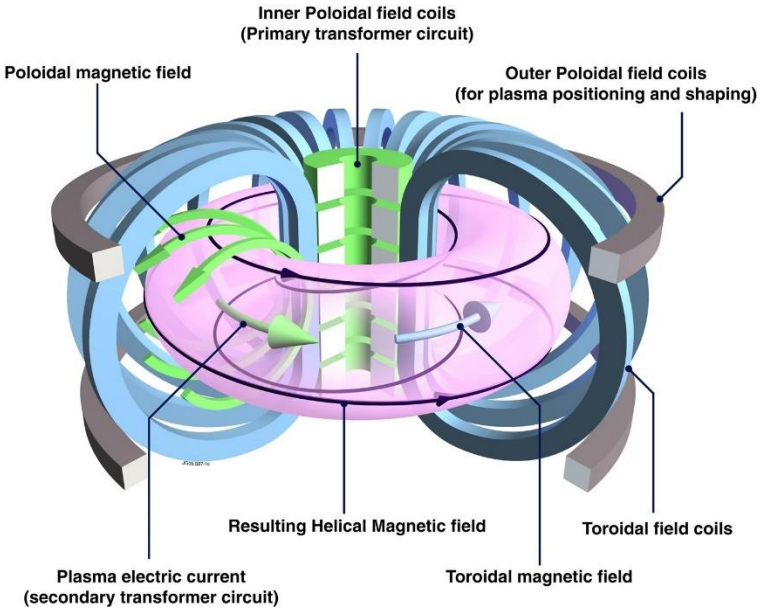

Figure 2 – Tokamak magnetic configuration [1].

The α-particles generated by fusion reactions are confined, owing to their charge, and deliver their energy to the bulk plasma; therefore, they can compensate the energy losses and might make the reaction self-sustaining. The kinetic energy of the fast neutrons can be converted to heat in a blanket which covers the inner surface of the vacuum vessel and then into electricity using conventional technology (turbine + alternator).

To heat the plasma, the most common method is ohmic heating. In a tokamak the plasma acts as the secondary winding of a transformer, while the poloidal coils act as the primary winding. Since the plasma has finite resistance, the induced current produces heat (Joule effect).

Another method is the injection of a beam of neutral particles, which typically are Hydrogen isotopes; they have to be neutral to cross the magnetic field and penetrate the plasma. By colliding with plasma particles, the neutral beam transfers its kinetic energy and increases the plasma temperature.

The last method is radio-frequency heating. Resonant particles are excited by injected radio frequency waves; then, they transfer their kinetic energy to non-resonant particles through collisions.

Several tokamaks have been built. The biggest tokamaks presently in operation are the Joint European Torus (JET) in the UK, EAST in China, KSTAR in Republic of Korea and, very soon, the upgraded Japanese tokamak JT-60SA. The next main step in controlled thermonuclear fusion research will be

ITER experiment, which is under construction in France and will be the largest tokamak when it will start its operation in the 2020s. ITER aims to demonstrate the technological and scientific feasibility of fusion energy. The industrial and commercial exploitation of fusion energy will be investigated through a few DEMO experiments, which are now under conceptual design within some of the ITER members (including Europe, China and Republic of Korea) and that should be operating by the middle of this century [1].

1.3 DEMO Experiment

DEMO (DEMOnstration Fusion Reactor) is the nuclear fusion power station prototype planned to be built following the ITER experiment. DEMO experiment will investigate on the feasibility of the electric energy production and should be the last step before the construction of the first commercial nuclear fusion power stations.

DEMO is presently in a pre-conceptual design phase and its final design will depend on the outcomes of the ITER experimental exploitation. The main objectives of EU DEMO project (the DEMO reactor under design within European Union) are [2]:

- conversion of heat into electricity (~500 MW);
- reasonable availability up to several full-power years;
- closed tritium fuel cycle and self-sufficiency;
- minimization of radioactive wastes, with no-long-term storage;
- extrapolation to a commercial fusion power plant.

2 ITER Power Supply System

2.1 ITER Experiment

ITER will be the largest tokamak in the world, aimed at proving the feasibility of net energy production from a magnetic-confinement fusion device, paving the way for the next generation of fusion reactors capable to provide electricity into the grid. ITER is under construction at Cadarache, in France, and it has been designed to produce 500 MW of fusion power with Q=10 (ratio between output fusion power and input power) [1]. The actual world record for fusion power production is held by the European tokamak JET that in 1997 produced 16 MW from a total input power of 24 MW (Q=0.67).

The ITER main parameters are listed below in Table 1.

Table 1 – ITER main parameters

	Value
Total fusion power	500 MW
Q=fusion power/auxiliary heating power	≥10
Average neutron wall loading	0.57 MW/m^2
Plasma inductive burn time	≥400 s
Plasma major radius	6.2 m
Plasma minor radius	2.0 m
Plasma current	15 MA
Plasma volume	837 m^3
Plasma surface	678 m^2
Installed auxiliary heating/current drive output power	73 MW

The main topic of this thesis is the Coil Power Supply System (CPSS) so in the following paragraphs the ITER magnet system and the ITER power supply system will be described.

2.2 ITER Magnet System

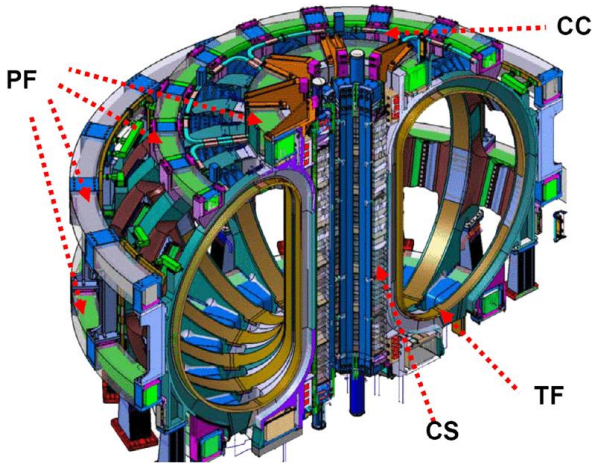

Figure 3 – The ITER coils [3]

The ITER magnet system consists of 4 superconducting coil sets which use both NbTi and Nb_3Sn-based conductors and will be cooled with supercritical Helium at inlet temperature of 4.5 K [3]:

1) **18 Toroidal Field coils (TF)**: the TF coils produce the field that confines the charged particles in the plasma during an ITER pulse. On the inner side, these coils are structurally joined by three upper and three lower pre-compression rings; externally, they are connected by four sets of Outer Inter-coil Structures (OIS).

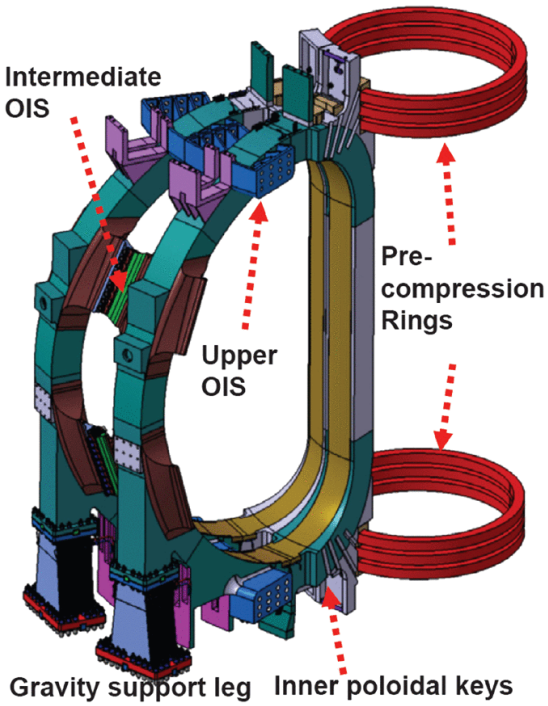

Figure 4 – Two TF coils and the pre-compression rings [3]

2) **6 Poloidal Field coils (PF)**: the six PF coils provide plasma vertical stability and are attached to the TF coil cases through flexible plates or sliding supports allowing radial displacements.

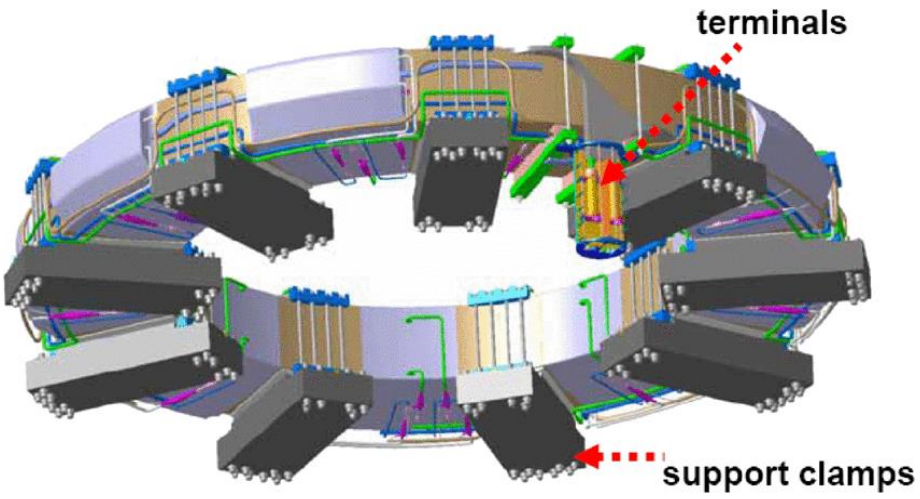

Figure 5 – The PF6 coil and the support clamps [3]

3) **6 Central Solenoid coils (CS)**: the Central Solenoid coils, held together in a vertical stack, provide the inductive flux slope necessary to ramp-up and sustain the plasma current. They will be composed of six independent winding packs, held together by a vertical pre-compression structure; at the bottom there is a sliding connection to provide the centring function and the support against horizontal forces.

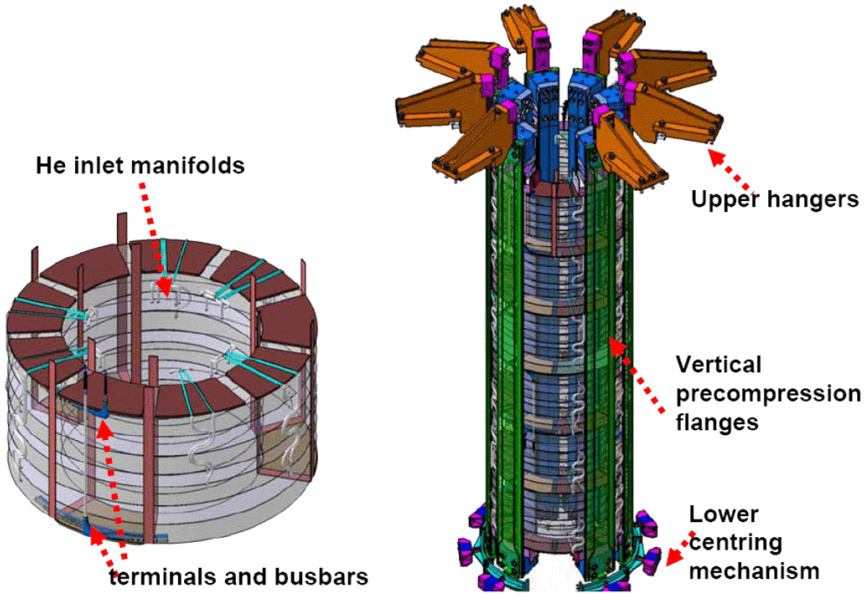

Figure 6 – CS module and stack arrangement [3]

4) **18 Correction Coils (CCs)**: outside the TF coils, three independent sets of CCs are located, each consisting of six coils, as shown in Figure 7. Within each set, pairs of coils on opposite sides of the machine are connected in series. These coils make possible to correct error fields (particularly toroidal asymmetry) from positioning and manufacturing errors in the TF, CS and PF coils. They can also correct error fields caused by the neutral beam systems or other ITER systems.

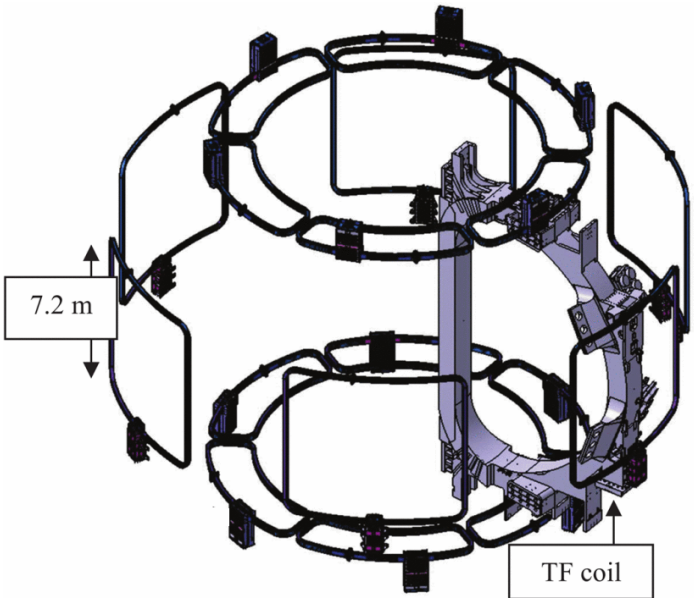

Figure 7 – Correction Coils [4]

TF, CS and PF coils are made with a cable-in-conduit superconductor consisting of about 1000 strands cabled around a small central cooling tube. The operating currents are ±45 kA for the CS, ±55 kA for the PF coils and 68 kA for the TF coils. The CC coils are made with a reduced size superconductor, 10 kA of rated current, with about 300 strands and without the central cooling channel. The Table 2 shows the coils main parameters [5].

Table 2 – ITER coils main parameters

Parameters	TF	CS	PF
Number of coils	18	6	6
Number of turns per coil	134	549	115-459
Maximum operating current [kA]	68	45	55
Nominal Peak field [T]	11.8	13.0	6.0
Stored magnetic energy [GJ]	41	6.4	4
Conductor total length [m]	82260	36114	63142
Coil total weight (with case and structures) [t]	310 (1 coil)	954 (all)	2163 (all)

2.3 ITER Coil Power Supply and Distribution System

ITER distribution system is connected to the 400 kV France grid, having a short-circuit power of about 11.7 GVA, capable to provide high active power (up to 500 MW), but with a severe limitation on the maximum allowed reactive power (around 200 MVAR). The ITER power supply network basically consists in two parts, as can be seen in Figure 8:

1) **The steady state electrical network (SSEN)**:

It supplies the power needed to operate the plant. The major loads are the cooling water and cryogenic systems requiring together about 80% of the SSEN total demand.

2) **The pulsed power electrical network (PPEN)**:

Provides the power needed to supply the superconducting coils and the heating and current drive systems.

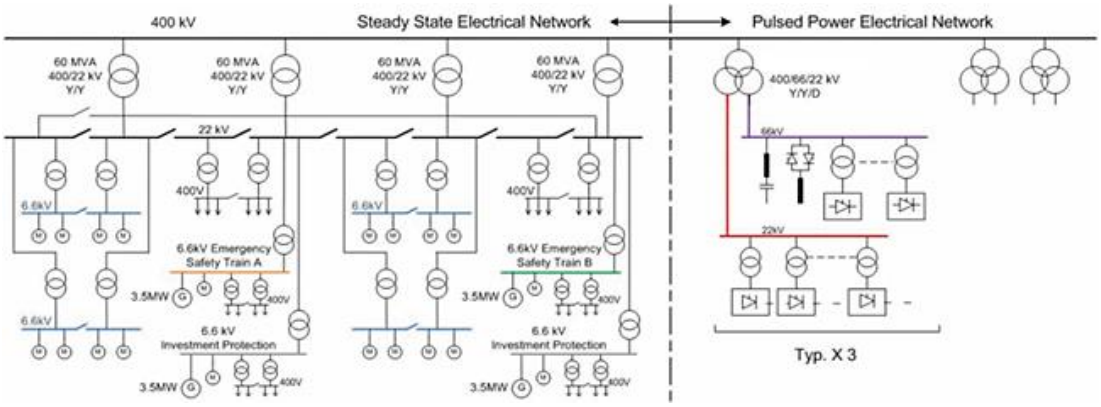

Figure 8 – ITER distribution system [6]

2.3.1 Steady State Electrical Network

ITER plant always works in one of four Global Operational States:

- Long Term Maintenance (LTM), used for long term maintenance or upgrade.

- Short Term Maintenance (STM), used after a failure. In this period the vessel is evacuated, all magnets are at zero current but are cooled (the magnets cool-down is an operation that takes several days).
- Test and Conditioning State (TCS), in which most systems are ready for plasma operation.
- Plasma Operation State (POS), that includes the waiting, countdown, execution and end of plasma pulse.

The following table shows SSEN active power consumption during the different operating states.

Table 3 – SSEN active power consumption [MW]

	LTM	STM	TCS	POS
Cooling Water System	20	40	60	60
Cryoplant	10	40	40	40
Buildings	16	14	12	12
Various	20	10	15	20
Total	66	104	127	132

2.3.2 Pulsed Power Electrical Network

The pulsed electrical network supplies the Coil Power Supply System (CPSS) and the Heat and Current Drive system (H&CD). The CPSS has an installed power of nearly 2.2 GVA [7] and provides controlled DC current to the superconducting magnets for plasma operation.

The following figure represents the ITER pulsed AC distribution system connected to the double 400 kV line. Three 3-winding step-down transformers, rated 300/250/150 MVA, supply the three independent 66 kV busbars and three independent 22 kV busbars. The loads will be distributed between these three sections. To satisfy the limit on the reactive power (200 MVAR) in order to respect voltage variation constrains (less than 2%), a Reactive Power Compensation and Harmonic Filtering (RPC&HF) is required, with a total compensation capacity of 750 MVAR.

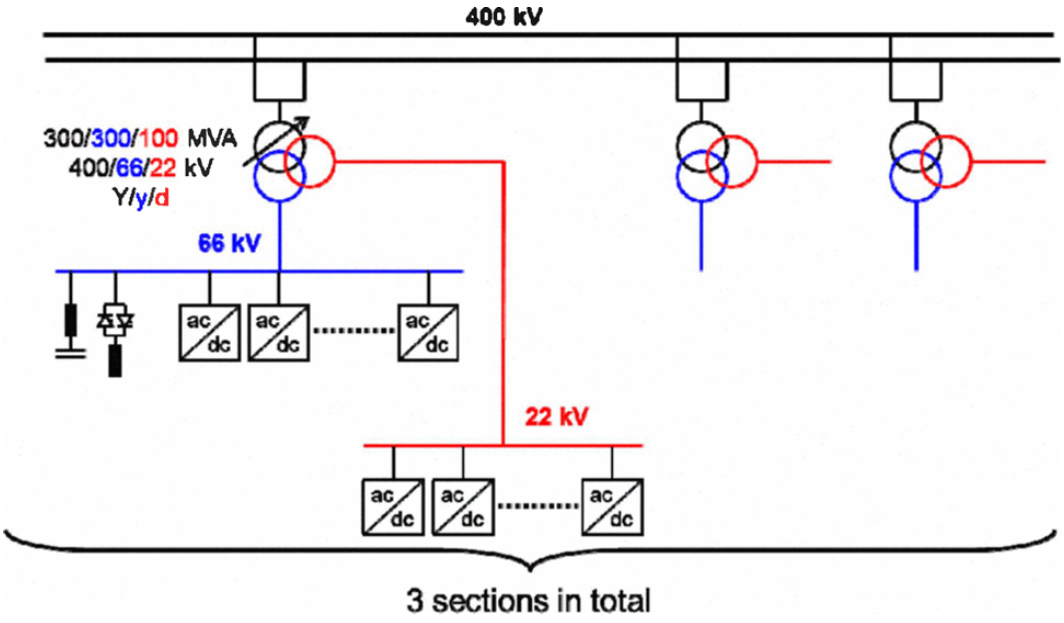

Figure 9 – ITER pulsed AC distribution system [8]

2.3.2.1 Coil Power Supply System

ITER CPSS consists in the following subsystems [8]:

- one power supply circuit for 18 series-connected TF coils;
- one power supply circuit for the CS1U and CS1L coils connected in series and four power supply circuits for the CS3U, CS2U, CS2L, CS3L coils;
- two individual power supply circuits for PF1 and PF6, and one common circuit for PF2, PF3, PF4, PF5;
- a power supply to provide a differential voltage between PF2, PF3 and PF4, PF5, for vertical stabilization purpose (VS);
- nine power supply circuits for the 18 CCs (CCs are connected in series two by two).

All these subsystems are shown below with their relationship with the magnets.

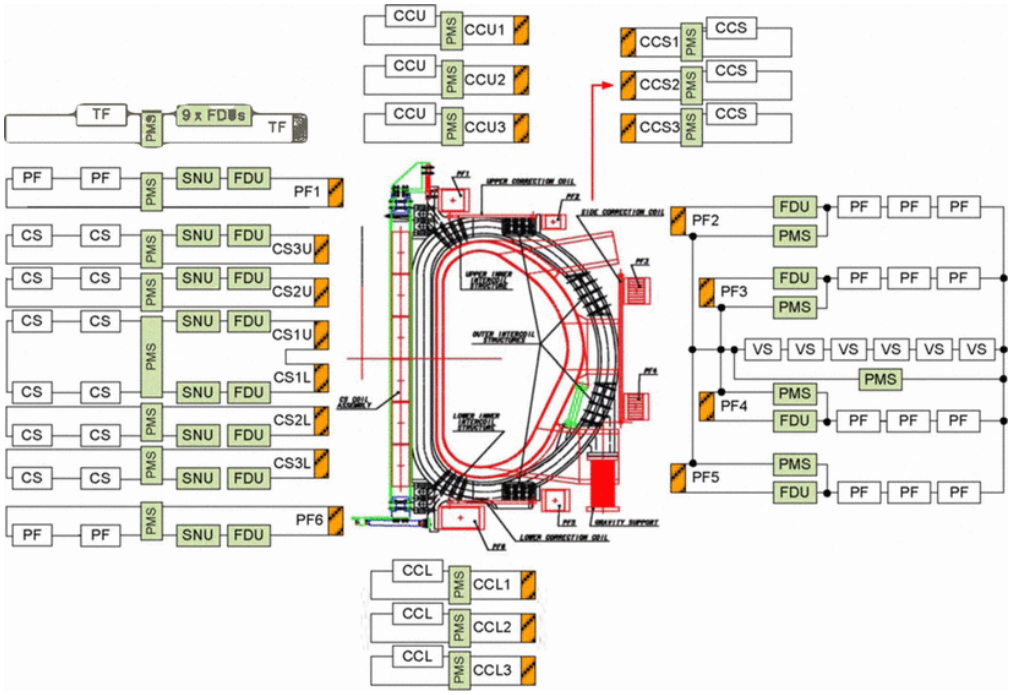

Figure 10 – ITER magnets and CPSS subsystems [8]

In general, each CPSS circuit includes a AC/DC converter unit connected in series with Switching Network Units (SNU) and Fast Discharge Units (FDU).

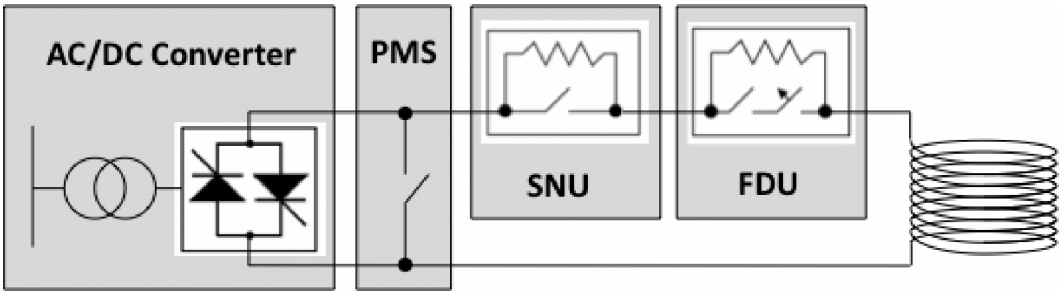

Figure 11 – CPSS subsystem [7]

- **Protective Make Switch (PMS)**: it is a bypass switch that guarantees the circuit continuity in case of a component fault, isolating the coil from the supply.
- **Fast discharging unit (FDU)**: it inserts a resistor in series in the circuit to dissipate quickly the coil magnet energy, to protects the superconducting coil from quench.
- **Switching Network Unit (SNU)**: for some circuit, it is necessary to provide an extra-voltage for plasma initiation. This is provided by opening a DC circuit breaker, such to insert of a resistor in the circuit that produces the additional voltage at the coil terminals.

ITER AC/DC converter units are based on thyristor technology. To reach the required output voltage, the converters are connected in series with a modular approach. Four converters types are required to supply different coil sets, as indicated in Table 4 [7].

Table 4 – ITER converter types

Coil	Requirement	Design Solution
TF	High current, unipolar, dual voltage (for charge and discharge), continuous-rated bypass.	2-quadrants, 12-pulse with tap changer on converter transformer, connected to 66 kV bus.
PF and CS	High current, high voltage for plasma ramping, low voltage for plasma flat top, pulse-rated bypass.	Multi-series 4-quadrants, 12-pulse with sequential control, connected to 66 kV bus.
VS	Medium current, bipolar, high voltage, fast response, pulse-rated bypass.	Multi-series 4 -quadrant, 6- pulse with sequential control, connected to 66 kV bus.
CC	Low current, bipolar, low voltage, pulse-rated bypass.	4-quadrant, 12-pulse, connected to 22 kV bus.

The TF converter transformer can provide two levels of secondary voltage (650 V and 160 V), using a no-load tap changer (see Figure 13). In steady-state conditions, the TF converter is fed with the lowest voltage, in order to reduce the reactive power consumption when providing the rated current (68 kA). To realize the accelerated discharge (within 30 mins under abnormal conditions), the TF converter is connected to the high secondary voltage.

CS and PF systems require 12-pulse/four-quadrants converters units. Each unit comprises four 6-pulse bridges, decoupled by external inductors and supplied by two step-down transformers. The transformers provide 30 degrees shifted voltages to realize the 12-pulse operation. In each bridge arm the thyristors are connected in parallel, each in series with its own fuse, in order to satisfy the current requirement, as we can see in the following figures.

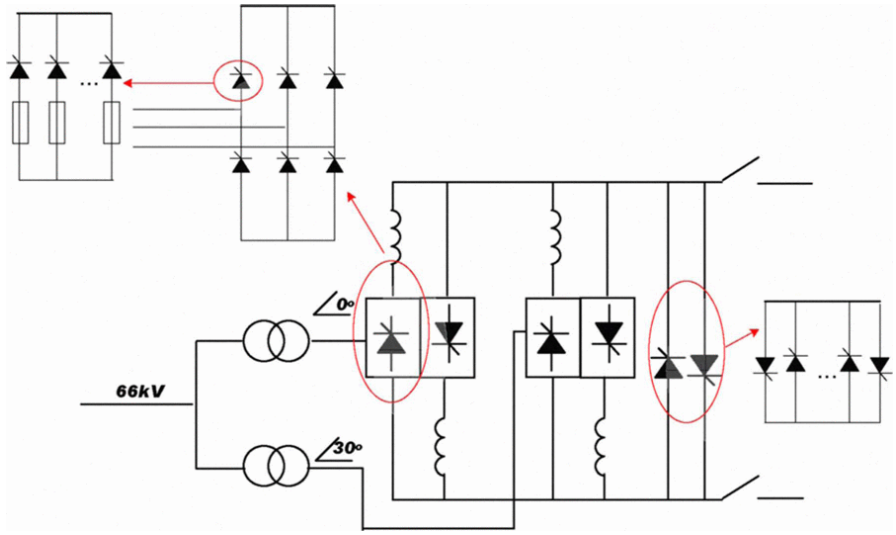

Figure 12 – PF and CS converters topology [8]

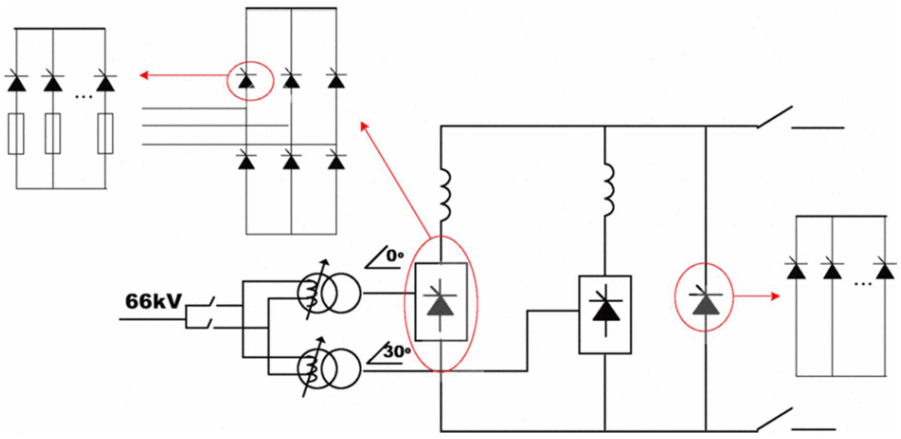

Figure 13 – TF converter topology [8]

In the following table, the ratings of each set of base converters are described.

Table 5 - Ratings and connection of AC/DC converters

Circuit	Unit no-load voltage (kV)	Rated current (kA)	Number of units in series	Total number of basic bridges	Thyristors in parallel for each arm
CS	±1.35	±45	2 per coil circuit	12	12
PF	±1.35	±55	2 for PF1 and PF6. 3 for PF2, PF3, PF4, PF5	16	12
VS	±1.35	±22.5	6	6	6
TF	±0.9	+68	1 for all TF coils	1	14
CCS	±0.45	±10	1 for each circuit	3	4
CCU and CCL	±0.09	±10	1 for each circuit	6	4

CS and PF converters are described in more detail in Table 6.

Table 6 – CS and PF converters ratings

Name	On-load voltage rating [kV]	Current rating [kA]	Thyristors in parallel in each arm	Number of units in series
CS1U	±2.1	±45	12	2
CS1L	±2.1	±45	12	2
CS2U	±2.1	±45	12	2
CS2L	±2.1	±45	12	2
CS3U	±2.1	±45	12	2
CS3L	±2.1	±45	12	2
PF1	±2.1	±55	12	2
PF2	±3.15	±55	12	3
PF3	±3.15	±55	12	3
PF4	±3.15	±55	12	3
PF5	±3.15	±55	12	3
PF6	±2.1	±55	12	2

As it's shown in Figure 12 and Figure 13, an external thyristor bypass is adopted to provide the freewheeling path of superconducting coil current in fault condition, in order to avoid converter and coil damages. However, the thyristor bypass is not rated for the full current in steady-state conditions, therefore a mechanical bypass switch with continuous rating (PMS) is foreseen in parallel.

The converters were designed taking into account electrical fault suppression capability under short circuit conditions: thyristors are sized by ensuring that thyristors retain the blocking reverse voltage capability after a short-circuit at DC side, until external thyristor bypass handle the current. Therefore, the junction temperature must remain under its maximum rated value (125°C) for four electrical cycles (80ms).

In TF converters, the external thyristor bypass is also used to assist the transition between the two levels of the secondary voltage.

Figure 14 shows the layout of one AC/DC converter. The converter transformers (1), installed outdoor, are connected to the 6-pulse bridges (3) by AC busbars (2), then the DC outputs are connected to the DC inductors (7) and DC disconnecting switches (DCDS) by vertical busbars (4, 6) and DC inter-connecting busbars (5) and finally connected to DC busbars (8) running toward the superconducting coils.

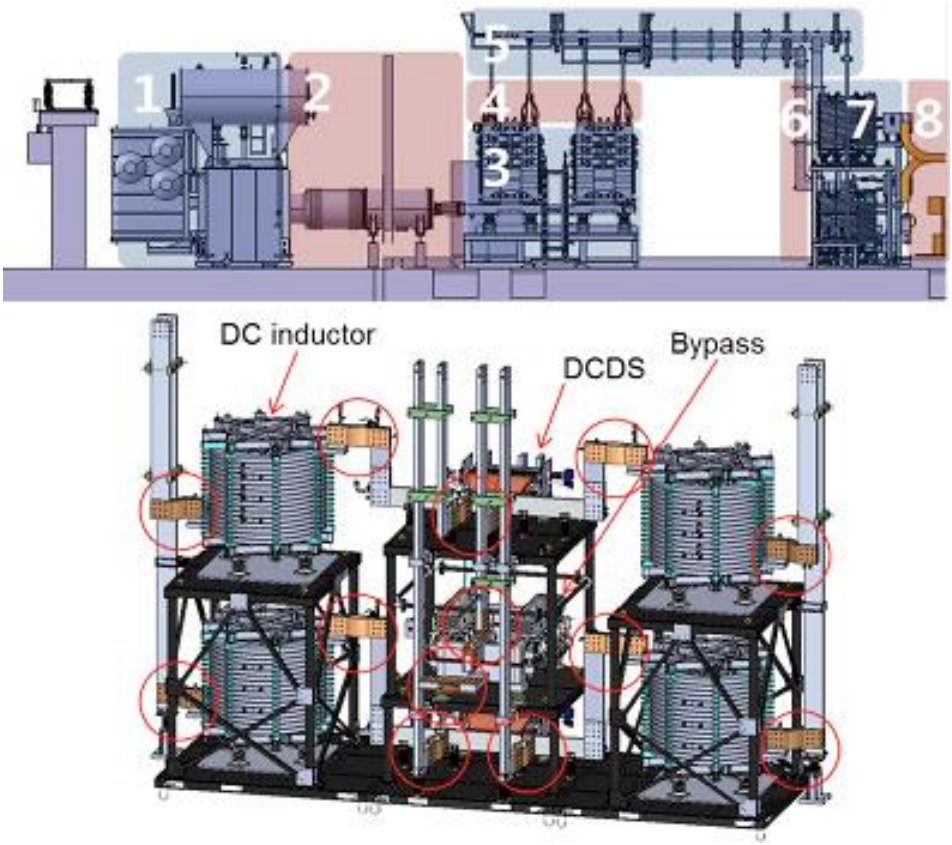

Figure 14 – AC/DC converter structure [9]

2.3.2.2 ITER Load Profile

As investigated in [10], ITER typical cycling pulsed power demand lasts 1000 seconds with a repetition time of 1800 seconds and is mainly composed of power required for the PF scenarios, power needed for the plasma current, position and shape control and power to supply the H&CD. The total amount of active power (without auxiliaries, that require about 130 MW of constant load) does not exceed 500 MW. As regards the reactive load, the peak value reaches 900 MVAR to 1000 MVAR. Figure 16 shows ITER active and reactive load profile.

2.3.2.3 Reactive Power Compensation and Harmonic Filtering System

The RPC&HF system in ITER has the task to compensate the reactive power required by base converters and to eliminate current harmonics. The system is based on static VAR compensation (SVC) technology consisting of thyristor-controlled reactors (TCR) and fixed capacitors (FC). An On Load Tap Changer (OLTC) is installed on the primary winding of each main transformer (see Figure 9) that will compensate daily and seasonal fluctuation outside ITER Pulse operation.

As mentioned in the previous paragraph, the reactive power peak values during pulse operation is about 1000 MVAR against the limited grid capacity to provide 200 MVAR, therefore substantial reactive power compensation is needed at ITER plant.

The RPC&HF system, in combination with the OLTC, has 4 main tasks:

- to reduce the reactive power required from the grid to 200 MVAR limiting the voltage variation, on the 400 kV line, between ±3%;
- to limit the voltage variation on 66 kV busbars between 62 kV and 72.5kV (-6% to 10%) during normal plasma operation;

- to limit the total harmonic distortion (THD) to a level defined in IEC 61000-3-6, to reduce voltage and current distortion on the grid;
- to limit the overvoltage on the busbars during plasma disruption or magnet quench.

Three 250 MVAR RPC&HF units, each connected to a 66 kV busbar, are adopted. In fact, on the 66 kV busbars there is the largest reactive power demand. Thyristor based AC/DC converters produce also low-order harmonics at ac side, therefore five fixed harmonic filters tuned on 3rd, 5th, 7th, 11th and 13th are included, plus a filter for high frequency harmonics. The filters generate a total reactive power of 250 MVAR at 50 Hz and are connected together with TCR to the 66 kV busbars, as shown in Figure 15.

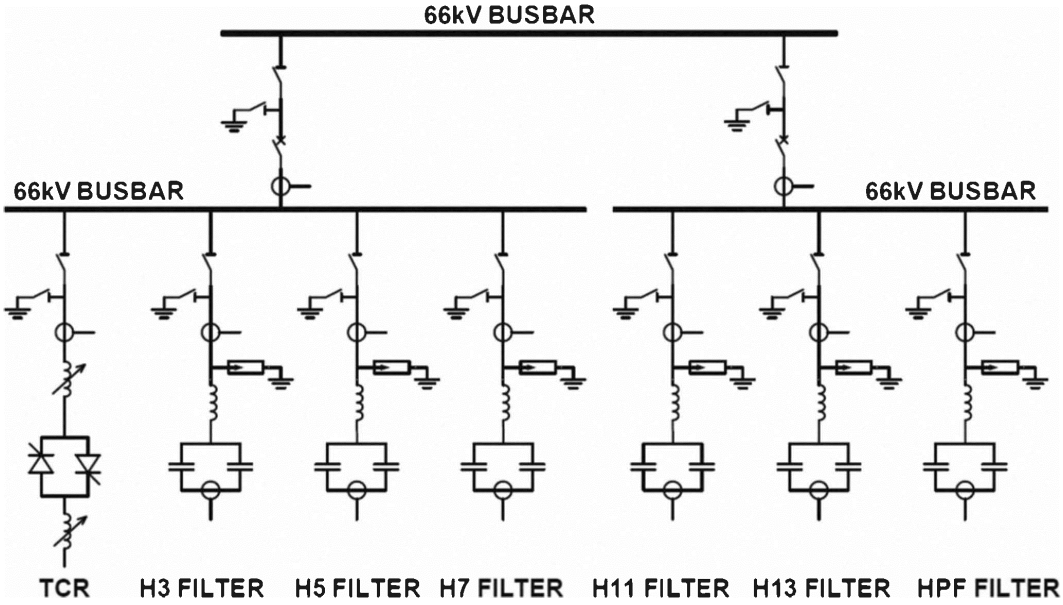

Figure 15 – Simplified diagram of RPC&HF system unit [10]

The filters are singled tuned RLC filter. The capacitor banks, considering the power system impedance, have an inherent oscillation frequency between 100 Hz and 150 Hz, therefore 3rd order harmonic filters have been included to avoid parallel resonance instabilities. The RCP&HF parameters are described in the following table.

Table 7 – RPC&HF unit design parameters

Parameter	**Unit**	**TCR**	**Filter Circuit**					
Harmonic Order			3	5	7	11	14	HPF
Reactive Power	MVAR	250	15	60	50	60	50	15
Inductance	mH	2*57.4	118.2	9.87	5.9	1.96	1.67	1.77
Capacitance	µF		9.71	41.9	35.8	43.6	36.7	11
Quality Factor			2	50	50	50	50	2

In case of unequal firing angles between positive and negative half-cycles, TCR would generate non-characteristic harmonics, mainly of the second order, that are proportional to the delay angle difference between anti-parallel thyristors. Therefore, the current generated by TCR will be permanently monitored by RPC&HF system and all differences between positive and negative half-waves will be equalised to hold the DC component at zero in each TCR phase.

Figure 16 shows simulated ITER active and reactive power demand at 400 kV busbar and RPC contribution. As can be seen the RPC system (rated 750 MVAR) limits the requested reactive power under 200 MVAR [10].

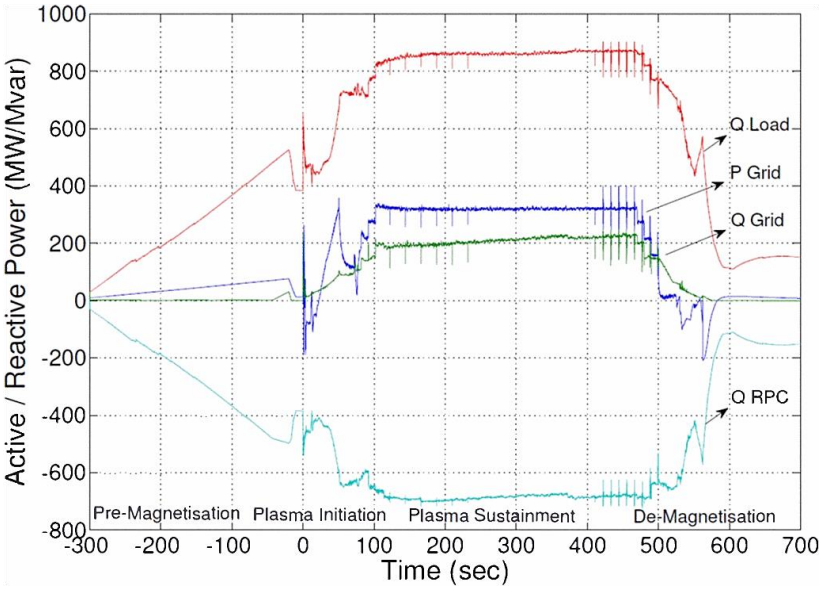

Figure 16 – Active and reactive power profiles at 400 kV [10]

3 DEMO Reactive Power Computation

3.1 Calculation of the Main Design Parameters

As mentioned in [11], in ITER, a certain number of converter units are put in series, with a modular approach, to produce the required coil voltage. CS and PF units have the following ratings:

Table 8 - Ratings of ITER CS and PF converters units

	CS	**PF**
No-load voltage	±1.35 kV	±1.35 kV
On-load voltage	±1.05 kV	±1.05 kV
Rated current	±45 kA	±45 kA

Each CS and PF unit is 12-pulse/4-quadrant and has the scheme represented in Figure 17.

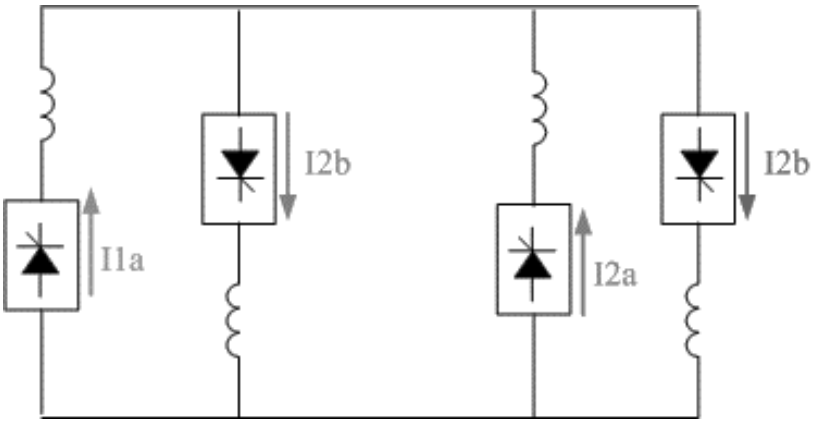

Figure 17 - ITER 12-pulse 4-quadrant converter configuration

For ITER, the thyristors ABB 5STP 52U5200 have been considered, having the following ratings [12]:

Table 9 - ABB 5STP 52U5200 ratings

Average on-state current (T_C = 70 °C), I_{TAV} (A)	5060
RMS on-state current, I_{TRMS} (A)	7940
Max. operating junction temperature, T_{vj} (°C)	125
Max repetitive peak forward and reverse blocking voltage, V_{DRM} (V)	5200

The topology of each ac/dc converter unit assumed for DEMO is the same of a ITER base converter unit, i.e. four 6-pulse converters, arranged as a couple of 12-pulse converters, capable to generate the output current in both directions (see section 2.3.2.1), such to realize a four-quadrant converter unit.

Supposing to adopt the same voltage safety factor, K_{vsf}=3.4 as is computed in [13], each three-phase/6-pulse basic bridge of DEMO CS and PF converters is realized with the parallel connection of 12 thyristors. as reported in Table 10. The number of DEMO units in series has been scaled up to account for the higher voltages required. As it can be noted, this number ranges between 8 and 10 for CS and

PF circuits. The current rating, instead, is the same or a bit lower than ITER, therefore the number of parallel thyristors is the same.

Table 10 – Tentative configuration of DEMO magnet base converters and comparison with ITER [11]

Name	On-load voltage rating [kV]	Current rating [kA]	Thyristors in parallel	Units in series	ITER on-load voltage rating [kV]	ITER current rating [kA]	Thyristors in parallel (ITER)	Units in series (ITER)
CS1U	±8	±45	12	8	±2.1	±45	12	2
CS1L	±8	±45	12	8	±2.1	±45	12	2
CS2U	±8	±45	12	8	±2.1	±45	12	2
CS2L	±8	±45	12	8	±2.1	±45	12	2
CS3U	±8	±45	12	8	±2.1	±45	12	2
CS3L	±8	±45	12	8	±2.1	±45	12	2
PF1	±8	±45	12	8	±2.1	±55	12	2
PF2	±10	±45	12	10	±3.15	±55	12	3
PF3	±10	±45	12	10	±3.15	±55	12	3
PF4	±10	±45	12	10	±3.15	±55	12	3
PF5	±10	±45	12	10	±3.15	±55	12	3
PF6	±8	±45	12	8	±2.1	±55	12	2

The transformer no-load secondary voltage of ITER CS and PF converter units is 1012 V, the converter unit required on-load voltage is ±1050 V and rated current is respectively ±45 kA and ±55 kA. Similarly, it is assumed for DEMO CS and PF converter unit an on-load voltage of ±1000 V and a rated current of ±45 kA [11]. Scaling ITER data it is obtained the transformer no-load secondary voltage equal to V_{20} = 964 V.

The rated power of transformers of the ITER CS and PF converter units is 32 MVA and scaling this power for DEMO we obtain a similar value equal to 31 MVA.

In ITER the maximum thyristors firing angle (alphamax) is 135° (multiple-parallel devices have a negative impact), and the minimum (alphamin) is 15°, adopted to assure safe converter operation. A minimum value of the firing angle has to be imposed to assure direct voltage across the high number of thyristors in parallel, to avoid misfiring inside the same bridge branch. As discussed in [14], generally, 180°-alphamax is greater than alphamin. Therefore, when one subunit operates as rectifier and one as inverter (i.e. in circulating current mode, see section 0), the maximum output voltage (for $I_d > 0$) or the minimum one (for $I_d < 0$) is limited by 180°-alphamax (Figure 18).

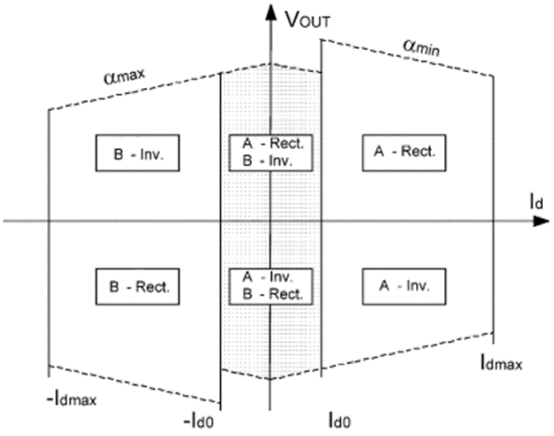

Figure 18 - Converter unit four-quadrant operation [14]

3.2 Introduction to Simulink Models

In order to compute the active and reactive power demand of DEMO assuming the same ITER technology (i.e., thyristor bridges), the Author developed two Simulink models, with two different solutions aiming at minimizing the reactive power demand:

- Bypass Model: Simulink model including converter bypasses;

- Sequential-control Model: Simulink model with sequential control of series-connected converters.

Each model receives as input the voltages and currents required from each ac/dc converter. In the model, only the power supplies for the poloidal field coils are considered, and in particular the converters for the CS coils (CS3U, CS2U, CS1U, CS1L, CS2L, CS3L) and the converters for the PF coils (P1, P2, P3, P4, P5, P6) as it can be seen in Figure 19. The converters for the TF coils are not included in the models, since their contribution on the active and reactive power demand is minor.

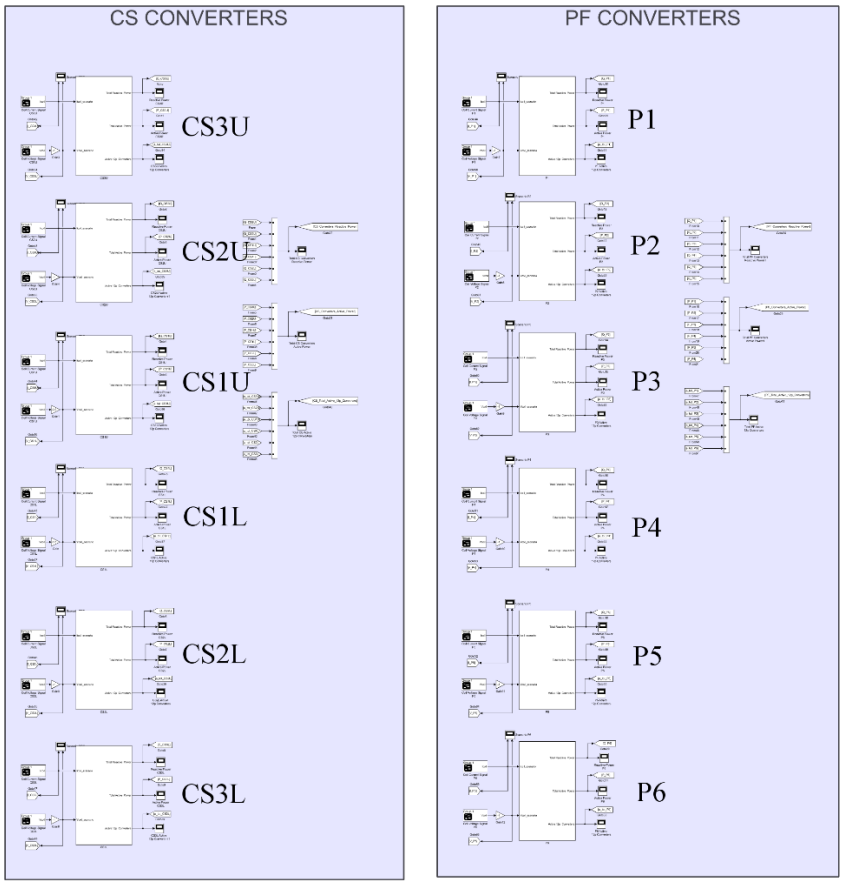

Figure 19 – Simulink model for the estimation of the DEMO active and reactive power demand. The blocks representing the converters considered in the analyses are shown.

In each converter block there are: a MATLAB function that implements the converter controls and calculates the firing angles necessary to produce the required output voltage, and a MATLAB function (Current Control Algorithm) that distributes the total current of each coil among the four 6-pulse converters of each converter unit, as in ITER. In the models, there is a number of blocks representing the units in series (Figure 20), each containing blocks (Figure 21) that calculate the active and reactive power of each 6-pulse/2-quadrant thyristor bridge of the converter unit (see section 3.4).

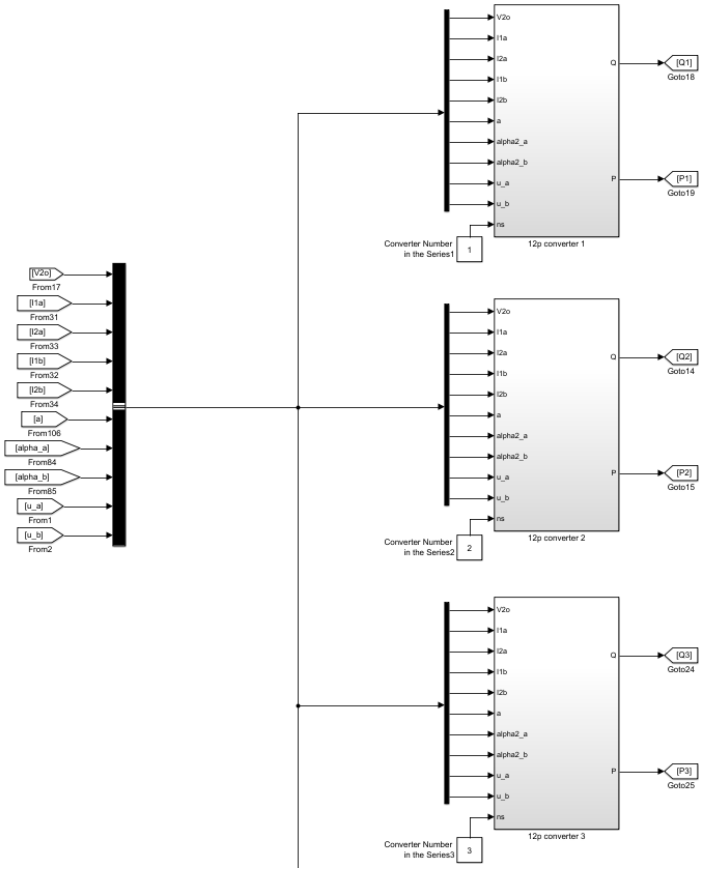

Figure 20 – Blocks of the Simulink models representing the converter units

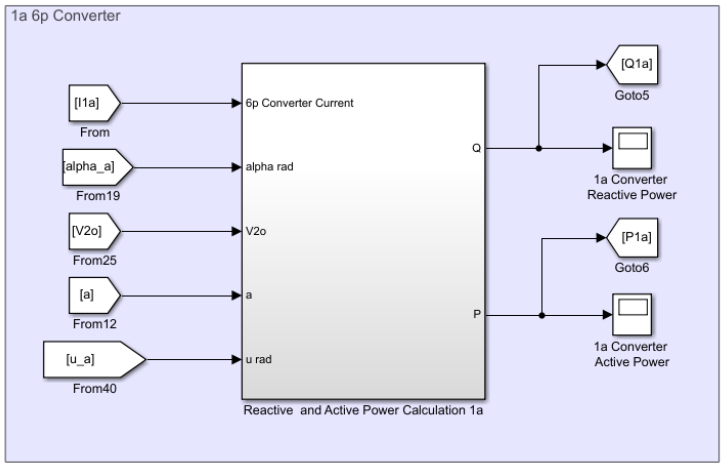

Figure 21 – Block of the Simulink models which calculate the active and reactive power demand of a 6-pulse/2-quadrant thyristor bridge

The following table defines the variables used in the model:

Table 11 - Variables used in the model

Icoil	Coil current
Vcoil	Coil voltage
Ir	12-pulse converter rated current
I1a	I1a converter current
I2a	I2a converter current
I1b	I1b converter current
I2b	I2b converter current
I6p	12-pulse to 6-pulse mode current threshold (p.u.)
Icircul	6-pulse to circulating mode current threshold (p.u.)
alpha_a	1a and 2a converter firing angle
alpha_b	1b and 2b converter firing angle
V_{20}	Secondary no-load voltage
Vconvmax_vector	Vector containing the maximum output voltages which can be generated by the 12-pulse converters
Vconvmin_vector	Vector containing the minimum (negative) output voltages which can be generated by the 12-pulse converters
s	Number of converter units in series

3.3 CREATE Scenario Data for DEMO

The current and voltage waveforms (I_{coil} and V_{coil}) to be generated by the base converters are the input of the model. In this thesis, the scenarios provided by C.R.E.A.T.E. consortium, on the basis of a Finite-Element models of the tokamak and considering variable plasma configurations, are adopted. These scenario, illustrated in Appendix A, are divided into plasma breakdown, plasma ramp-up and plasma ramp-down phases. At the moment, an overall scenario for the whole plasma discharge is not available.

3.4 Active and Reactive Power Computation

Simulink models compute active and reactive power of each 6-pulse/2-quadrant thyristor bridge as follows [15]:

$$P(t) = 1.35 \times V_{20} \times \cos\left(\alpha(t) + \frac{u(t)}{2}\right) \times I_{coil}(t) \tag{3.1}$$

$$Q(t) = 1.35 \times V_{20} \times \sin\left(\alpha(t) + \frac{u(t)}{2}\right) \times I_{coil}(t) \tag{3.2}$$

where V_{20} is the phase-to-phase transformer secondary voltage (RMS), α is the firing angle of the thyristor bridge and u is the overlapping angle determined with the following equation [15]:

$$u(t) = \operatorname{acos}\left[\cos(\alpha(t)) - \frac{2 \times \omega \times L_{cc}}{\sqrt{2} \times V_{20}} \times I_{coil}(t)\right] - \alpha(t) \tag{3.3}$$

DEMO transformers short-circuit reactance is supposed to be equal to the ITER one, so X_{cc}=0.175 pu from which L_{cc} is derived (transformer short-circuit inductance). To compute deltav_dc_a and deltav_dc_b, that represent the decrease of mean value of dc voltage caused by thyristors commutation, the following equation is used in the models [15]:

$$\Delta V_{DC}(t) = 6 \times f \times L_{cc} \times I_d(t) \tag{3.4}$$

The active and reactive power equations assume a linear shape of the current during the commutation therefore the angle in equations (3.1) and (3.2) is α+u/2. This simplification can be avoided for the active power with the following equation:

$$P(t) = V_{coil}(t) \times I_{coil}(t) \tag{3.5}$$

3.5 Current Control Algorithm

Due to the specific function of poloidal and central solenoid magnetic fields, each poloidal field (PF) and central solenoid (CS) coil needs to be excited by an independent four-quadrant converter system, giving a variable output current and voltage. To perform four-quadrants operation and realize smooth transition at zero-crossing of the load current, the operation of ITER PF and CS converters includes three different operation modes, as shown in Figure 22:

1. **12-pulse mode with positive Icoil:** if Icoil > I6p the converter unit operates in 12-pulse mode and Icoil is equally divided between the 6-pulse/2-quadrant converters 1a and 2a;
2. **6-pulse mode with positive Icoil:** if Icircul < Icoil < I6p the converter unit operates in 6-pulse mode and I1a is equal to Icoil;
3. **Circulating current mode:** if -Icircul < Icoil < Icircul the converter unit operates in circulating mode; an additional circulating current is imposed to 1a and 2b antiparallel sub-units to control without discontinuity the coil voltage during the current polarity inversion. The current difference between the two sub-units flows in the coil;
4. **6-pulse mode with negative Icoil:** if -I6p < Icoil < - Icircul the converter unit operates in 6-pulse mode and I2b is equal to Icoil;
5. **12-pulse mode with negative Icoil:** if Icoil < -I6p the converter unit operates in 12-pulse mode and Icoil is equally divided between I1b and I2b.

In ITER, it is I6p = 0.3 × Ir and Icircul = 0.15 × Ir.

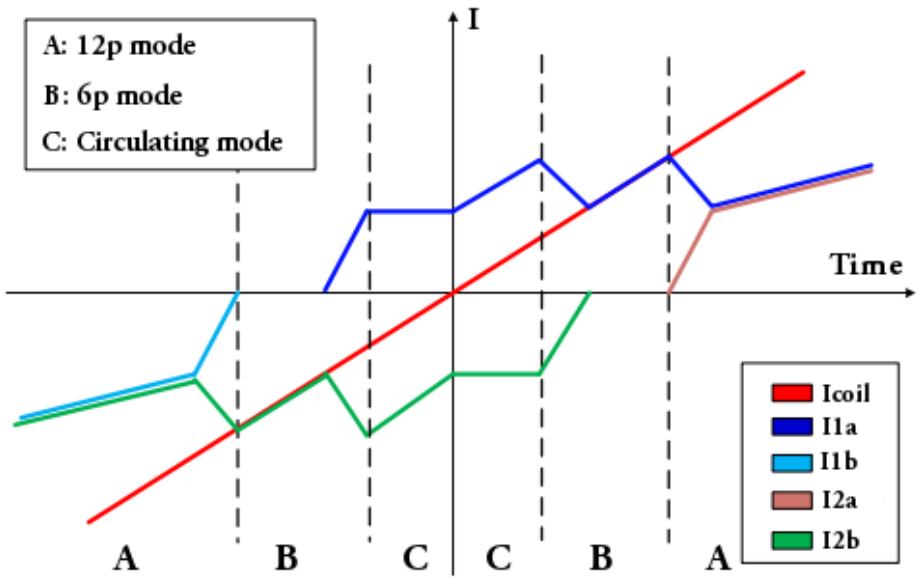

Figure 22 – AC/DC converter 4-quadrant drive concept [16]

The four 6-pulse/2-quadrant converters which compose the converter unit are supplied by two transformers installed in the same housing. The windings of two transformers are organized in a 12-pulse configuration by supplying voltage with 30° of phase difference between the two pairs of 6-pulse converters. 1a and 1b are connected to the same secondary winding and 2a and 2b to the other one.

The current control Matlab® function of the Simulink models, shown hereafter, implements the circulation-current control algorithm described above:

```
function [I1a,I1b,I2a,I2b] = fcn(Icoil,Ir)

I6p=0.3;
Icircul=0.15;
I1a=6000;
I1b=6000;
I2a=6000;
I2b=6000;
if Icoil>=(I6p*Ir)
    I1a=0.5*Icoil;
    I2a=0.5*Icoil;
    I1b=0;
    I2b=0;
end
if (Icircul*Ir<=Icoil && Icoil<(I6p*Ir))
    I1a=Icoil;
    I2a=0;
    I1b=0;
    I2b=0;
end
if (0<=Icoil && Icoil<(Icircul*Ir))
    I1a=Icoil+(Icircul*Ir);
    I2b=-(Icircul*Ir);
    I1b=0;
    I2a=0;
end
if (0>Icoil && Icoil>=-(Icircul*Ir))
    I2b=Icoil-(Icircul*Ir);
    I1a=Icircul*Ir;
    I1b=0;
    I2a=0;
```

```
end
if (-(Icircul*Ir)>Icoil && Icoil>=-(I6p*Ir))
    I2b=Icoil;
    I1b=0;
    I1a=0;
    I2a=0;
end
if Icoil<-(I6p*Ir)
    I1b=0.5*Icoil;
    I2b=0.5*Icoil;
    I1a=0;
    I2a=0;
end
```

Figure 23 – Current control function of the Simulink models

Figure 24 shows the result of a current control simulation in which a current (I_{coil}) with a linear shape from +40 kA to -40 kA is imposed as input. As can been seen, the sum of the four 6-pulse converter currents follow the reference and the current is distributed among the thyristor bridges according to the circulation-current control algorithm.

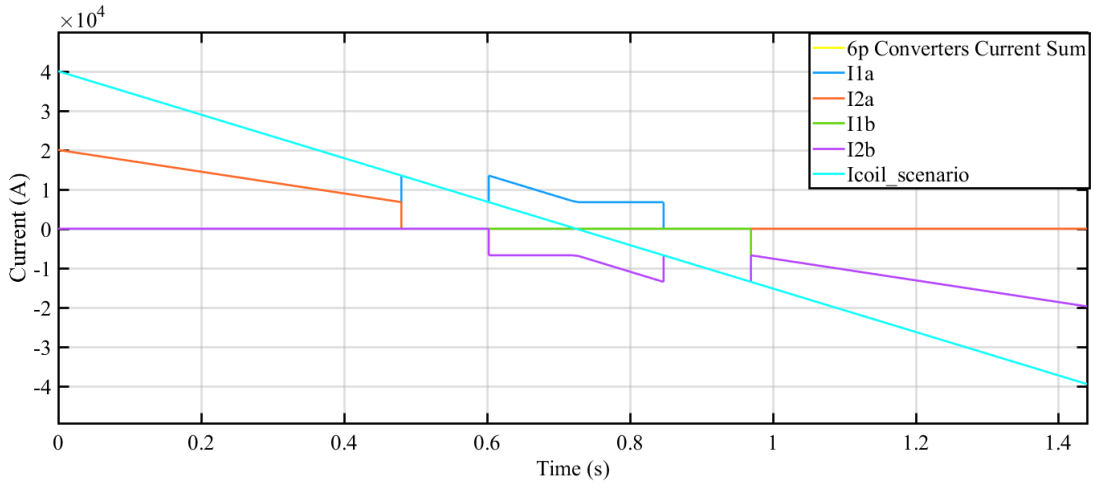

Figure 24 – Current control algorithm simulation

3.6 Sequential Control Model

This Simulink model implements the converter sequential control described in [17]. In ITER, the sequential control is adopted to reduce the reactive power demand of series-connected converter units.

In fact, with the symmetrical control, the firing delay angle is the same for all the 6-pulse converters with the same orientation. Therefore, if the output voltage of the converter is high, the reactive power is small, but if the output voltage is around zero, at nominal output current, the reactive power becomes very high.

Instead, by operating the converters (two in series, for example) with the sequential control, the reactive power is much reduced. This because, with the sequential control, the output voltage of one converter is always fixed at its maximum or minimum, where its reactive power demand is minimum, and the regulation of the output voltage is performed by varying the delay angle of the other converter.

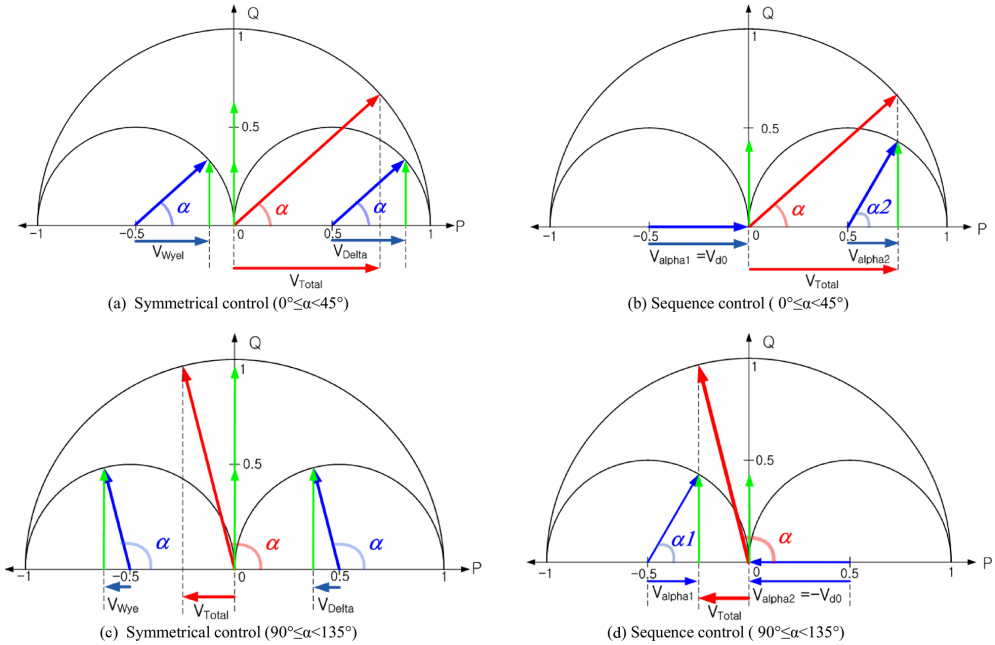

Figure 25 – Power Diagrams showing the reduction of reactive power demand with sequential control with respect to symmetrical control [17]

Symmetrical control is shown in Figure 25 (a), (c) and sequence control in Figure 25 (b), (d). The principle of the symmetrical control is shown in Figure 25 (a), (c), while the sequential control is shown in Figure 25 (b), (d). With the same total active power (P, horizontal axis), the reactive power (Q, vertical axis) is clearly reduced with the sequential control.

In the real case, the reactive power demand of the converters giving maximum or minimum voltage is not zero, due to the limitations on firing angle. This make the sequential control logic worse in respect of converter reactive power demand with respect to the bypass control logic described in the next chapter.

In case of more than two converters in series controlled with the sequential logic, according to the required output voltage, only one converter regulates the output voltage, while the others supply the maximum ore the minimum voltage. When some of 12-pulse/4-quadrant converters in series have to produce zero voltage they work in pairs: one produces the minimum voltage (negative, with alpha=alphamax) and the other produces an equal but positive voltage (with alpha=180-alphamax). This logic is shown in Figure 26, for three converters.

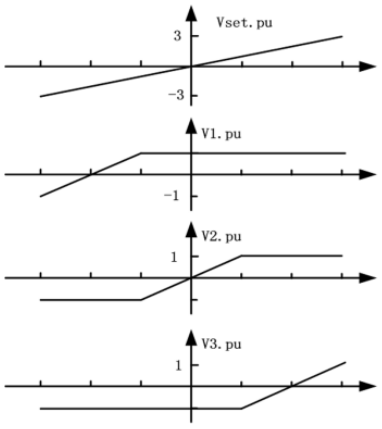

Figure 26 – Sequential control of three units in series [18]

The sequential control algorithm which calculates the firing delay angles is implemented with the following Matlab® function (Figure 27):

```
function [a,aa,alpha_a,alpha_b,deltav_dc_a,deltav_dc_b,u_a,u_b,Vdc]  =
fcn(Sn,V2o,deltavcc,I1a,I2b,Vcoil,alphamax,alphamin)

%This function
%generates a vector 'a' in which every position matches with the respective
%12p converter.
%If the value in the i-th position is 1 the i-th the converter modulates the voltage
%to follow Vcoil, all
%the inferior converters (all have a=1) provide the maximum or the minimum voltage and
%the i-th converter a variable voltage to follow Vcoil.
%If the value in the i-th position is 0 the converter
%works in pair with another converter (with a=0) to produce a null voltage.
%Two converters with a=0 work in pairs: one gives the maximum voltage and
%the other gives the opposite voltage.
%If the i-th value is 2 the converter is part in the pair
%that work with sequential control.
%Then the function generates the vectors alpha_a and alpha_b that contain the
%firing angle of a and b 6p converters.

s=8;
Vconvmax_vector=zeros(s,1);
Vconvmin_vector=zeros(s,1);

I2n=Sn/(sqrt(3)*V2o);                %tranformer secondary rated current
Xcc=(deltavcc*V2o)/((sqrt(3))*I2n);  %short circuit reactance (deltavcc [pu])

%the following function part computes the decrease of dc voltage due to
%commutation and the maximum and minimum tension that the converters can supply

deltav_dc_a=abs((3*Xcc*I1a)/pi);
deltav_dc_b=abs((3*Xcc*I2b)/pi);

Vconvmax_a=1.35*V2o*cos(alphamin)-deltav_dc_a;
Vconvmin_a=1.35*V2o*cos(alphamax)-deltav_dc_a;
Vconvmax_b=-(1.35*V2o*cos(alphamax))+deltav_dc_b;
Vconvmin_b=-(1.35*V2o*cos(alphamin))+deltav_dc_b;

i=1;
while i<=s
if I1a~=0 && I2b~=0                          %circulating mode
    if abs(Vconvmax_a)>=abs(Vconvmax_b)
        Vconvmax_vector(i)=Vconvmax_b;
    else
        Vconvmax_vector(i)=Vconvmax_a;
    end
    if abs(Vconvmin_a)>=abs(Vconvmin_b)
        Vconvmin_vector(i)=Vconvmin_b;
    else
        Vconvmin_vector(i)=Vconvmin_a;
    end
else
    if I1a~=0                                %6p or 12p mode with Icoil>0
        Vconvmax_vector(i)=Vconvmax_a;
        Vconvmin_vector(i)=Vconvmin_a;
else                                         %6p or 12p mode with Icoil<0
        Vconvmax_vector(i)=Vconvmax_b;
        Vconvmin_vector(i)=Vconvmin_b;
    end
end
i=i+1;
end

%the following function part computes the vector 'a'

i=1;
alpha_a=zeros(s,1);
alpha_b=zeros(s,1);
a=zeros(s,1);
aa=zeros(s,1);
```

```
Vdc=zeros(s,1);
u_a=zeros(s,1);
u_b=zeros(s,1);

while i<=s
    Vbmax=sum(Vconvmax_vector(1:(i-1),1));
    Vbmin=sum(Vconvmin_vector(1:(i-1),1));
    if Vbmax<Vcoil || Vbmin>Vcoil
        a(i,1)=1;
    else
        if i==s
            a(i,1)=2;
            a(i-1,1)=2;
            i=s+1;
        else
            ii=i;
            while ii<s
                a(ii,1)=0;
                a(ii+1,1)=0;
                ii=ii+2;
            end
            if ii==s
                a(i,1)=2;
                a(i-1,1)=2;
                i=s+1;
            end
            i=s+1;
        end
    end
    i=i+1;
end

%the following function part computes the vectors alpha_a and alpha_b

i=1;
while i<=s
    if a(i,1)==0
        if Vconvmax_vector(i,1)<abs(Vconvmin_vector(i,1))
            wa=(Vconvmax_vector(i,1)+deltav_dc_a)/(1.35*V2o);
            wb=(-Vconvmax_vector(i,1)+deltav_dc_b)/(1.35*V2o);
            alpha_a(i,1)=acos(wa);
            alpha_b(i,1)=acos(wb);
            wa1=(-Vconvmax_vector(i,1)+deltav_dc_a)/(1.35*V2o);
            wb1=(Vconvmax_vector(i,1)+deltav_dc_b)/(1.35*V2o);
            alpha_a(i+1,1)=acos(wa1);
            alpha_b(i+1,1)=acos(wb1);
            i=i+2;
        else
            wa=(-Vconvmin_vector(i,1)+deltav_dc_a)/(1.35*V2o);
            wb=(Vconvmin_vector(i,1)+deltav_dc_b)/(1.35*V2o);
            alpha_a(i,1)=acos(wa);
            alpha_b(i,1)=acos(wb);
            wa1=(Vconvmin_vector(i,1)+deltav_dc_a)/(1.35*V2o);
            wb1=(-Vconvmin_vector(i,1)+deltav_dc_b)/(1.35*V2o);
            alpha_a(i+1,1)=acos(wa1);
            alpha_b(i+1,1)=acos(wb1);
            i=i+2;
        end
    else
        if a(i,1)==2
            if Vcoil>0
                Vconvmax_vector(i,1)=-Vconvmin_vector(i+1,1);
                Vseq=Vcoil-(sum(Vconvmax_vector(1:(i-1),1)));
                wa=(Vconvmax_vector(i,1)+deltav_dc_a)/(1.35*V2o);
                wb=(-Vconvmax_vector(i,1)+deltav_dc_b)/(1.35*V2o);
                alpha_a(i,1)=acos(wa);
                alpha_b(i,1)=acos(wb);
                wa1=(Vseq-Vconvmax_vector(i,1)+deltav_dc_a)/(1.35*V2o);
                wb1=(-Vseq+Vconvmax_vector(i,1)+deltav_dc_b)/(1.35*V2o);
                alpha_a(i+1,1)=acos(wa1);
                alpha_b(i+1,1)=acos(wb1);
                i=i+2;
            else
                Vconvmin_vector(i+1,1)=-Vconvmax_vector(i,1);
```

```
                Vseq=Vcoil-(sum(Vconvmin_vector(1:(i-1),1)));
                wa=(Vseq-Vconvmin_vector(i,1)+deltav_dc_a)/(1.35*V2o);
                wb=(-Vseq+Vconvmin_vector(i,1)+deltav_dc_b)/(1.35*V2o);
                alpha_a(i,1)=acos(wa);
                alpha_b(i,1)=acos(wb);
                wa1=(Vconvmin_vector(i,1)+deltav_dc_a)/(1.35*V2o);
                wb1=(-Vconvmin_vector(i,1)+deltav_dc_b)/(1.35*V2o);
                alpha_a(i+1,1)=acos(wa1);
                alpha_b(i+1,1)=acos(wb1);
                i=i+2;
            end
        else   %a=1
            if Vcoil>0
                Vseq=Vcoil-(sum(Vconvmax_vector(1:(i-1),1)));
                if Vseq>=Vconvmax_vector(i,1)
                    if I1a~=0 && I2b~=0
                        wa=(Vconvmax vector(i,1)+deltav dc a)/(1.35*V2o);
                        wb=(-Vconvmax_vector(i,1)+deltav_dc_b)/(1.35*V2o);
                        alpha_a(i,1)=acos(wa);
                        alpha_b(i,1)=acos(wb);
                        i=i+1;
                    else
                        alpha_a(i,1)=alphamin;
                        alpha_b(i,1)=alphamax;
                        i=i+1;
                    end
                else
                    wa=(Vseq+deltav dc a)/(1.35*V2o);
                    wb=(-Vseq+deltav_dc_b)/(1.35*V2o);
                    alpha_a(i,1)=acos(wa);
                    alpha_b(i,1)=acos(wb);
                    i=i+1;
                end
            else
                Vseq=Vcoil-(sum(Vconvmin_vector(1:(i-1),1)));
                if Vseq<=Vconvmin_vector(i,1)
                    if I1a~=0 && I2b~=0
                        wa=(Vconvmin_vector(i,1)+deltav_dc_a)/(1.35*V2o);
                        wb=(-Vconvmin_vector(i,1)+deltav_dc_b)/(1.35*V2o);
                        alpha_a(i,1)=acos(wa);
                        alpha_b(i,1)=acos(wb);
                        i=i+1;
                    else
                        alpha_a(i,1)=alphamax;
                        alpha_b(i,1)=alphamin;
                        i=i+1;
                    end
                else
                    wa=(Vseq+deltav_dc_a)/(1.35*V2o);
                    wb=(-Vseq+deltav_dc_b)/(1.35*V2o);
                    alpha_a(i,1)=acos(wa);
                    alpha_b(i,1)=acos(wb);
                    i=i+1;
                end
            end
        end
    end
end
```

Figure 27 – Sequential control function of the Simulink Sequential Control Model

3.7 Bypass Model

In ITER baseline design, an internal bypass solution was proposed for both reactive power reduction and as freewheeling path for the load current in case of fault or activation of the Quench Protection Circuits, before the closure of the external mechanical switch. The internal bypass is realized by switching on the thyristors of the same leg of the bridge, such to provide zero voltage at the output. The bypass function is performed by all the three legs in sequence, in order to spread the thermal losses. In this way, if no voltage is required from the converter unit, the bypass function is activated, so its reactive

power demand is zero. The internal bypass function was combined with the sequential control of series-connected units, as shown in Figure 28. Only one converter unit of the series at time regulates the output voltage, while the others supply maximum or minimum voltage or operate in bypass mode if their voltage is not required.

Figure 29 shows the internal bypass scheme [19].

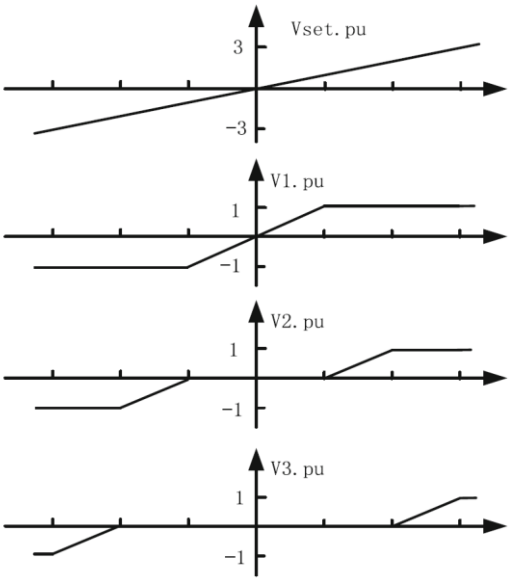

Figure 28 – Sequential control of three units in series, with bypass operation [19].

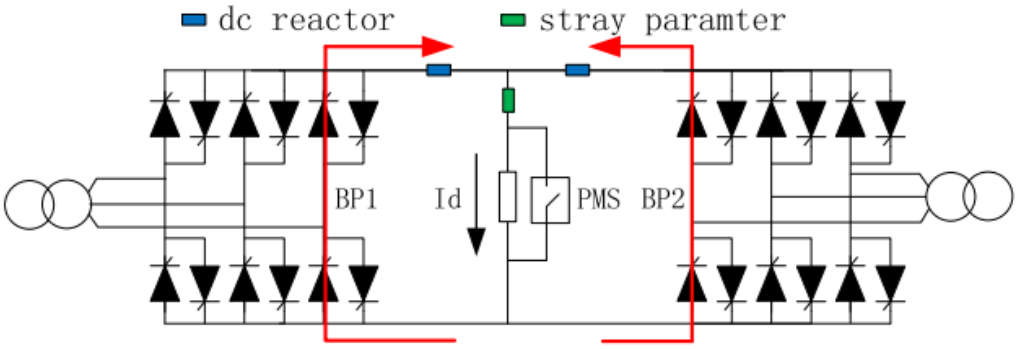

Figure 29 – Internal bypass scheme [19]

The transition from normal to bypass operation and vice-versa is critical for ITER converter units, since it causes current unbalance between the two 6-pulse/4-quadrant subunits connected in parallel. that can trigger overcurrent protection system. In [20] these transitions are analyzed and the conditions to avoid or minimize current unbalance are defined. However, for ITER the internal bypass solution was finally rejected and the converters will be controlled with the sequential control only. This choice has been motivated by considering that the frequent transitions from normal to bypass mode and vice-versa would imply frequent overcurrents and consequent overheat of the thyristor junctions, requiring a higher number of thyristors in parallel [19].

In this model the transition from normal to bypass operation and vice-versa is considered instantaneous. The bypass control algorithm which calculates the firing delay angles is implemented with the following Matlab® function:

```
function [a,alpha_a,alpha_b,deltav_dc_a,deltav_dc_b,u_a,u_b,Vdc]  =
fcn(Sn,V2o,deltavcc,I1a,I2b,Vcoil,alphamax,alphamin)

%This function determines which 12p converters must be active. It
%generates a vector 'a' in which every position matches with the respective 12p
%converter. If the value in the i-th position is 1 the i-th the converter is
%active, if it's 0 the converter is bypassed.
%Then the function generates the vectors alpha_a and alpha_b that contain the
%firing angle of 'a' and 'b' 6p converters.

s=8;
Vconvmax_vector=zeros(s,1);
Vconvmin_vector=zeros(s,1);

I2n=Sn/(sqrt(3)*V2o);                    %transformer secondary rated current
Xcc=(deltavcc*V2o)/((sqrt(3))*I2n);      %short circuit reactance (deltavcc [pu])

%the following function part computes the decrease of dc voltage due to %commutation
and the maximum and minimum voltage that the converters can supply

deltav_dc_a=abs((3*Xcc*I1a)/pi);
deltav dc b=abs((3*Xcc*I2b)/pi);

Vconvmax_a=1.35*V2o*cos(alphamin)-deltav_dc_a;
Vconvmin_a=1.35*V2o*cos(alphamax)-deltav_dc_a;
Vconvmax_b=-(1.35*V2o*cos(alphamax))+deltav_dc_b;
Vconvmin_b=-(1.35*V2o*cos(alphamin))+deltav_dc_b;

i=1;
while i<=s
    if I1a~=0 && I2b~=0                              %circulating mode
        if abs(Vconvmax_a)>=abs(Vconvmax_b)
            Vconvmax_vector(i)=Vconvmax_b;
        else
            Vconvmax_vector(i)=Vconvmax_a;
        end
        if abs(Vconvmin_a)>=abs(Vconvmin_b)
            Vconvmin_vector(i)=Vconvmin_b;
        else
            Vconvmin_vector(i)=Vconvmin_a;
        end
    else
        if I1a~=0                                    %6p or 12p mode with Icoil>0
            Vconvmax_vector(i)=Vconvmax_a;
            Vconvmin_vector(i)=Vconvmin_a;
        else                                         %6p or 12p mode with Icoil<0
            Vconvmax_vector(i)=Vconvmax_b;
            Vconvmin_vector(i)=Vconvmin_b;
        end
    end
    i=i+1;
end

%the following function part computes the vector 'a'

i=1;
alpha_a=zeros(s,1);
alpha_b=zeros(s,1);
a=zeros(s,1);
Vdc=zeros(s,1);
u_a=zeros(s,1);
u_b=zeros(s,1);

while i<=s
    Vbmax=sum(Vconvmax_vector(1:(i-1),1));
    Vbmin=sum(Vconvmin_vector(1:(i-1),1));
    if Vbmax<Vcoil || Vbmin>Vcoil
        a(i,1)=1;
    else
        a(i,1)=0;
    end
    i=i+1;
end
```

```
%the following function part evaluates the vectors alpha_a and alpha_b

i=1;
while i<=s
    if a(i,1)==0
            alpha_a(i,1)=0;
            alpha_b(i,1)=0;
            i=i+1;
    else    %a=1
        if Vcoil>0
            Vseq=Vcoil-(sum(Vconvmax_vector(1:(i-1),1)));
            if Vseq>=Vconvmax_vector(i,1)
                if I1a~=0 && I2b~=0
                    wa=(Vconvmax_vector(i,1)+deltav_dc_a)/(1.35*V2o);
                    wb=(-Vconvmax_vector(i,1)+deltav_dc_b)/(1.35*V2o);
                    alpha_a(i,1)=acos(wa);
                    alpha_b(i,1)=acos(wb);
                    i=i+1;
                else
                    alpha_a(i,1)=alphamin;
                    alpha_b(i,1)=alphamax;
                    i=i+1;
                end
            else
                wa=(Vseq+deltav_dc_a)/(1.35*V2o);
                wb=(-Vseq+deltav_dc_b)/(1.35*V2o);
                alpha_a(i,1)=acos(wa);
                alpha_b(i,1)=acos(wb);
                i=i+1;
            end
        else
            Vseq=Vcoil-(sum(Vconvmin_vector(1:(i-1),1)));
            if Vseq<=Vconvmin_vector(i,1)
                if I1a~=0 && I2b~=0
                    wa=(Vconvmin_vector(i,1)+deltav_dc_a)/(1.35*V2o);
                    wb=(-Vconvmin_vector(i,1)+deltav_dc_b)/(1.35*V2o);
                    alpha_a(i,1)=acos(wa);
                    alpha_b(i,1)=acos(wb);
                    i=i+1;
                else
                    alpha_a(i,1)=alphamax;
                    alpha_b(i,1)=alphamin;
                    i=i+1;
                end
            else
                wa=(Vseq+deltav_dc_a)/(1.35*V2o);
                wb=(-Vseq+deltav_dc_b)/(1.35*V2o);
                alpha_a(i,1)=acos(wa);
                alpha_b(i,1)=acos(wb);
                i=i+1;

            end
        end
    end
end
```

Figure 30 – Bypass control function of the Simulink Bypass Model

3.8 Example of results achievable with Bypass Model and Sequential Control

To easily evaluate the difference between the two control methods, a simulation with only one converter (CS3U) has been performed. CS3U, rated for 8 kV, 45 kA, is considered being composed by eight converter units in series, assuming to adopt the same design of ITER (with same voltage margin). A constant coil current I_{coil} equal to 40 kA is considered, in order to operate in 12-pulse mode, and the coil voltage V_{coil} is assumed being a ramp from +6 kV to -6 kV. The following figure shows I_{coil} and V_{coil} as function of time.

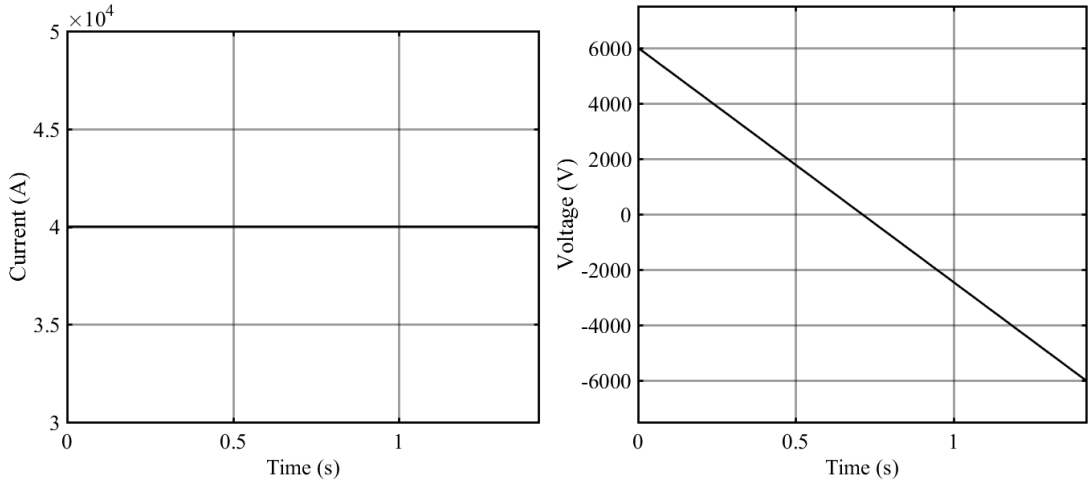

Figure 31 – Coil current and voltage waveforms assumed in the following example

With the symmetrical control, the firing angle is the same for all the eight converters, therefore the reactive power at ac side is maximum when the output voltage is near zero (where the firing angles are about 90°). With sequential control or bypass logic control there is a great reduction of reactive power, especially when V_{coil} is close to zero, as shown in Figure 32. From this Figure, it is clear the necessity to implement a control aimed at reducing the reactive power demand under acceptable levels.

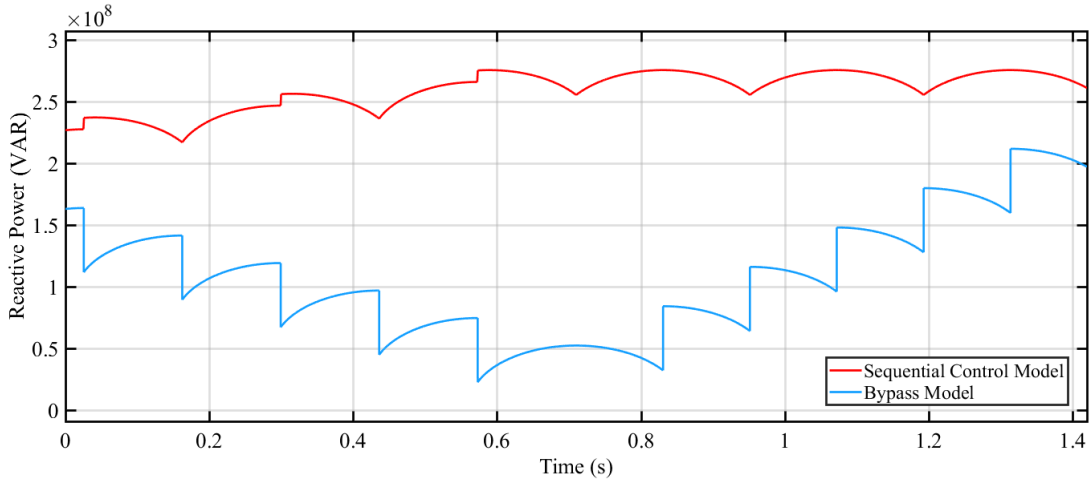

Figure 32 – Reactive power demand at ac side of CS3U achieved with the Simulink models, with dc output voltage and current as in Figure 31.

With positive I_{coil} and negative V_{coil} there is a greater request of reactive power due to the limit on the firing angle equal to 135 degrees. The better reduction of reactive power demand achievable with the bypass logic control with respect to sequential control is evident from Figure 32..

3.9 Simulation results in plasma breakdown, ramp-up and ramp-down phases

In this chapter, the total active and reactive power demand obtained with the two models described above for the plasma breakdown, plasma ramp-up and plasma ramp-down phases given by CREATE team (Section 3.3) are shown. In the models, the tentative configuration of DEMO magnet base converters described in Section 3.1 is implemented. In general, the model implementing the converter

bypass logic control and that for sequential control give the same active power but different reactive powers.

3.9.1 Plasma Breakdown Phase

The plasma breakdown phase given by CREATE lasts 1.46 seconds; the results are shown in Figure 33, Figure 34, Figure 35 and Table 12.

Table 12 – Active and reactive power comparison in plasma breakdown phase

	Bypass Model	**Sequential Control Model**
P max	1.35 GW	1.35 GW
P min	-1.66 GW	-1.66 GW
Q max	1.91 GVAR	2.41 GVAR
Q min	0.89 GVAR	2.05 GVAR

As can be seen, with bypass logic control, the maximum reactive power is lower, since the unnecessary converters do not exchange reactive power at ac side; instead, with sequential control, unnecessary converters produce reactive power even though their voltage is maximum or minimum, because of the firing angle limitations. In principle, without these limitations and considering overlapping angle only, the two models would give similar results.

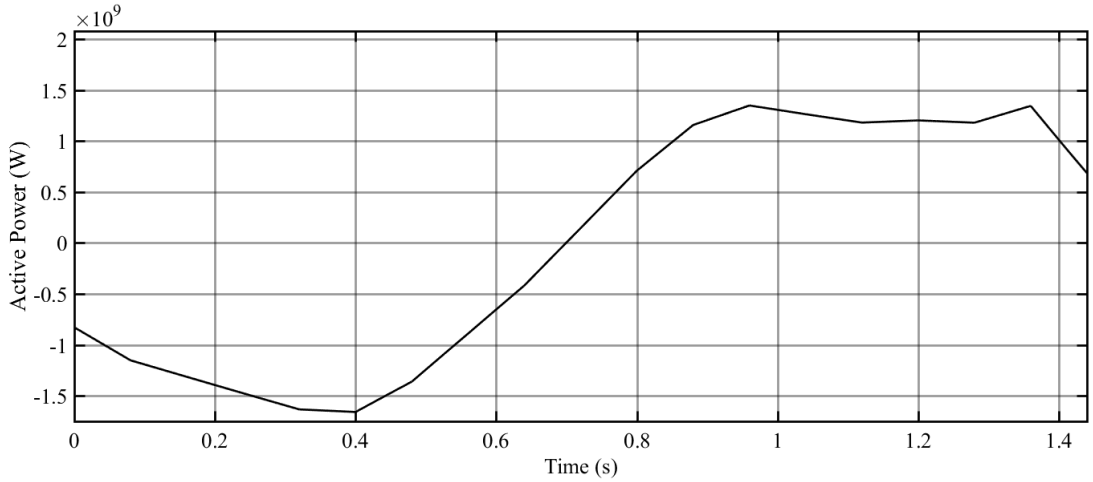

Figure 33 – Active power obtained in plasma breakdown phase with Bypass Model and Sequential Control Model

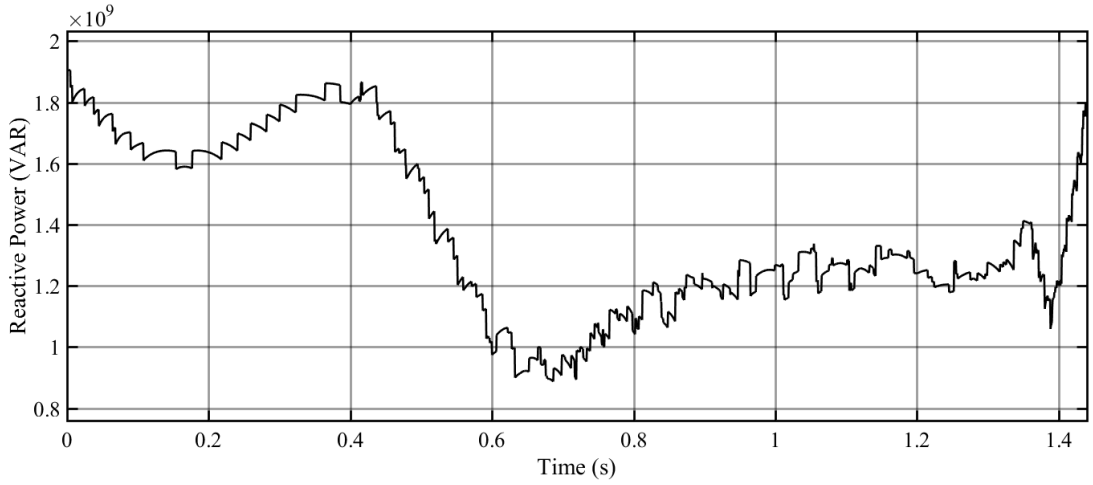

Figure 34 – Reactive power obtained in plasma breakdown phase with Bypass Model

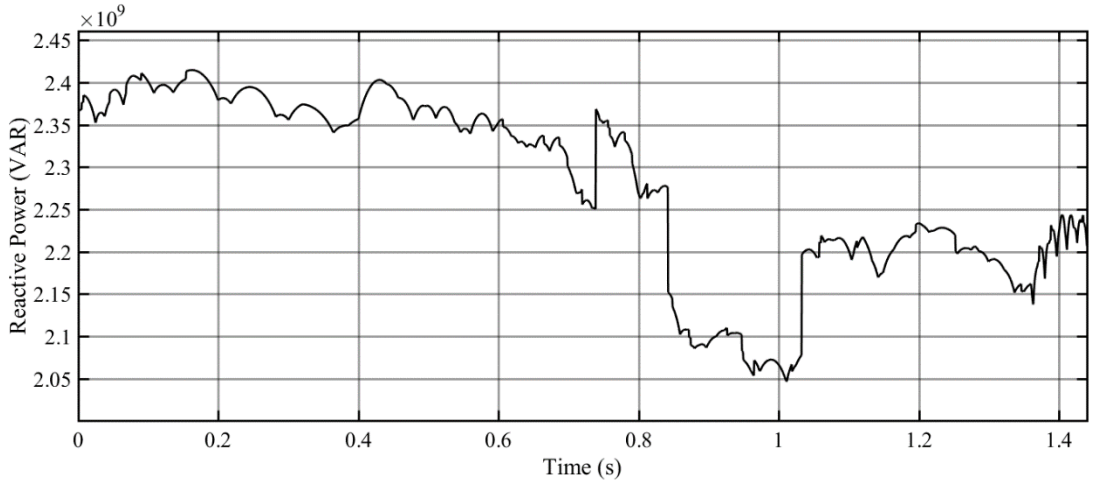

Figure 35 – Reactive power obtained in plasma breakdown phase with Sequential Control Model

3.9.2 Plasma Ramp-up Phase

For DEMO plasma ramp-up phase given by CREATE, the resulting active power is much lower than in plasma breakdown phase (due to lower output voltages), but the reactive power demand, especially with sequential control, has the same order of magnitude.

Plasma ramp-up phase lasts 146 seconds; the results are shown in Figure 36, Figure 37, Figure 38 and Table 13.

Table 13 – Active and reactive power comparison in plasma ramp-up phase

	Bypass Model	**Sequential Control Model**
P max	136 MW	136 MW
P min	-11 MW	-11 MW
Q max	303 MVAR	2009 MVAR
Q min	236 MVAR	1373 MVAR

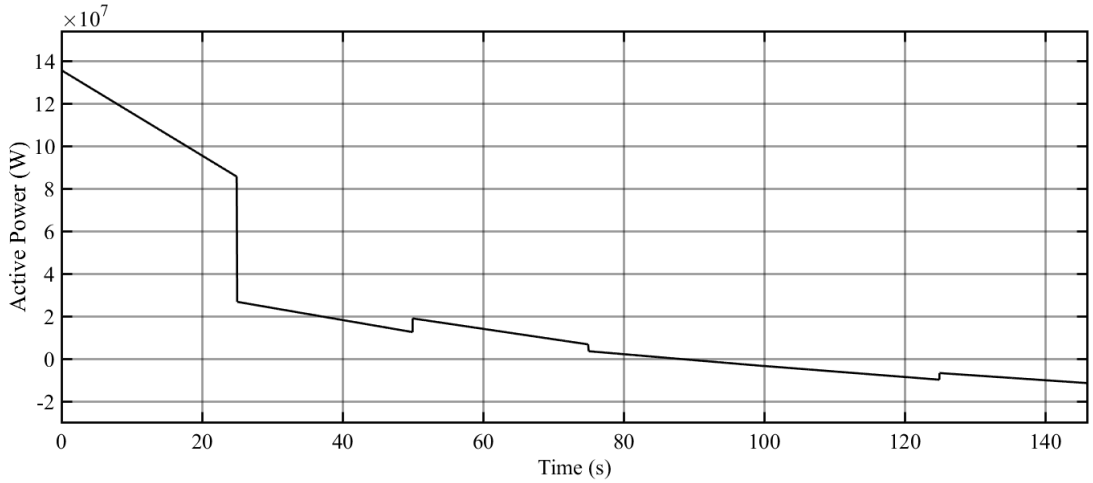

Figure 36 - Active power obtained in plasma ramp-up phase scenario with Bypass Model and Sequential Control Model

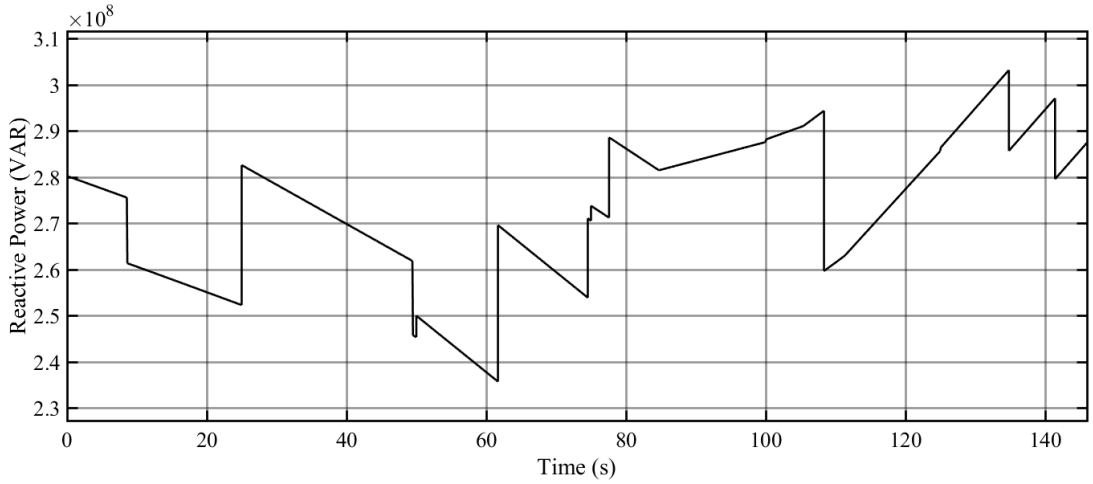

Figure 37 – Reactive power obtained in plasma ramp-up phase scenario with Bypass Model

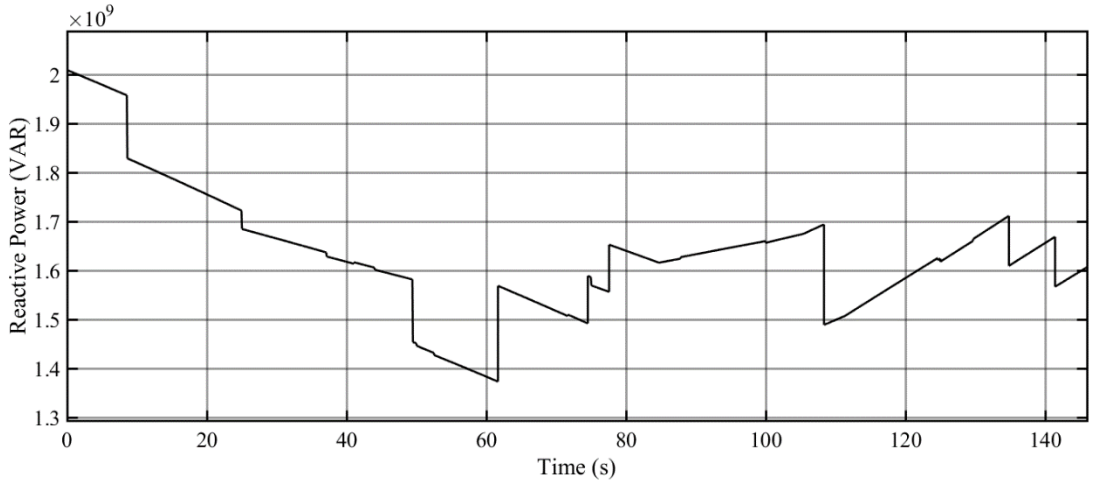

Figure 38 – Reactive power obtained in plasma ramp-up phase with Sequential Control Model

3.9.3 Plasma Ramp-down Phase

In DEMO plasma ramp-down phase given by CREATE team, the active and reactive power values are similar to those achieved in plasma ramp-up phase.

The plasma ramp-down phase lasts 146 seconds; the results are shown in Figure 39, Figure 40, Figure 41 and Table 14

Table 14 – Active and reactive power comparison in plasma ramp-down phase

	Bypass Model	**Sequential Control Model**
P max	113 MW	113 MW
P min	-28 MW	-28 MW
Q max	466 MVAR	2417 MVAR
Q min	286 MVAR	1702 MVAR

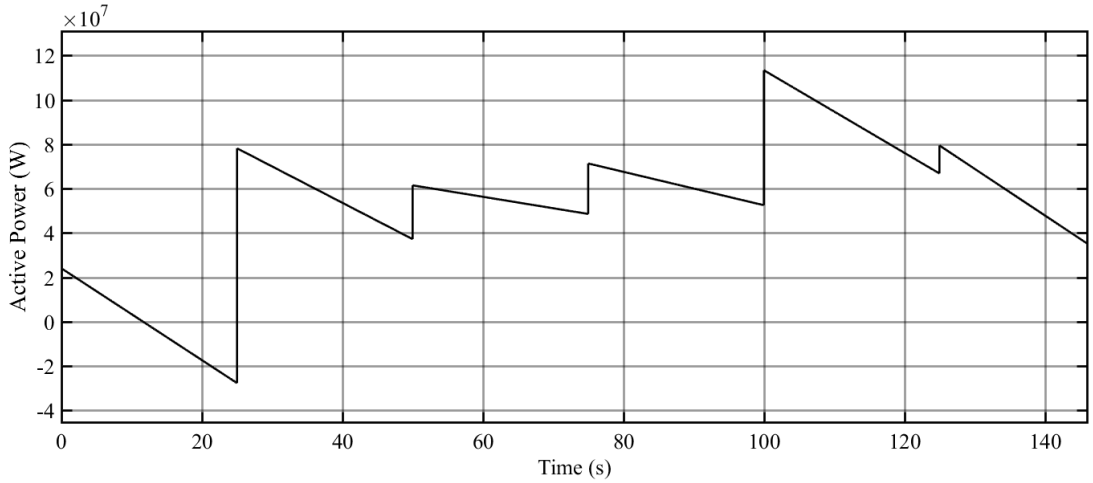

Figure 39 – Active power obtained in plasma ramp-down phase with Bypass Model and Sequential Control Model

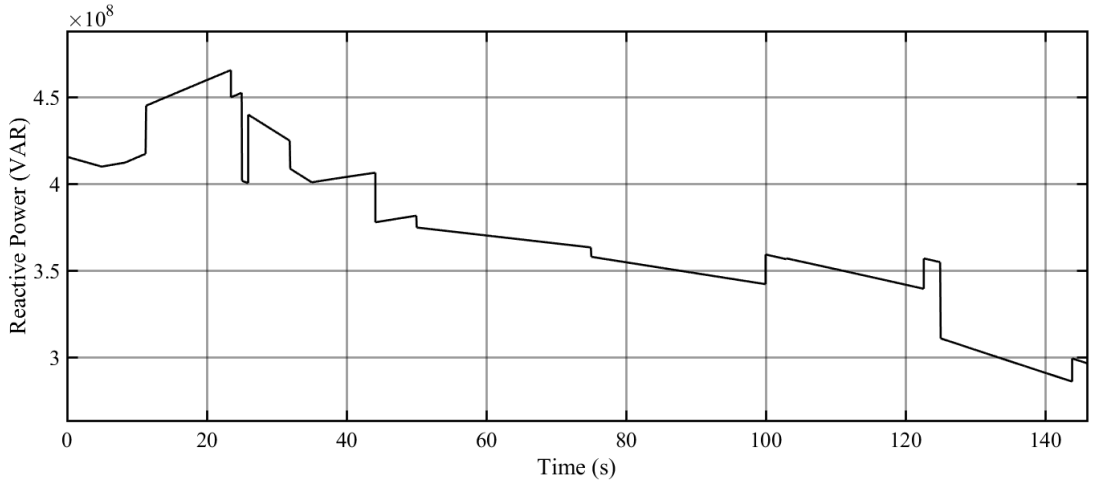

Figure 40 – Reactive power obtained in plasma ramp-down phase with Bypass Model

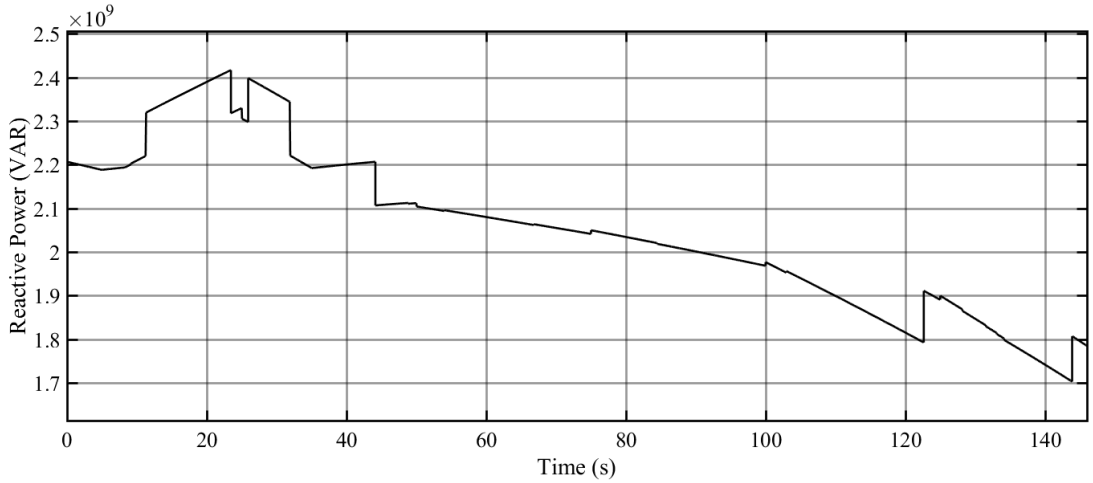

Figure 41 – Reactive power obtained in plasma ramp-down phase with Sequential Control Model

3.9.4 Conclusions

From the results shown in the previous sections, it can be noticed that the differences between the requested reactive power with sequential control and bypass logic control are greater in ramp-up and ramp-down operations than in the breakdown operation, as shown in Table 15. This because the bypass logic control leads to a higher reduction of the reactive power demand at ac side with respect to sequential control especially when low output voltages are required. With sequential control, the maximum reactive power demand is very high, in the order of 2.4 GVAR. It has to be underlined that the scenarios considered in these simulations do not necessarily represent the worst case. However, this reactive power needs to be compensated with a RPC&HF to satisfy the limitations imposed by the grid network, and this RPC&HF would be much larger if sequential control is adopted.

Table 15 – Comparison of maximum reactive power required with bypass logic control and sequential control

	Breakdown Q_{max} [MVAR]	**Ramp-up Q_{max} [MVAR]**	**Ramp-down Q_{max} [MVAR]**
Bypass Model	1910	303	466
Sequential Control Model	2410	2009	2417
Q_{MAX} reduction in Bypass Model with respect to Sequential Control Model	-21%	-85%	-81%

4 Study of Active Front End Design for DEMO CS and PF Coils Power Supply

In ITER, the superconducting coils are supplied by thyristor-based converters. To achieve acceptable reactive power absorption and current harmonic content from the grid, a large Reactive Power Compensation and Harmonic Filtering system (RPC&HF) is adopted, rated for a total power of 750 MVAR and based on Thyristor Controlled Reactors and tuned filters (as described in paragraph 2.3.2.3). Besides its cost and area occupancy, the high dynamics required to satisfy the reactive power limit in transient conditions represents a further severe challenge. These problems would be much amplified in DEMO where the power ratings of the base converters are about five times higher than those of ITER.

In this chapter, an alternative solution for DEMO base converters, based on Active Front End (AFE), is investigated. The AFE topology includes a line-side ac/dc converter based on fully controlled active switches, such as IGCT (Integrated Gate-Commutated Thyristors), a dc-link capacitor bank and a load-side inverter. In the following, only the DEMO base converters with a voltage rating of 8 kV are considered.

The line-side converter, commonly referred as PWM rectifier, can operate both as a rectifier and as an inverter, feeding power back to the line; it basically works as a boost converter, i.e. the intermediate dc-link voltage has to be higher than the peak of the grid side phase voltage, to avoid saturation of the PWM controller, which would lead to line side harmonics [21].

The topology selected for the coil-side converter is a five-level cascaded H-bridge (5L-CHB) composed of two cells. This converter topology allows reaching a modular approach in base converter structure and it is made by less components in respect with other solutions, such as Neutral Point Clamped (NPC) Converter. Each cell is fed by its own PWM rectifier, that supplies a dedicated dc-link capacitors bank and a full bridge converter. The PWM rectifier is fed by a secondary winding of a step-down transformer, fed in turn by the Medium Voltage distribution board. The two cells are put in series at the coil-side, to generate the requested voltage level. The topology adopted for the AFE converter is shown in Figure 42. The solution conceived for the DEMO base converters rated for 10 kV is similar, but with three cells in series instead of two. In that case, the coil-side converters would be controlled as a single seven-level cascaded H-bridge (7L-CHB).

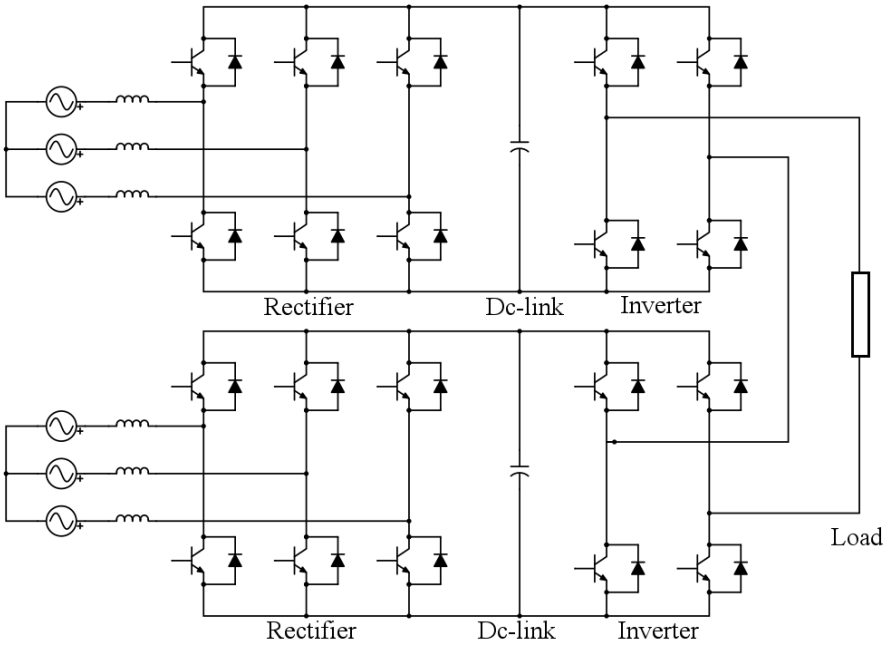

Figure 42 – converter topology for DEMO base converter rated for 8 kV

4.1 AC/DC Converter

4.1.1 The d-q Theory

Clarke transformation, or alpha-beta (αβγ) transformation, is a mathematical transformation used to simplify the analysis of three-phase circuits. This transformation allows us to represent a three-phase balanced system by an equivalent two-phase system. We consider a three-phase system with sinusoidal and time-varying voltages (e_a, e_b, e_c) and a stationary two-axis coordinate system where α-axis is aligned with e_a, β-axis is orthogonal to the α-axis and γ-axis orthogonal to the previous two. The three-phase voltages have component in the three axes (if it is symmetric and balanced the components on γ-axis are equal to zero) and it can be expressed as:

$$e_{\alpha\beta\gamma}(t) = T_C * e_{abc}(t) = \sqrt{\frac{2}{3}} * \begin{bmatrix} 1 & -\frac{1}{2} & -\frac{1}{2} \\ 0 & \frac{\sqrt{3}}{2} & -\frac{\sqrt{3}}{2} \\ \frac{1}{2} & \frac{1}{2} & \frac{1}{2} \end{bmatrix} * \begin{bmatrix} e_a(t) \\ e_b(t) \\ e_c(t) \end{bmatrix} \tag{4.1}$$

where $e_{abc}(t)$ is the generic three-phase voltage sequence and $e_{\alpha\beta\gamma}(t)$ is the corresponding voltage sequence in the coordinate reference αβγ. The coefficient $\sqrt{2/3}$ is used to make the two coordinate systems equivalent as regard the instantaneous power (power invariant transformation). The inverse transformation is:

$$e_{abc}(t) = {T_C}^{-1} * e_{\alpha\beta\gamma}(t) = \sqrt{\frac{3}{2}} * \begin{bmatrix} \frac{2}{3} & 0 & \frac{\sqrt{2}}{3} \\ -\frac{1}{3} & \frac{1}{\sqrt{3}} & \frac{\sqrt{2}}{3} \\ -\frac{1}{3} & -\frac{1}{\sqrt{3}} & \frac{\sqrt{2}}{3} \end{bmatrix} * \begin{bmatrix} e_\alpha(t) \\ e_\beta(t) \\ e_\gamma(t) \end{bmatrix} \tag{4.2}$$

Note that parameters $e_\alpha(t)$ $e_\beta(t)$ $e_\gamma(t)$ are still time-varying. In order to improve the dynamic performance of the models that use this coordinate system, the Park transformation is proposed. With this transformation the reference frame axes rotate with an angular speed ω. If this speed is equal to the angular frequency of time-varying parameters, then all the parameters in this reference frame became time invariant.

The direct transformation from the frame reference abc to the rotating frame reference dq0 is:

$$e_{dq0}(t) = T_{CP} * e_{abc}(t) = \sqrt{\frac{2}{3}} * \begin{bmatrix} \cos(\vartheta) & \cos\left(\vartheta - \frac{2}{3}\pi\right) & \cos\left(\vartheta + \frac{2}{3}\pi\right) \\ -\sin(\vartheta) & -\sin\left(\vartheta - \frac{2}{3}\pi\right) & -\sin\left(\vartheta + \frac{2}{3}\pi\right) \\ \frac{\sqrt{2}}{2} & \frac{\sqrt{2}}{2} & \frac{\sqrt{2}}{2} \end{bmatrix} * \begin{bmatrix} e_a(t) \\ e_b(t) \\ e_c(t) \end{bmatrix} \tag{4.3}$$

where the orthogonal axes d and q are rotating at angular speed ω and ϑ is the angular displacement between α and d such that,

$$\omega = \frac{d\vartheta}{dt} \tag{4.4}$$

The inverse transformation is:

$$e_{abc}(t) = {T_{CP}}^{-1} * e_{dq0}(t) = \sqrt{\frac{2}{3}} * \begin{bmatrix} \cos(\vartheta) & -\sin(\vartheta) & \frac{\sqrt{2}}{2} \\ \cos\left(\vartheta - \frac{2}{3}\pi\right) & -\sin\left(\vartheta - \frac{2}{3}\pi\right) & \frac{\sqrt{2}}{2} \\ \cos\left(\vartheta + \frac{2}{3}\pi\right) & -\sin\left(\vartheta + \frac{2}{3}\pi\right) & \frac{\sqrt{2}}{2} \end{bmatrix} * \begin{bmatrix} e_d(t) \\ e_q(t) \\ e_0(t) \end{bmatrix} \tag{4.5}$$

4.1.2 Operating Principle

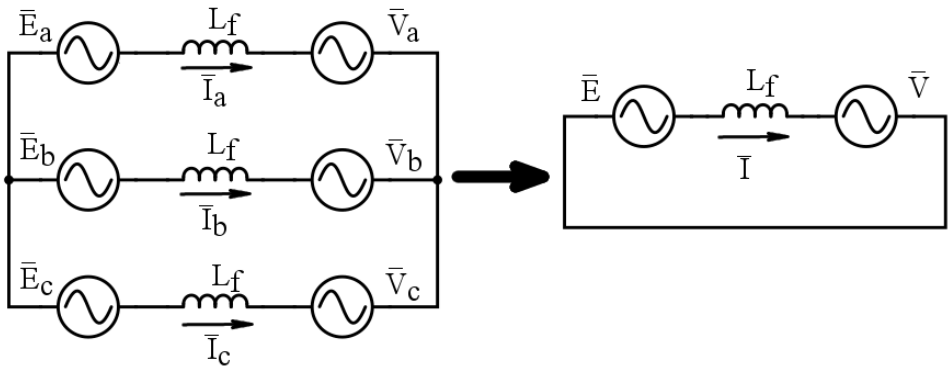

Figure 43 – Three-phase and equivalent single-phase circuit

The ac/dc converter is connected to the step-down transformer through a reactance (L_f) that incorporates the L-filter and the equivalent leakage inductance of the step-down transformer. On the left-side of Figure 43 it is shown the equivalent circuit seen from the grid, in which V represents phase to phase voltage at the ac/dc converter ac input, E is the grid voltage and L_f is the inductance mentioned above. On the right side, a single phase equivalent circuit of this circuit is shown.

Considering only the fundamental harmonic, to achieve a unity power factor in rectifier mode, the converter voltage V must be greater than the grid voltage E in magnitude, as shown in Figure 44 (where φ is the angle between line current and phase voltage).

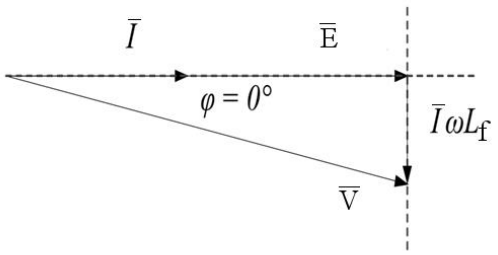

Figure 44 – Unity power factor in rectifier mode

As shown in Figure 45 and equations (4.6) and (4.7), the active power flow is controlled by changing the converter voltage component V_q (which leads E by an angle of 90 degrees) and the reactive power flow by changing the converter voltage component V_d (in phase with E). The angle δ is called the power angle because the power flow between the grid and the ac/dc converter can be controlled by varying this angle.

$$P = 3EI\cos(\varphi) = 3EI_d = \frac{3EV\sin(\delta)}{X} = \frac{3EV_q}{X} \tag{4.6}$$

$$Q = 3EI\sin(\varphi) = 3EI_q = \frac{3E(V\cos(\delta) - E)}{X} = \frac{3E(V_d - E)}{X} \tag{4.7}$$

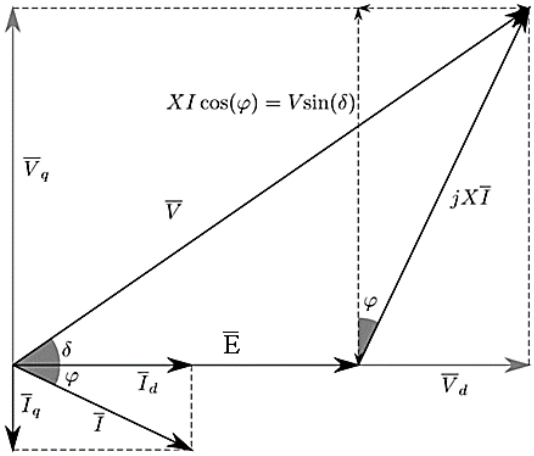

Figure 45 – Vector diagram

4.1.3 Control Scheme

The control scheme of the ac/dc converter has two main duties:

- to keep the dc-link voltage equal to the reference value;
- to produce a sinusoidal current on the grid side, in phase with the respective phase voltage, in order to achieve a power factor close to one in any operative condition.

The block diagram of the control scheme is shown in Figure 46. It can be noted that:

- the voltage controller receives as input the dc-link voltage reference (u^*_{dc}) and the measured instantaneous dc-link voltage (u_{dc}), and gives at the output the reference i^*_d. Its function is to keep the dc-link voltage maintains equal to the reference;
- the current controller takes as input the current references i^*_d, i^*_q and the measured values of i_d, i_q, e_d, e_q producing the reference voltages u_d and u_q for the converter. This control forces i_d and i_q to follow their references, minimizing at the same time the generation of high-order harmonics.

To achieve a good control dynamics, the control operates in the dq0 frame reference. The transformation from abc frame reference to dq0 frame reference is analysed in the previous paragraph.

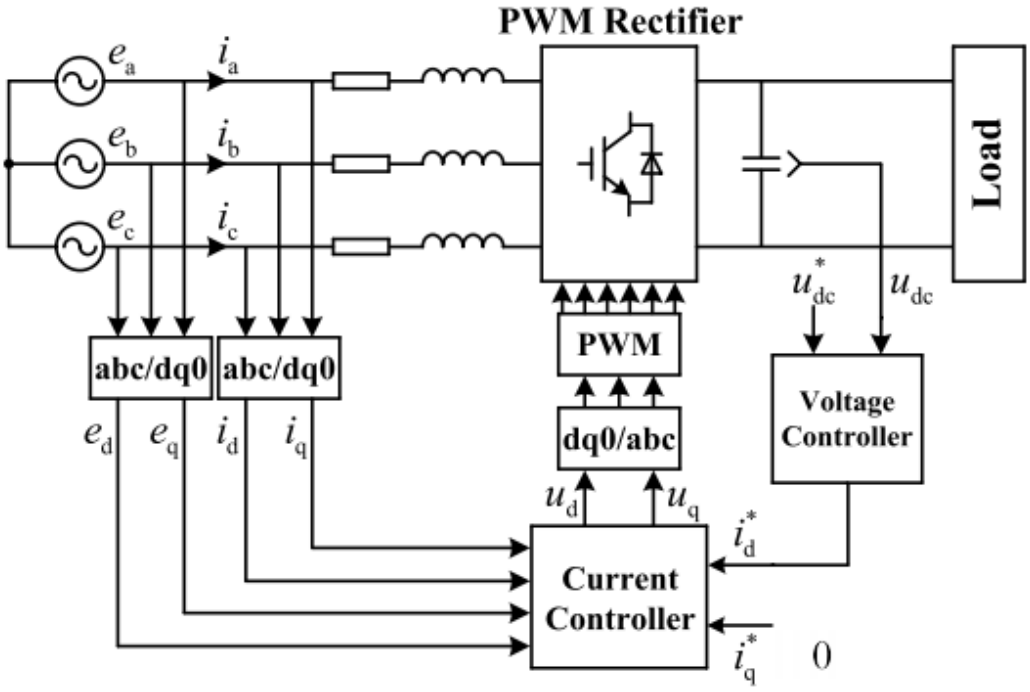

Figure 46 – Control Block Diagram of the ac/dc converter

4.1.4 Deriving d-q Model

Figure 47 represents the scheme of the ac/dc converter, which is a voltage source PWM rectifier that produces the grid-side voltages V_a, V_b and V_c and is supplied by grid voltages E_a, E_b and E_c. L is the total inductance of the ac-side filter reactor and the transformer. V_{dc} is the dc-link voltage and C is the dc-link capacitance. i_{dc} is the total dc-link current, which is the sum of the load current (i_L) and the capacitor current (i_c). i_c can be expressed as:

$$i_c = C\frac{dV_{dc}}{dt} = i_{dc} - i_L \tag{4.8}$$

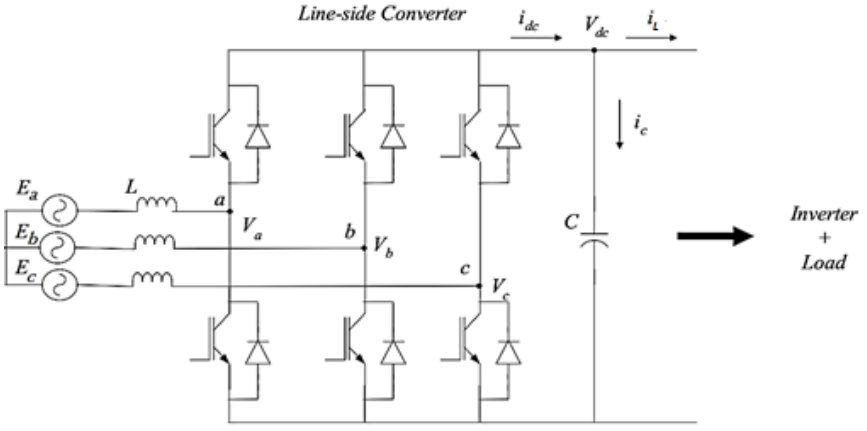

Figure 47 – Scheme of the ac/dc converter

The grid-side phase voltages produced by the converter are:

$$\begin{cases} V_a = S_a V_{dc} \\ V_b = S_b V_{dc} \\ V_c = S_c V_{dc} \end{cases} \tag{4.9}$$

where S_a, S_b and S_c are the converter legs states that assume the values +1 if upper switch is in conducting state or 0 if lower switch is in conducting state.

The dynamic equations which describe the converter are:

$$\begin{cases} e_a = L\dfrac{di_a}{dt} + Ri_a + V_a \\ e_b = L\dfrac{di_b}{dt} + Ri_b + V_b \\ e_c = L\dfrac{di_c}{dt} + Ri_c + V_c \end{cases} \tag{4.10}$$

By using Park Transformation from abc to dq0 rotating frame we can write [22] [23],

$$\begin{cases} e_d = Ri_d + L\dfrac{di_d}{dt} - \omega L i_q + V_d \\ e_q = 0 = Ri_q + L\dfrac{di_q}{dt} + \omega L i_d + V_q \\ e_0 = Ri_0 + L\dfrac{di_0}{dt} + V_0 \end{cases} \tag{4.11}$$

To the previous equations shall be added the dc-link voltage dynamic equation,

$$C\frac{dv_{dc}}{dt} = \frac{3}{2}\left(i_d s_d + i_q s_q\right) - i_L \tag{4.12}$$

s_d and s_q are switching function in rotating d-q coordinate. From equations (4.11) and (4.12) we can derive the block diagram of the converter in dq0 frame Figure 48.

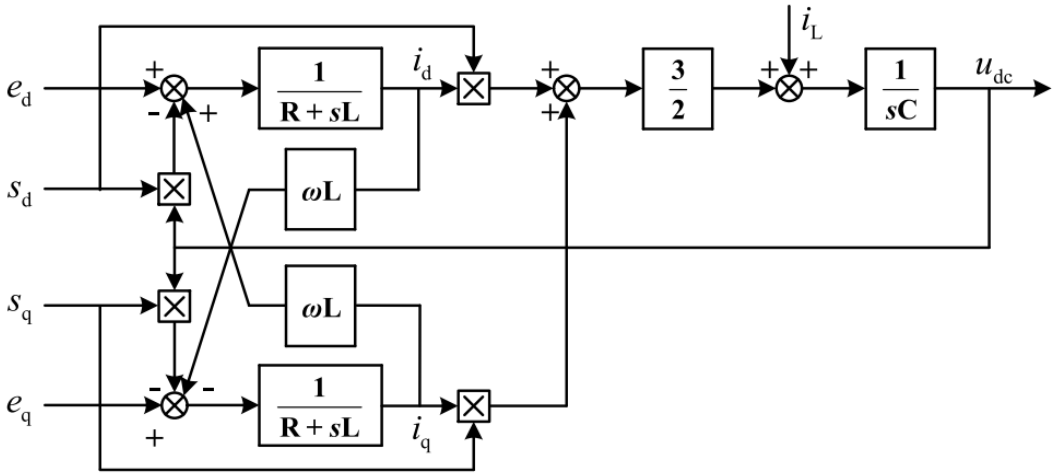

Figure 48 – Mathematical Model of ac/dc converter in dq0 frame

Note that grid voltage q component is equal to zero because the ϑ reference is chosen to obtain e_q=0. In the synchronous dq0 frame reference active and reactive power may be written as:

$$P = e_d i_d + e_q i_q = e_d i_d \tag{4.13}$$

$$Q = e_q i_d - e_d i_q = -e_d i_q \tag{4.14}$$

From equations (4.12) and (4.13) can be noticed that the active power is controlled by varying the current component i_d, while the reactive power by varying the current component i_q. The equation (4.13) also shows that, when i_q is positive, the reactive power is negative, so the active rectifier is feeding the reactive power back to the grid. Alternatively, when i_q is negative, the converter is absorbing reactive power from the grid.

4.1.5 Dc-link Voltage Control

From equation (4.8), it can be noted that, if i_{dc}-i_L is positive the dc-link voltage rises, while if it is negative the dc-link voltage decreases. If i_{dc}-i_L is equal to zero, the dc-link voltage remains constant.

Equation (4.13) shows that the active power is controlled by i_d, therefore the dc-link voltage control has to produce the proper i_d reference to achieve the desired dc-link voltage.

In the dc-link voltage control, a dc-link voltage reference $V_{dc\ ref}$ is compared to the instantaneous measured dc-link voltage v_{dc}. The resulting error feeds a PI controller that gives the direct current reference $i_{d\ ref}$ that will be used in the current control to ensure constant dc-link voltage as shown in Figure 49 and in equation (4.15):

$$\begin{cases} i_{d_{ref}} = \left(K_p + \dfrac{K_I}{s}\right)\left(V_{dc_{ref}} - v_{dc}\right) \\ i_{q_{ref}} = 0 \\ i_{0_{ref}} = 0 \end{cases} \tag{4.15}$$

$i_{q\ ref}$ and $i_{0\ ref}$ are set equal to zero to achieve a reactive power compensation (see equation (4.13)), and to compensate the zero-sequence current, if any.

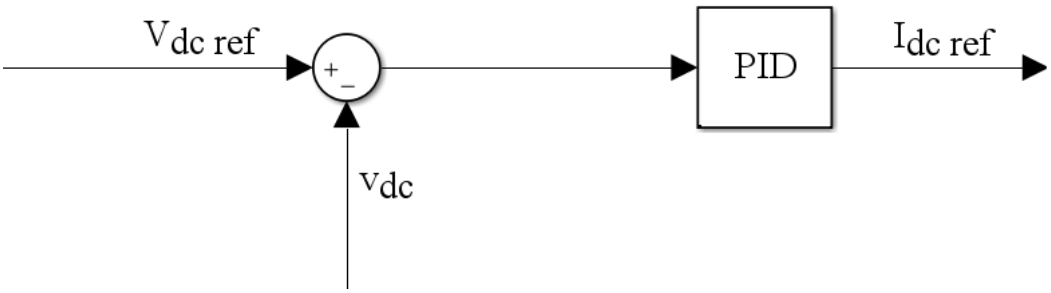

Figure 49 – Block Diagram of dc-link voltage control

4.1.6 Current Control

As derived previously with equations (4.11) and (4.12), the dynamics of the ac/dc converter is described by a system of non-linear differential equations. Equation (4.11) and Figure 48 show the coupling between the i_d and i_q current components. This coupling makes the control dynamic slow, especially for large variations of the dc-link voltage. During dc-link voltage variations, $i_{d\ ref}$ varies as function of V_{dc}, and the dynamics of i_d interferes with i_q dynamics, reducing the overall control performances.

The coupling between the current components can be effectively eliminated by considering an input-output linearization controller. In dynamic equations (4.11), V_d and V_q are the inputs, controlled such to generate the desired currents. The new variables V_d' and V_q' can be defined as follows [24]:

$$V'_d = V_d - E_d - \omega L i_q \tag{4.16}$$

$$V'_q = V_q - E_q + \omega L i_d \tag{4.17}$$

The new dynamic equations of the system for the d and q components become:

$$Ri_d + L\frac{di_d}{dt} = -V'_d \tag{4.18}$$

$$Ri_q + L\frac{di_q}{dt} = -V'_q \tag{4.19}$$

In the equations (4.18) and (4.19) the dynamics of i_d and i_q are decoupled. The new voltage references to be generated by the control system are:

$$V_{d_{ref}} = V'_d + E_d + \omega L i_q - R i_d \tag{4.20}$$

$$V_{q_{ref}} = V_q' + E_q - \omega L i_d - R i_q \quad (4.21)$$

The current control takes as inputs $i_{d\,ref}$, $i_{q\,ref}$ and $i_{0\,ref}$ coming from dc-link voltage control, and compare them with the measured instantaneous i_d, i_q and i_0. The respective errors are the inputs of PI controllers that generate $V_{d\,ref}$, $V_{q\,ref}$ and $V_{0\,ref}$. These references will be used to generate the command signals for the PWM rectifier switches with the Sinusoidal Pulse Width Modulation Technique (SPWM).

Figure 50 shows the overall control of the PWM rectifier, including both dc-link voltage control and current control, with the input-output linearization controller for the current components i_d and i_q.

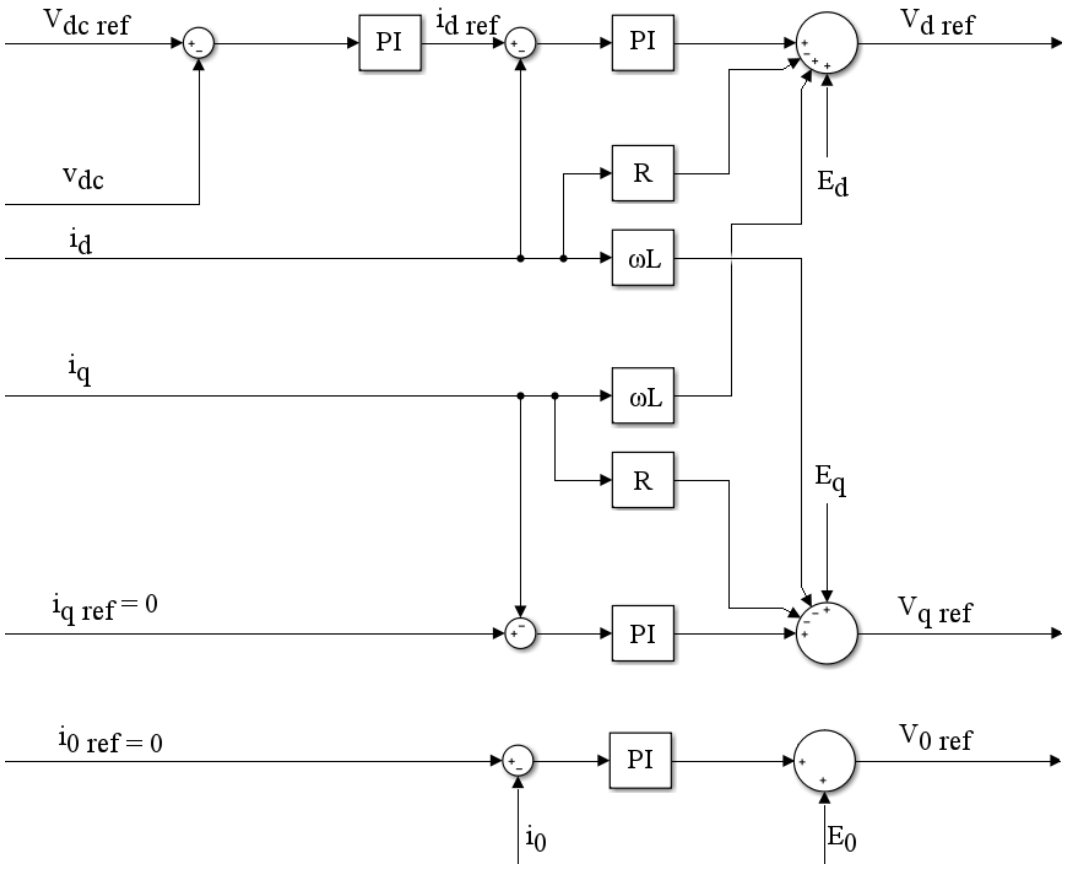

Figure 50 – Block Diagram of ac/dc converter current and voltage control

4.2 Load-Side Converter

As described in [25], the Five-Level Cascaded Half Bridge (5L-CHB) is composed by the connection in series of two H-Bridge inverters. Each H-Bridge is supplied by an isolated voltage source. Consider the load-side of the power cell presented in Figure 51. The switching state of the cell is determined by logical value of the two signals S_{k1} and S_{k2} (where k can be 1 or 2 depending on the units being considered), which can be "1" or "0" representing respectively the "on" and "off" state of the upper switches. This leads to four different binary combinations that generate three different output voltages $+V_{dc}$, zero and $-V_{dc}$.

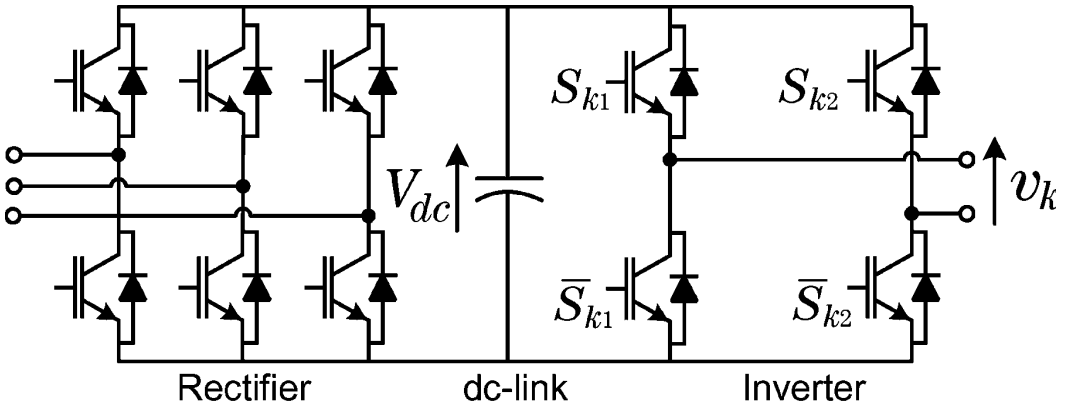

Figure 51 – AFE power cell [25]

The output voltage v_N of n cells in series is given by:

$$v_N = \sum_{k=1}^{n} v_k = \sum_{k=1}^{n} V_{dc}(S_{k1} - S_{k2}) \tag{4.22}$$

Considering n = 2, if we put all the possible binary combinations in the equation (4.22), the switching table is obtained, as shown in Table 16:

Table 16 – Five-Level Cascaded H-Bridge switching states

Output Voltage v_N	Cell 1			Cell 2		
	S_{11}	S_{12}	v_1	S_{21}	S_{22}	v_2
$2V_{dc}$	1	0	V_{dc}	1	0	V_{dc}
V_{dc}	1	0	V_{dc}	0	0	0
	1	0	V_{dc}	1	1	0
	0	0	0	1	0	V_{dc}
	1	1	0	1	0	V_{dc}
0	0	0	0	0	0	0
	0	0	0	1	1	0
	1	1	0	0	0	0
	1	1	0	1	1	0
	1	0	V_{dc}	0	1	$-V_{dc}$
	0	1	$-V_{dc}$	1	0	V_{dc}
$-V_{dc}$	0	1	$-V_{dc}$	1	1	0
	0	1	$-V_{dc}$	0	0	0
	0	0	0	0	1	$-V_{dc}$
	1	1	0	0	1	$-V_{dc}$

-2 V_{dc}	0	1	- V_{dc}	0	1	- V_{dc}

Note that there is more than one switching state for some voltage levels. This redundancy of the output voltage levels can be used for control purposes and increase proportionally with the number of levels.

4.2.1 Phase Disposition Strategy

To supply the coil with the requested voltage the Phase Disposition Pulse Width Modulation Strategy (PD-PWM) is adopted. As investigated in [26], for a N-level multilevel converter, N-1 triangular carriers with the same amplitude and frequency have to be generated. The N-1 carriers are disposed in order to fully occupy in contiguous bands the range $+NV_{dc}$ to $-NV_{dc}$, V_{dc} being the dc-link voltages (considered equal in each converter). A single reference is compared with each carrier, as we can see in Figure 52, and the multilevel converter signals pattern is generated.

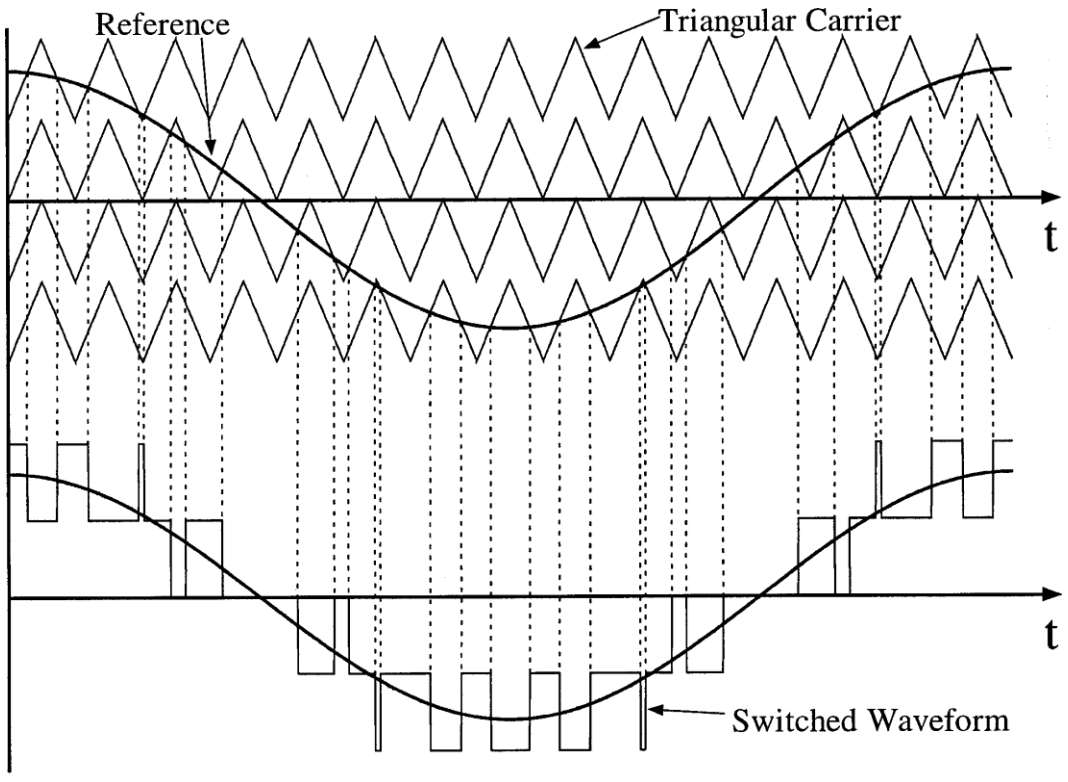

Figure 52 – Reference and Carriers Arrangement for Phase Disposition Pulse Width Modulation of a 5L-CHB Converter [26]

4.3 AFE Converter Design

4.3.1 Ratings and Main Design Choices

The input data considered in the AFE converter design are:

- rated load voltage: 8 kV;
- rated load current: 45 kA;
- rated load power = 380 MVA (45 kA × 8 kV);

- dc-link voltage:
    - nominal value = 4 kV;
    - maximum variation under stationary regimes = ±5%;
    - maximum variation under transients = ±15%;
- grid voltage:
    - nominal value = 66 kV;
    - maximum value = 72 kV (+10%);
    - minimum value = 62 kV (-6%);

The AFE converter topology (Figure 42) proposed is composed by two cells in series. Each cell has a PWM rectifier that operates with a SPWM control given by the dual-closed-loop control (dc-link voltage control as outer loop and current control as inner loop). The cell dc-link voltage reference is equal to 4 kV and the two H-bridge inverters in series operate with a PD-PWM strategy to generate the requested coil voltage. For the maximum variations of the dc-link under stationary regimes, a reasonable value has been assumed; the accuracy required is not so high, since the load-side converter can compensate these variations with its own real-time control system. For the maximum variations of the dc-link under transients, it has been considered that the worst load power step (±100 %) would occur only in case of fault or anomalous conditions. For the grid voltage, the same medium voltage level of ITER has been tentatively considered, with the same variation range.

The grid-side rms phase to phase no-load voltage (V_{ll}) can be computed with the following equation [15]:

$$V_{ll} = V_{dc,min*} m_a * \frac{\sqrt{3}}{2\sqrt{2}} * \frac{1}{1.1} = 3600 * 1 * \frac{\sqrt{3}}{2\sqrt{2}} * \frac{1}{1.1} = 2004.13\ V \tag{4.23}$$

with m_a=1 has been assumed as the maximum modulation index, to avoid the saturation of the modulation and the consequent distortion of the ac currents. The multiplication factor 1/1.1 takes into account the maximum grid voltage (72 kV).

Considering the high voltage and current ratings, for both the ac/dc converter and the load-side converter, Integrated Gate-Commutated Thyristors (IGCTs) have to be adopted. For the selection of their repetitive peak off-state voltage, taking into consideration the high reliability required for the DEMO base converters, it is considered a safety margin of 1.6 with respect to the nominal dc-link voltage:

$$V_{DRM} \geq 4000 * 1.6 = 6400\ V \tag{4.24}$$

V_{DRM} being the repetitive peak off-state voltage. The Asymmetric IGCT 5SHY42L6500 produced by ABB has been considered in the AFE converter design, having an adequate V_{DRM} of 6500 V. The selection of mentioned component allows avoiding IGCTs in series in bridge arms which would lead to a more complex structure to guarantee the voltage balance between the devices.

For the selection of Diodes repetitive peak reverse voltage (V_{RRM}), it is considered a safety margin of 2 with respect to the nominal dc-link voltage:

$$V_{RRM} \geq 4000 * 2 = 8000\ V \tag{4.25}$$

The soft freewheeling Diode D4600U45X172 produced by Infineon has been considered. Having a V_{RRM} of 4500 V, two Diodes in series must be used to respect the limit on the V_{RRM}.

The ratings of these two components are summarized in Table 17 and Table 18 [27] [28].

Table 17 – IGCT 5SHY426500 ratings

Parameter	Description	Value
V_{dc}	Permanent DC voltage	4000 V
I_{TGQM}	Maximum controllable turn-off current	3800 A
V_{DRM}	Repetitive peak off-state voltage	6500 V
r_T	Slope resistance	0.56 mΩ
V_{TO}	Threshold voltage	1.88 V
$R_{th(j-c)}$	Thermal resistance junction-to-case of GCT	8.5 K/kW
$R_{th(c-h)}$	Thermal resistance case-to-heatsink of GCT	3 K/kW
E_{on}	Turn-on energy per pulse @ V_D=4 kV, I_{TGQ}=4 kV	3.1 J
E_{off}	Turn-off energy per pulse @ V_D=4 kV, I_{TGQ}=4 kV	44 J
$t_{d(on)}$	Turn-on delay time @ V_D=4 kV, I_{TGQ}=4 kV	4 µs
t_r	Rise time	1 µs
$t_{d(off)}$	Turn-off delay time @ V_D=4 kV, I_{TGQ}=4 kV	7 µs
T_{vj}	Operating junction temperature range	125°C

Table 18 – Soft freewheeling Diode D4600U45X172 ratings

Parameter	Description	Value
V_{dc}	Permanent DC voltage	2800 V
I_{FSM}	Maximum peak non-repetitive surge current	80 kA
V_{RRM}	Repetitive peak reverse voltage	4500 V
r_T	Slope resistance	0.3 mΩ
V_{TO}	Threshold voltage	1.25 V
$R_{th(j-c)}$	Thermal resistance junction-to-case of diode	3.71 K/kW
$R_{th(c-h)}$	Thermal resistance case-to-heatsink of diode	1 K/kW
E_{off}	Turn-off energy per pulse @ V_D=3.3 kV, I_{TGQ}=1.8 kA	24 J
I_{RM}	Reverse recovery current	5500 A
T_{vj}	Operating junction temperature range	140°C

The frequency of the PWM carrier of the ac/dc converter shall be chosen among triple odd multiple of fundamental frequency to avoid ac current harmonics even or with orders being multiple of three of the fundamental [15]. A tentative value of 450 Hz has been assumed, as a trade-off between the switching losses on the power switches, the dc-link capacitance necessary to satisfy the maximum dc-link voltage variations under transients, and the line inductance necessary to achieve a reasonable current ripple.

4.3.2 Simulink Circuit Model

To carry out the thermal analysis and to verify the dynamic performance of the converter, a detailed Simulink model has been developed, including both the power section and the feedback controls.

The model is composed by the following main sections:

- ac/dc converter (Figure 53);
- load-side converter (Figure 54);
- dc-link voltage control (Figure 55), which generates the current references;
- ac/dc converter current control (Figure 56), that generates the voltage references and switching signals pattern from the current references;
- voltage controller of the load-side converter (Figure 57 and Figure 58): it is based on PD-PWM technique and it generates the switching signals pattern of the two H-bridge in series. It includes also the feedforward compensation of switches voltage drop and dc-link voltage fluctuations.

These sections are shown in the next figures.

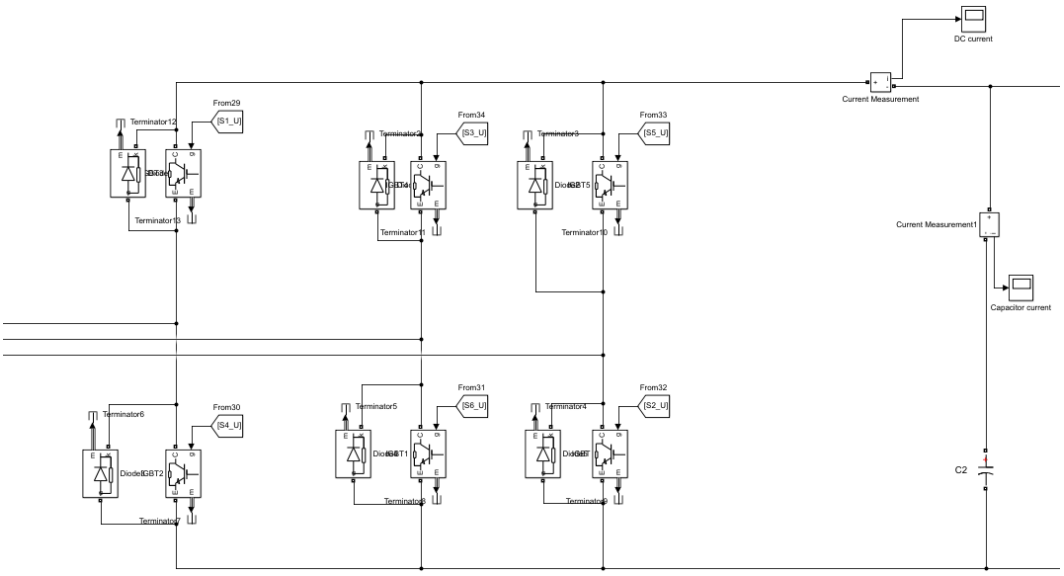

Figure 53 – Model of the ac/dc converter (of upper cell, that of lower cell is identical)

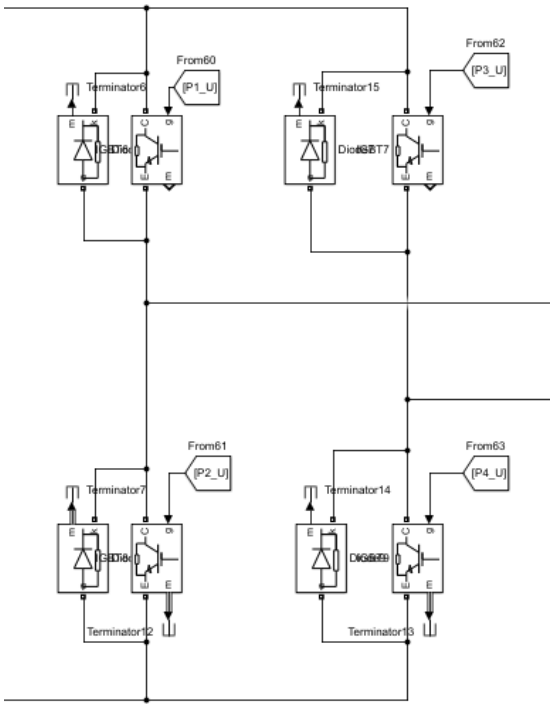

Figure 54 – Model of the load-side converter (of upper cell, that of lower cell is identical)

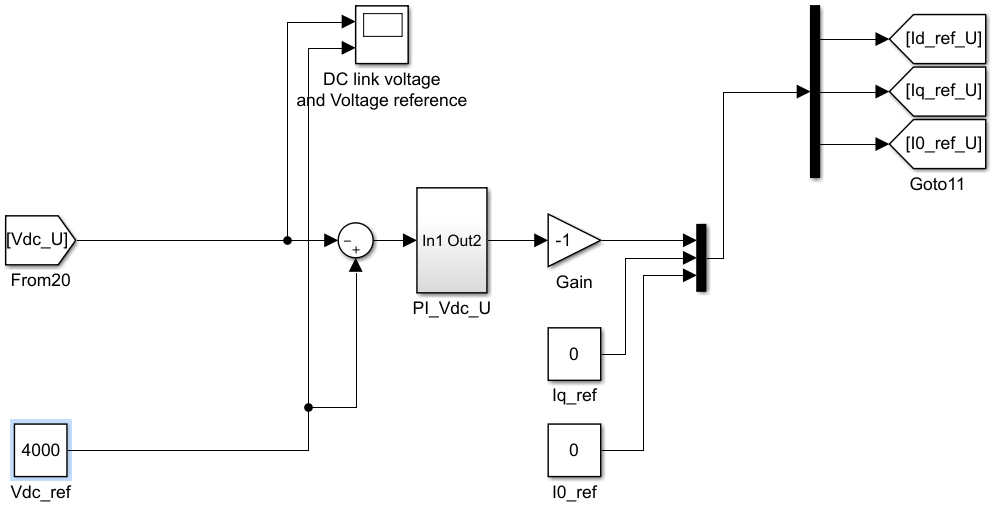

Figure 55 – Model of the dc-link voltage control (of upper cell, that of lower cell is identical)

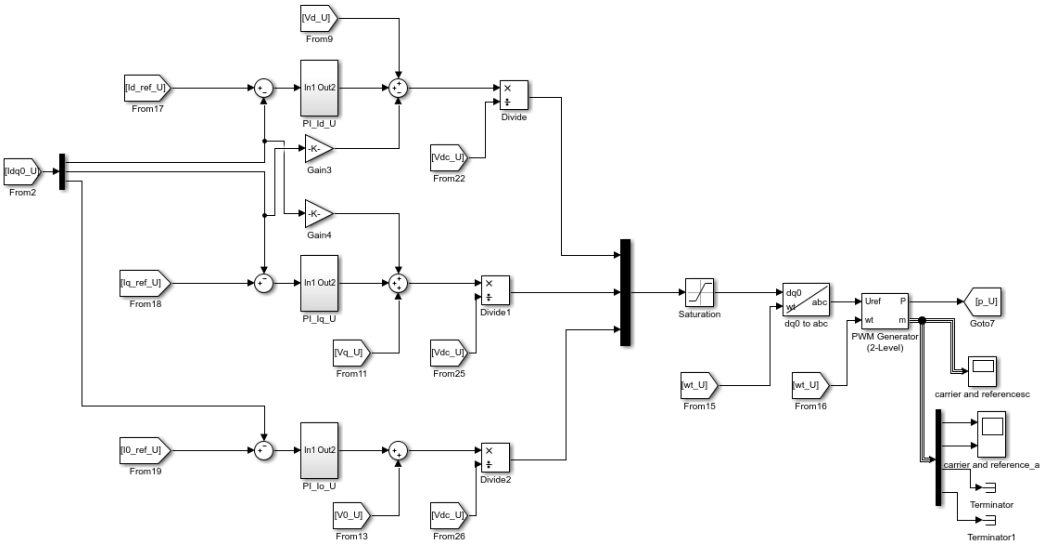

Figure 56 – Ac/dc converter current control (of upper cell, that of lower cell is identical)

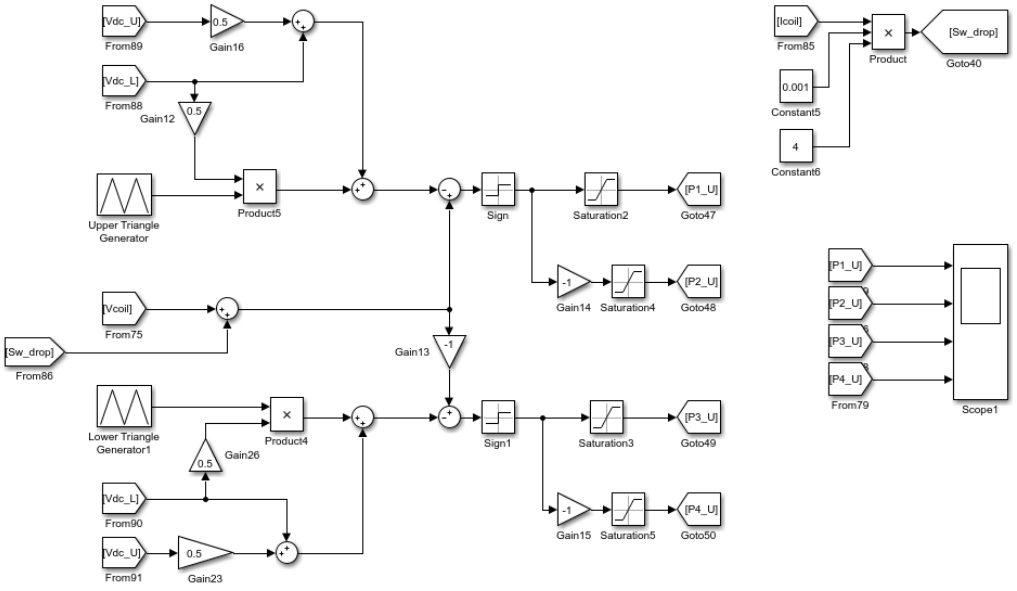

Figure 57 – Voltage controller of the load-side converter (upper H-Bridge)

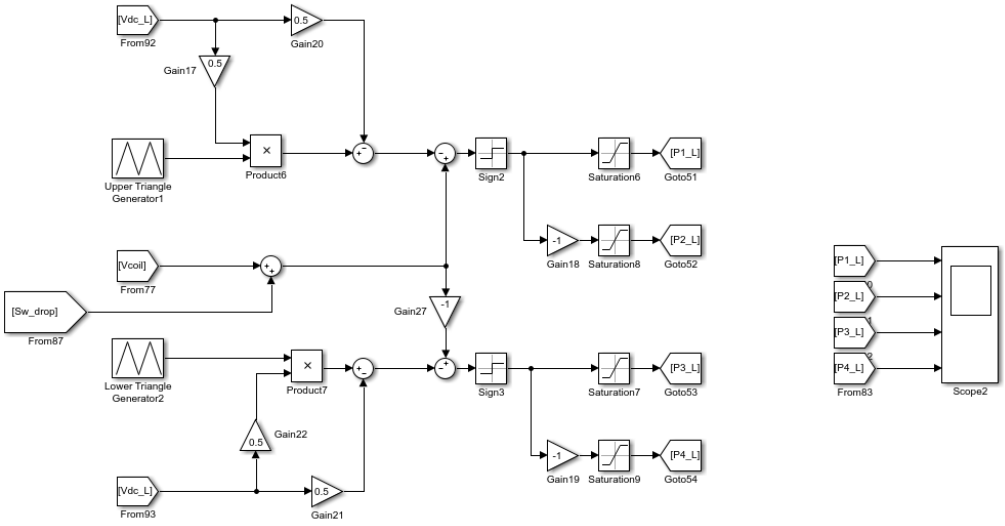

Figure 58 – Voltage controller of the load-side converter (lower H-Bridge)

The minimum capacitance of the dc-link capacitor bank in each cell is given by [29]:

$$C \geq \frac{T_r \Delta P_{max}}{2 V_{dc} \Delta U_{max}} = \frac{0.007 * 180000000}{2 * 4000 * 600} = 262.5\ mF \tag{4.26}$$

where T_r is the rise time of the dc current provided by the ac/dc converter and ΔU_{max} is a reasonable maximum allowed variation of the dc-link voltage with a full load step ΔP_{max}, i.e. 15% of the rated value (V_{dc} = 4 kV). ΔU_{max} has been selected to avoid ovestressing the capacitor bank in case sudden switch-off of the inverter (for example in case of fault) or voltage steps required at the output at high current. T_r has been tentatively supposed equal to 7 ms, taking into consideration the switching frequency of the rectifier and the expected dynamics. A simulation has been carried out with the resulting value of capacitance (262.5 mF), giving a rise time near 7 ms with an optimized PI regulator, confirming the first guess. The maximum variation of the two dc-link voltages remains within the limit of 15% with a full load step (360 MW in total, coil voltage and current equal to 8 kV and 45 kA respectively), as expected. The resulting dc-link voltage and current waveforms are shown in Figure 59, Figure 60 and Figure 61.

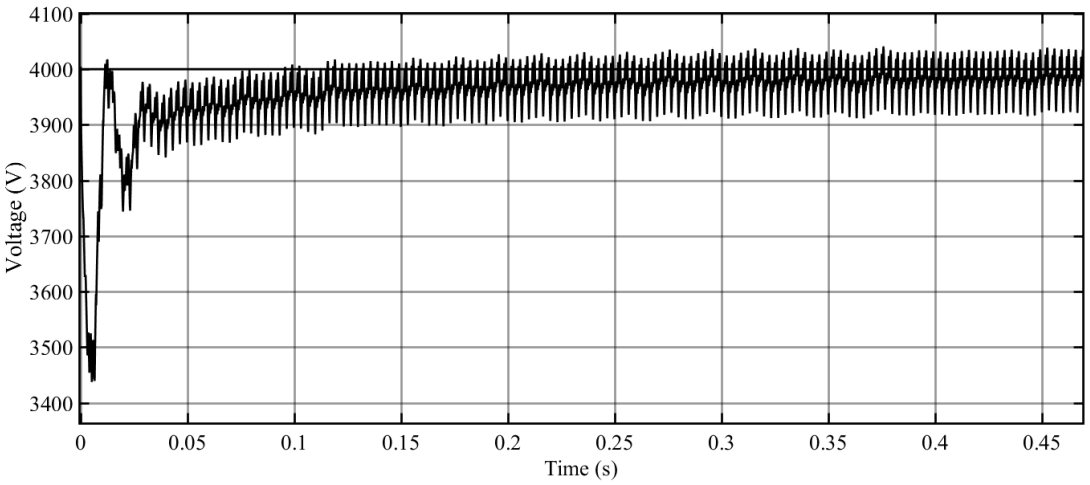

Figure 59 - Upper cell dc-link voltage with full load step (8 kV, 45 kA) applied at t = 0 s

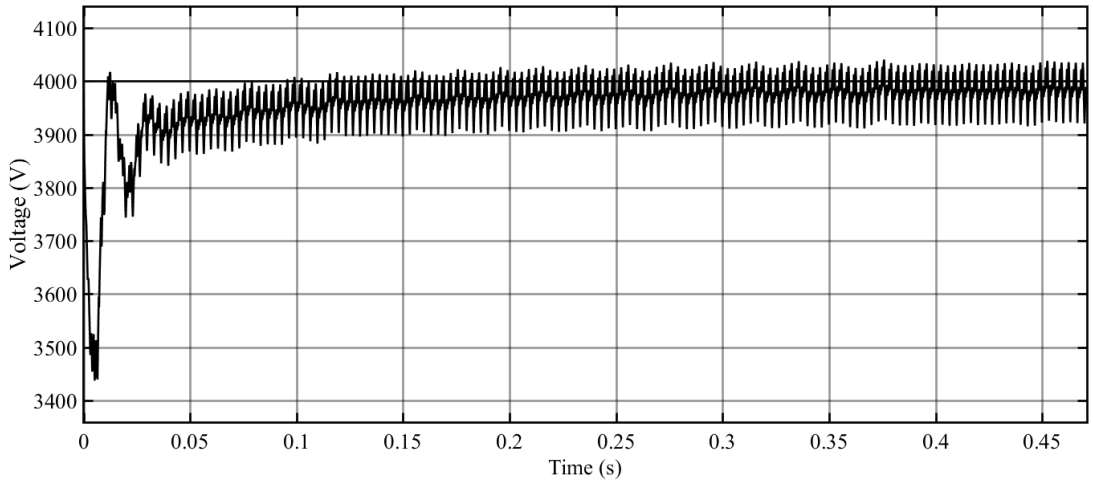

Figure 60 – Lower cell dc-link voltage with full load step (8 kV, 45 kA) applied at t = 0 s

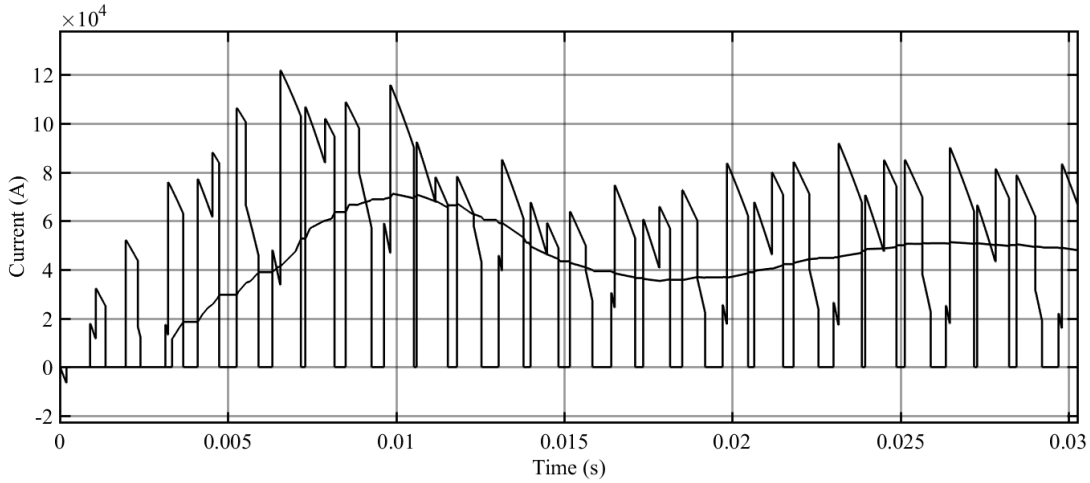

Figure 61 – Instantaneous upper cell dc-link current and its mean value, with full load step (8 kV, 45 kA) applied at t = 0 s

The selection of a reasonable current ripple on the rectifier is the criterion adopted for the filter inductor design. Negligible inductor resistance and no-load condition are considered; therefore, the grid-side phase voltages of the ac/dc converter shall be equal to the supply voltage. The modulation index, in no-load condition, is given by [30]:

$$m_a = \frac{2\sqrt{2}E}{V_{dc}} \tag{4.27}$$

where E is the RMS phase supply voltage. In these conditions, the peak to peak value of the current ripple can be calculated as follow:

$$I_{ripple_{pk-pk}} = \frac{m_a V_{dc}}{8\sqrt{3} f_{sw} L_f} = \frac{\sqrt{2}E}{4\sqrt{3} f_{sw} L_f} = \frac{E}{2\sqrt{6} f_{sw} L_f} \tag{4.28}$$

Through simulation (load: 8 kV x 45 kA) is measured a transformer secondary current fundamental of 77.08 kA (peak value), this value doesn't change varying L-filter. Considering a reasonable peak to peak value of the current ripple equal to 15 kA (19.5% of the nominal current), given the dc-link voltage and the selected switching frequency (450 Hz), the resulting filter inductance is [30]:

$$L_f = \frac{E}{2\sqrt{6} f_{sw} I_{ripple_{pk-pk}}} = \frac{1157.08}{2\sqrt{6} \cdot 450 \cdot 15000} = 34.99\ \mu H \tag{4.29}$$

Figure 62 shows transformer secondary current with the previously computed values of L_f and C.

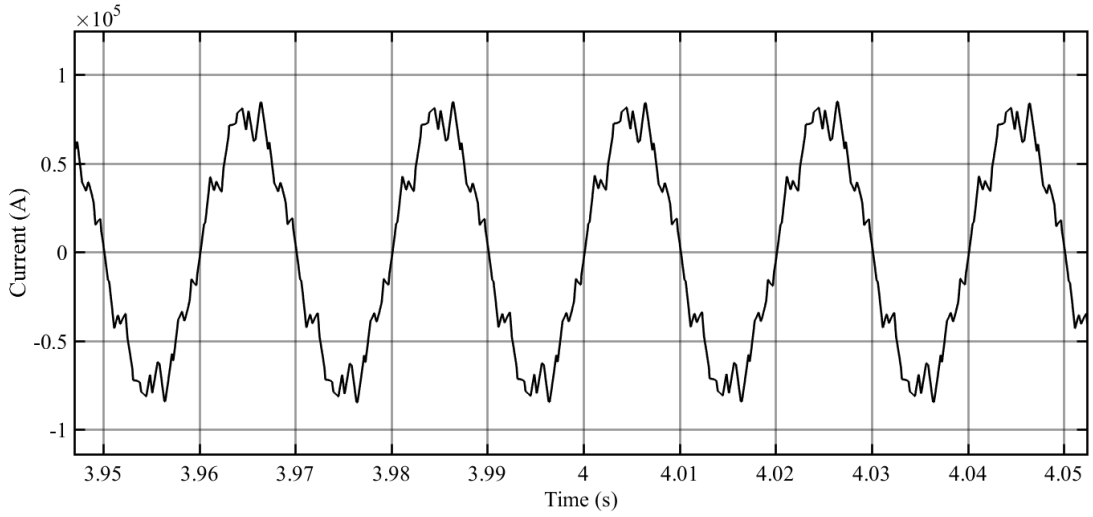

Figure 62 – Transformer secondary current with f_{sw}=450 Hz, L_f=34.99 µH and C=262.5 mF

4.3.3 Thermal Analysis

4.3.3.1 General Formulae

In the thermal analysis, the diodes and IGCTs cooling water temperature is supposed equal to 35°C and a margin of 15°C is taken with respect to the maximum junction temperature. With these assumptions, the maximum over temperatures on the junction of the two components are:

- IGCT: $\Delta T_{MAX}=T_{vj}$-15-35=125-50=75 K;
- diode: $\Delta T_{MAX}=T_{vj}$-15-35=140-50=90 K.

To calculate the over temperature in relation with the number of parallel components (N_c), the following equations are used, as described in [31].

The conducting losses can be calculated as follows, where I_{AV} and I_{RMS} are the average current and the RMS current of the switch, respectively:

$$P_{CON} = V_{TO}\left(\frac{I_{AV}}{N_C}\right) + r_T\left(\frac{I_{RMS}}{N_C}\right)^2 \tag{4.30}$$

The switch-on losses can be calculated as follows:

$$P_{SW_{ON}} = E_{ON} f \frac{V_{dc}}{V_D} \frac{\sum I_{COMM_{ON}}}{I_{TGQM}} \frac{1}{N_C} \tag{4.31}$$

while this formula is valid for the switch-off losses:

$$P_{SW_{OFF}} = E_{OFF} f \frac{V_{dc}}{V_D} \frac{\sum I_{COMM_{OFF}}}{I_{TGQM}} \frac{1}{N_C} \tag{4.32}$$

where E_{ON} and E_{OFF} are the energy dissipated during switch-on and switch-off respectively, with the dc-link voltage V_{dc} and commutation current I_{TGQ} specified in the data-sheet. f is the fundamental frequency (50 Hz) and I_{COMMON} and $I_{COMMOFF}$ are the current commutated at each switch-on or switch-off respectively. The switching losses have been calculated in a cycle of the fundamental frequency (50 Hz). The total losses are calculated as follows:

$$P_{TOT} = P_{CON} + P_{SW_{ON}} + P_{SW_{OFF}} \ [W] \tag{4.33}$$

The over-temperature can be calculated considering the thermal resistances of the component and of the heat-sink:

$$\Delta T = \left(R_{th(j-c)} + R_{th(c-h)} + R_{th(h-s)}\right) P_{TOT} \ [K] \tag{4.34}$$

where the heat sink thermal resistance $R_{th(h-s)}$ is supposed equal to 5 K/kW, which is a reasonable number for a water-cooled device.

4.3.3.2 AC/DC Converter Thermal Analysis

In sections 4.3.3.2.1 and 4.3.3.2.2, the over-temperatures of the diodes and IGCTs of the ac/dc converter are calculated on the basis of the current waveforms resulting from the model, assuming a switching frequency of 450 Hz. Different switching frequencies will be considered in Sections 4.3.3.2.3.

4.3.3.2.1 Diode Over-Temperature

The thermal analysis of the ac/dc converter diodes has been done with a load of 8 kV and 45 kA. This represents the worst case for the diodes because almost all the current flows thought them, leading to the higher over-temperature. Figure 63 shows the current of the upper diode of the phase "a" arm in this operating condition. The average current is I_{AV}=19860 A and the RMS current is I_{RMS}=35550 A.

Using equations (4.30), (4.32) and (4.34) (the switch-on losses are negligible), it is:

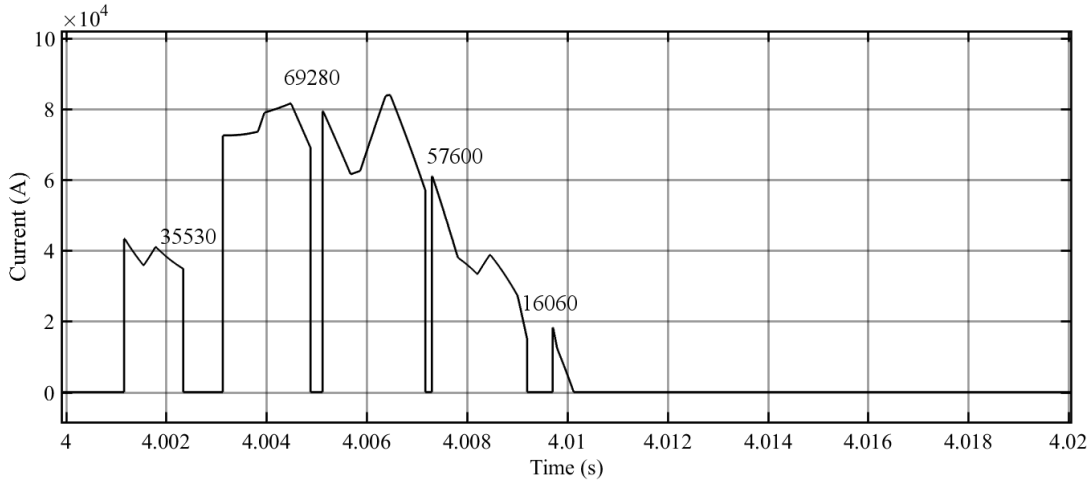

Figure 63 - Ac/dc converter diode current, switch-off commutation currents are indicated.

$$P_{CON} = V_{TO}\left(\frac{I_{AV}}{N_C}\right) + r_T\left(\frac{I_{RMS}}{N_C}\right)^2 = 1.25\left(\frac{19860 \cdot 1.2}{N_C}\right) + 0.3 \cdot 10^{-3}\left(\frac{35550 \cdot 1.2}{N_C}\right)^2 \quad (4.35)$$

$$P_{SW_{OFF}} = E_{OFF} \cdot f \cdot \frac{V_{dc}}{V_D} \cdot \frac{\sum I_{COMM_{OFF}}}{I_{FM}} \cdot \frac{1}{N_C} = 6.5 \cdot 50 \cdot \frac{2000}{2800} \cdot \frac{178470 \cdot 1.2}{4500} \cdot \frac{1}{N_C} \quad (4.36)$$

$$\Delta T = \left(R_{th(j-c)} + R_{th(c-h)} + R_{th(h-s)}\right)P_{TOT} = (0.00317 + 0.001 + 0.005) \cdot P_{TOT} \quad (4.37)$$

The factor 1.2 in the equations (4.35) and (4.36) takes into account the maximum current unbalance between parallel components. The same unbalance factor considered in the ITER base converters design has been assumed [32].

Table 19 shows the results of the thermal analysis for the diodes. 13+13 diodes in parallel per valve are needed to achieve an over temperature under 90 K.

Table 19 – Conducting and switching losses and junction over-temperature of the ac/dc converter diodes

N_c	P_{CON} [W]	$P_{SW\ ON}$ [W]	$P_{SW\ OFF}$ [W]	P_{TOT} [W]	ΔT [K]
10	8439	0	4079	12518	122
11	7220	0	3708	10929	106
12	6274	0	3399	9673	94
13	5522	0	3138	8660	84
14	4913	0	2914	7827	76
15	4412	0	2719	7132	69

4.3.3.2.2 IGCT Over-Temperature

The thermal analysis of the ac/dc converter IGCTs has been done with a load of 8 kV and -45 kA. This represents the worst case for the IGCTs because almost all the current flows thought them, leading to the higher over temperature. Figure 64 shows the current of the upper IGCT of the phase

"a" arm in this operating condition. The average current is I_{AV}=18070 A and the RMS current is I_{RMS}=31750 A.

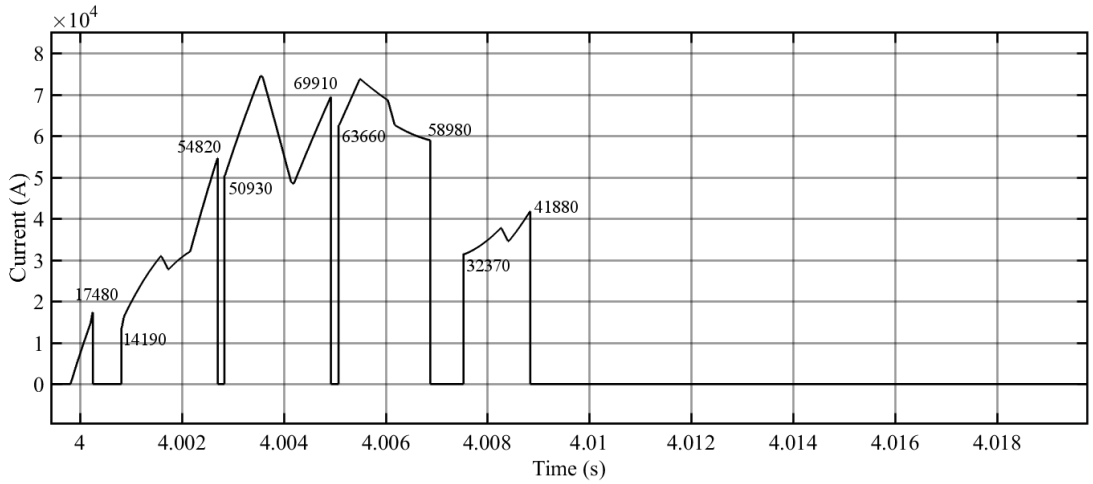

Figure 64 – Ac/dc converter IGCT current. Switch-on and switch-off commutation currents are indicated.

Using equations (4.30), (4.31), (4.32) and (4.32), it is:

$$P_{SW_{ON}} = E_{ON} \cdot f \cdot \frac{V_{dc}}{V_D} \cdot \frac{\sum I_{COMM_{ON}}}{I_{TGQM}} \cdot \frac{1}{N_C} = 3.1 \cdot 50 \cdot \frac{4000}{4000} \cdot \frac{161150 \cdot 1.2}{3800} \cdot \frac{1}{N_C} \tag{4.38}$$

$$P_{SW_{OFF}} = E_{OFF} \cdot f \cdot \frac{V_{dc}}{V_D} \cdot \frac{\sum I_{COMM_{OFF}}}{I_{TGQM}} \cdot \frac{1}{N_C} = 44 \cdot 50 \cdot \frac{4000}{4000} \cdot \frac{243070 \cdot 1.2}{3800} \cdot \frac{1}{N_C} \tag{4.39}$$

$$\Delta T = \left(R_{th(j-c)} + R_{th(c-h)} + R_{th(h-s)}\right) P_{TOT} = (0.0085 + 0.003 + 0.005) \cdot P_{TOT} \tag{4.40}$$

Table 19 shows the results of the thermal analysis for the IGCTs. 51 IGCTs in parallel per valve are needed to achieve an over temperature under 75 K.

Table 20 – Conducting and switching losses and junction over-temperature of the ac/dc converter IGCTs

N_c	P_{CON} [W]	$P_{SW\ ON}$ [W]	$P_{SW\ OFF}$ [W]	P_{TOT} [W]	ΔT [K]
50	1084	158	3377	4619	76
51	1057	155	3311	4522	75
52	1030	152	3247	4429	73
53	1005	149	3186	4340	72
54	981	146	3127	4255	70
55	959	143	3070	4172	69

4.3.3.2.3 Thermal Analysis with Higher Switching Frequencies

With the aim of reducing the line inductance of the L-filter and improving the dynamic performance such to reduce the dc-link capacitance, the thermal analysis has been repeated considering carrier frequencies equal to 750 Hz and 1050 Hz.

4.3.3.2.3.1 Thermal Analysis for f_{sw}=750 Hz

By increasing the switching frequency to 750 Hz, the rise time t_r is reduced to 5 ms, as can be seen in Figure 65. Using equation (4.26), the minimum capacitance of the dc-link capacitor bank in each cell results:

$$C \geq \frac{T_r \Delta P_{max}}{2 V_{dc} \Delta U_{max}} = \frac{0.005 * 180000000}{2 * 4000 * 600} = 187.5\ mF \tag{4.41}$$

The filter inductance is computed with equation (4.29) as follows:

$$L_f = \frac{E}{2\sqrt{6} f_{sw} I_{ripple_{peak}}} = \frac{1157.08}{2\sqrt{6} \cdot 750 \cdot 15000} = 20.99\ \mu H \tag{4.42}$$

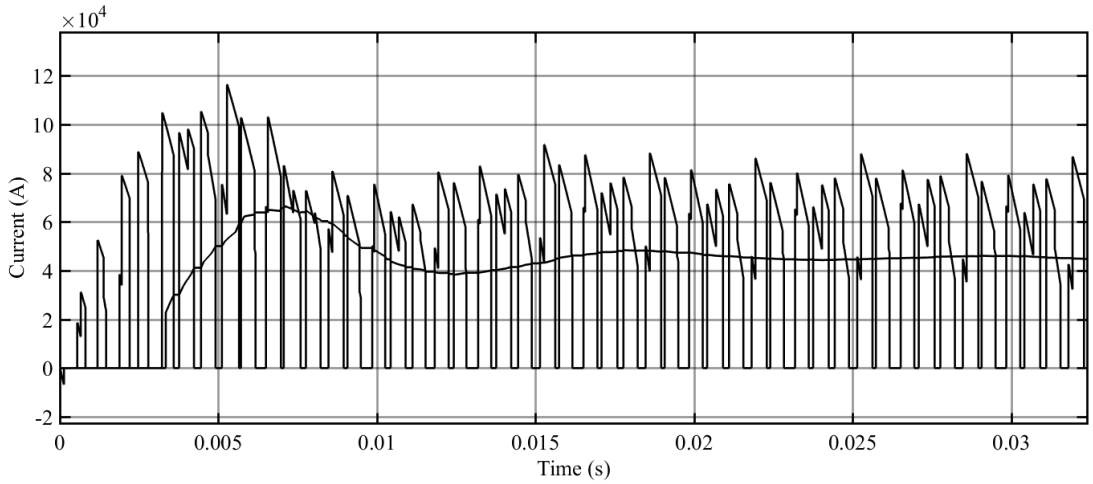

Figure 65 - Instantaneous upper cell dc-link current (orange line) and its mean value (blue line) with f_{SW}=750 Hz and full load step (8 kV, 45 kA) applied at t = 0 s

Figure 65 and Figure 66 show respectively the phase a upper diode and the phase a upper IGCT currents, calculated in the same operating conditions described in Section 4.3.3.2.1 and 4.3.3.2.2. For the diode, the average current is I_{AV}=19890 A and the RMS current is I_{RMS}=35570 A. For the IGCT, the average current is I_{AV}=17960 A and the RMS current is I_{RMS}=31510 A.

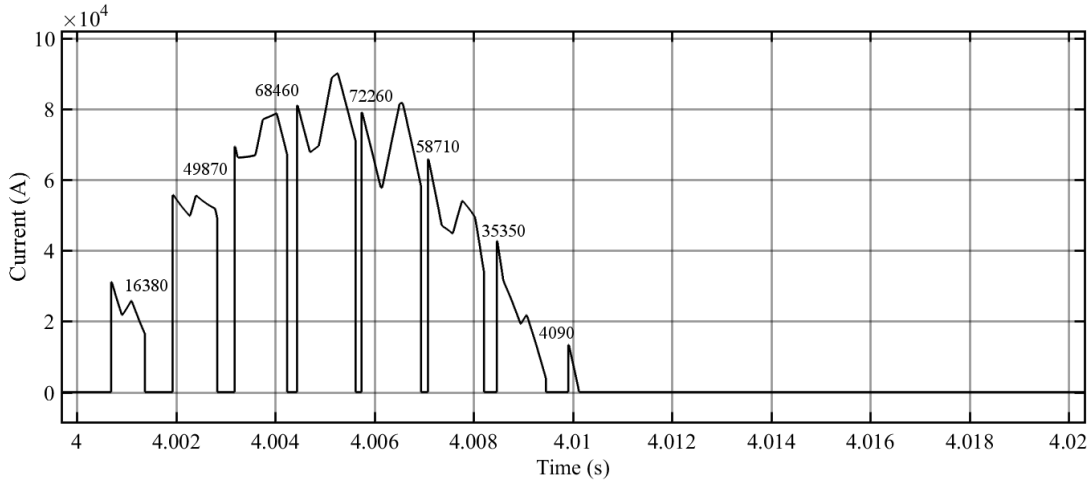

Figure 66 – Ac/dc converter diode current, for f_{SW}=750 Hz. Switch-off commutation currents are indicated

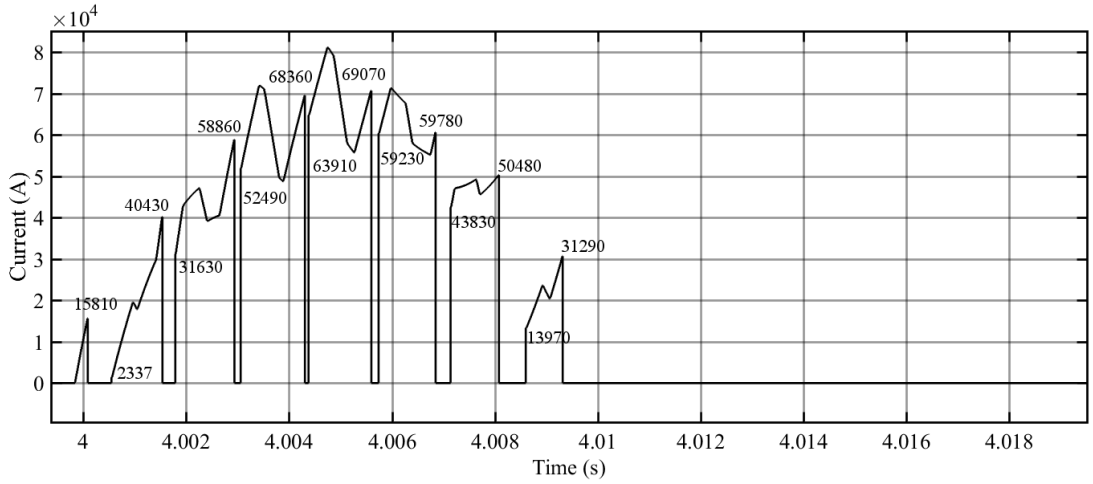

Figure 67 – Ac/dc converter IGCT current, for f_{SW}=750 Hz. Switch-off and switch-on commutation currents are indicated

The analysis results with a switching frequency equal to 750 Hz are shown in Table 21 and Table 22.

Table 21 – Conducting and switching losses and junction over-temperature of the ac/dc converter diodes, for f_{SW}=750 Hz

N_c	P_{CON} [W]	$P_{SW\ ON}$ [W]	$P_{SW\ OFF}$ [W]	P_{TOT} [W]	ΔT [K]
13	5529	0	5365	10894	106
14	4920	0	4982	9901	96
15	4418	0	4649	9068	88
16	4000	0	4359	8359	81
17	3646	0	4102	7749	75
18	3344	0	3875	7219	70

Table 22 – Conducting and switching losses and junction over-temperature of the ac/dc converter IGCTs, for f_{SW}=750 Hz

N_c	P_{CON} [W]	$P_{SW\ ON}$ [W]	$P_{SW\ OFF}$ [W]	P_{TOT} [W]	ΔT [K]
72	678	182	3803	4663	77
73	667	179	3750	4597	76
74	656	177	3700	4533	75
75	645	175	3650	4470	74
76	635	172	3602	4409	73
77	625	170	3556	4350	72

4.3.3.2.3.2 Thermal Analysis for f_{sw}=1050 Hz

By increasing the switching frequency to 1050 Hz, the rise time t_r is reduced to 4.25 ms, as can be seen in Figure 68. Using equation (4.26), the minimum capacitance of the dc-link capacitor bank in each cell results:

$$C \geq \frac{T_r \Delta P_{max}}{2 V_{dc} \Delta U_{max}} = \frac{0.00425 * 180000000}{2 * 4000 * 600} = 159.38\ mF \tag{4.43}$$

The filter inductance is computed with equation (4.29) as follows:

$$L_f = \frac{E}{2\sqrt{6} f_{sw} I_{ripple_{peak}}} = \frac{1157.08}{2\sqrt{6} \cdot 1050 \cdot 15000} = 14.99\ \mu H \tag{4.44}$$

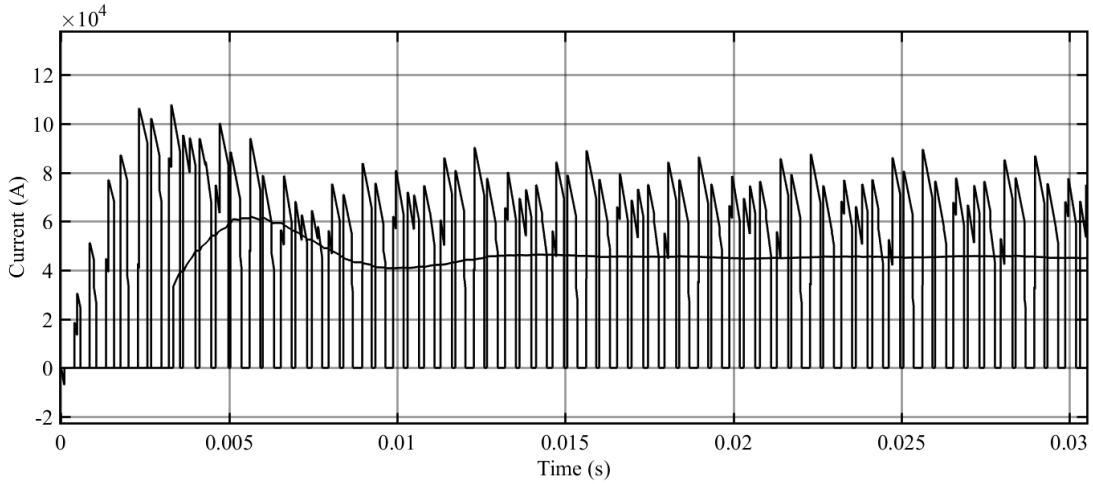

Figure 68 – Instantaneous upper cell dc-link current (orange line) and its mean value (blue line), with f_{SW}=1050 Hz and full load step (8 kV, 45 kA) applied at t = 0 s

Figure 69 and Figure 70 show respectively the S1 diode current and the S1 IGCT current, calculated in the same operating conditions described in Section 4.3.3.2.1 and 4.3.3.2.2. For the diode, the average current is I_{AV}=19790 A and the RMS current is I_{RMS}=35180 A. For the IGCT, the average current is I_{AV}=18230 A and the RMS current is I_{RMS}=32030 A.

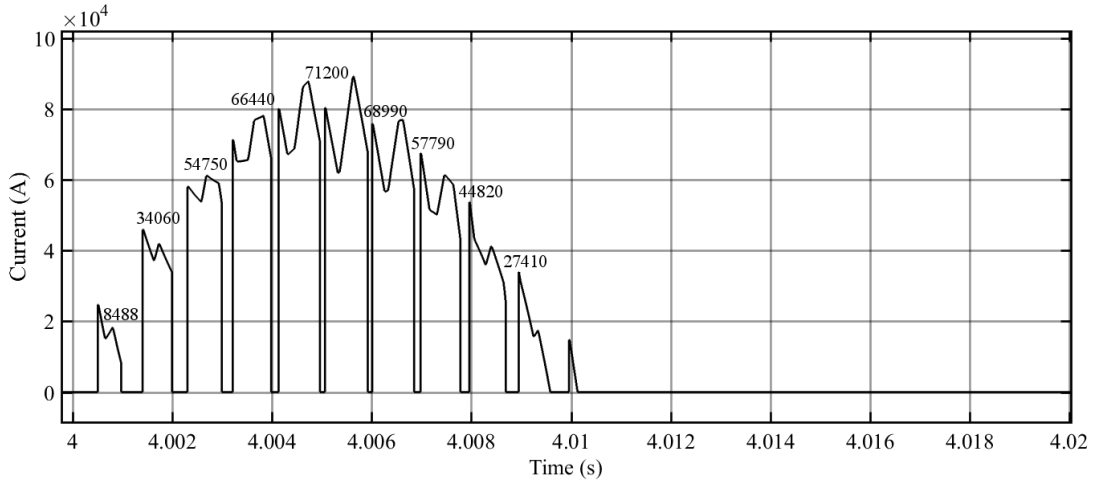

Figure 69 – Diode current for f_{SW}=1050 Hz. Switch-off commutation currents are indicated

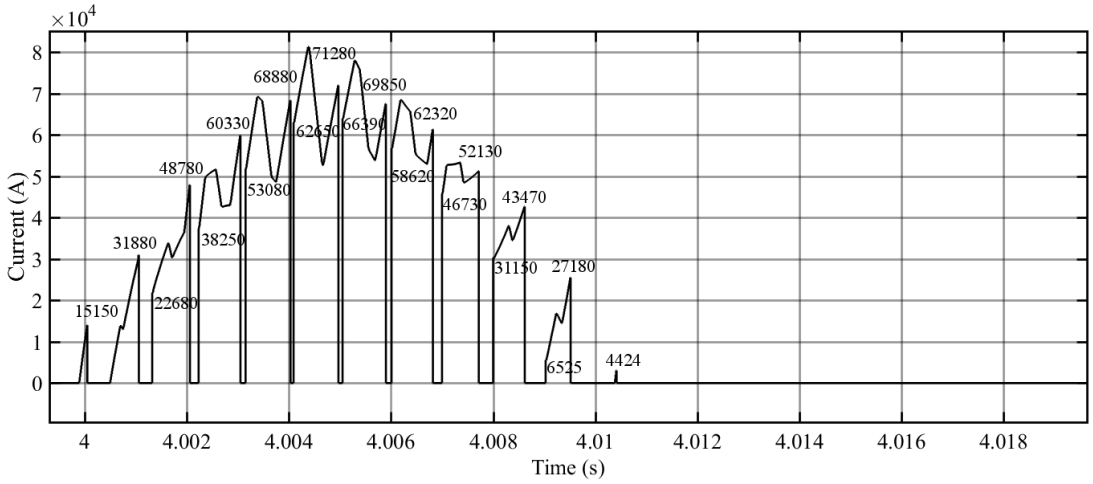

Figure 70 – IGCT current for f_{SW}=1050 Hz. Switch-off and switch-on commutation currents are indicated

The analysis results with a switching frequency equal to 1050 Hz are shown in Table 21 and Table 22.

Table 23 – Conducting and switching losses and junction over temperature of the ac/dc converter diodes, for f_{SW}=1050 Hz

N_c	P_{CON} [W]	$P_{SW\ ON}$ [W]	$P_{SW\ OFF}$ [W]	P_{TOT} [W]	ΔT [K]
15	4355	0	6613	10968	106
16	3944	0	6199	10143	98
17	3596	0	5835	9431	92
18	3299	0	5510	8810	86
19	3043	0	5220	8264	80
20	2821	0	4959	7780	76

Table 24 – Conducting and switching losses and junction over temperature of the ac/dc converter IGCTs, for f_{SW}=1050 Hz

N_c	P_{CON} [W]	$P_{SW\ ON}$ [W]	$P_{SW\ OFF}$ [W]	P_{TOT} [W]	ΔT [K]
97	483	195	3980	4657	77
98	477	193	3939	4609	76
99	471	191	3899	4561	75
100	466	189	3860	4515	74
101	460	187	3822	4469	73
102	455	185	3785	4425	73

4.3.3.3 Load-Side Converter Thermal Analysis

For the thermal analyses of the load-side converter, a tentative switching frequency of 300 Hz has been assumed, as a trade-off between the dynamic performance (which is not critical) and the commutation losses in the power switches.

To achieve more confidence that the selected switching frequency leads to an appropriate dynamic performance of the system, a simulation with CS3U plasma breakdown phase current as current reference is shown in Figure 71. It can be noted that the coil current follows the reference with good accuracy. This current scenario is not necessarily the worst case, but could represent a typical operative situation. Further simulations have been performed with more fast references, and the dynamic performance was still satisfactory.

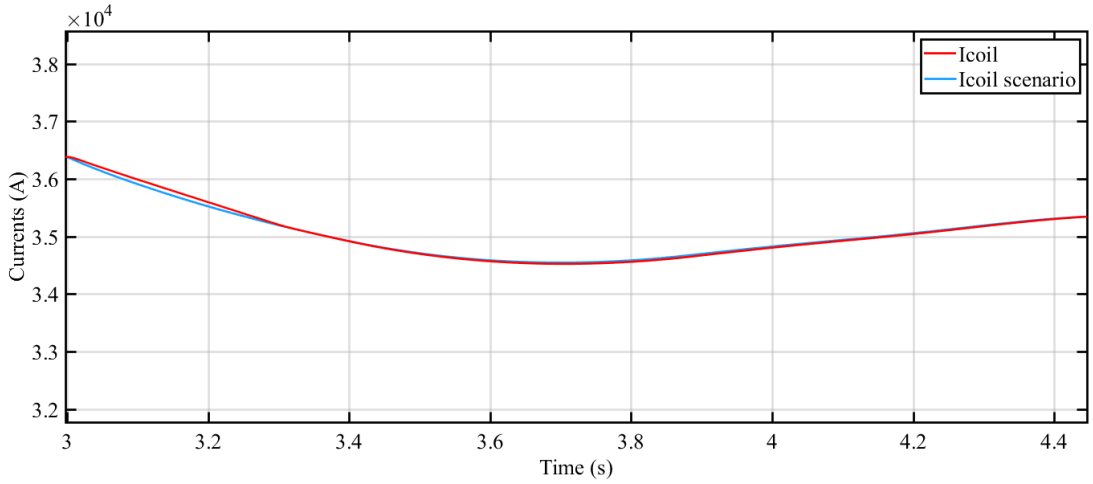

Figure 71 – Simulated CS3U plasma breakdown phase current.

4.3.3.3.1 Diode Over-Temperature

For the thermal analysis of the diodes of the load-side converter, an amplitude of the modulation index close to zero and a coil current equal to 45 kA have been selected, representing the worst case for the diodes. In this operating condition, in fact, almost all the load current flows through the freewheeling diodes, resulting in the maximum over-temperature. Figure 72 shows the diode current waveform; its average value is I_{AV}=42700 A, while the RMS value is I_{RMS}=43840 A.

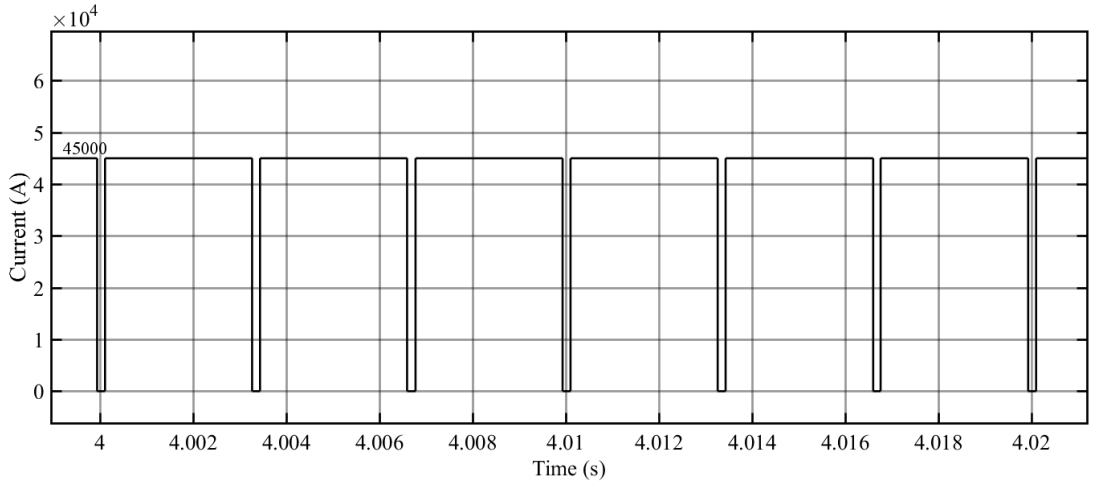

Figure 72 – Inverter diode current.

Table 25 shows that 19+19 diodes in parallel per valve are needed to satisfy the over-temperature limit. To compute the diode losses, the equations (4.35), (4.36) and (4.37) have been used.

Table 25 – Conducting and switching losses and junction over-temperature of the load-side converter diodes

N_c	P_{CON} [W]	$P_{SW\ ON}$ [W]	$P_{SW\ OFF}$ [W]	P_{TOT} [W]	ΔT [K]
17	6641	0	3630	10271	100
18	6121	0	3429	9549	93
19	5671	0	3248	8919	87
20	5278	0	3086	8364	81
21	4933	0	2939	7871	76

4.3.3.3.2 IGCT Over-Temperature

The IGCT maximum over-temperature occurs with an amplitude of the modulation index close to one and a load current equal to 45 kA. Figure 73 shows the IGCT current waveform; its average value is I_{AV}=41040 A, while the RMS value is I_{RMS}=42980 A.

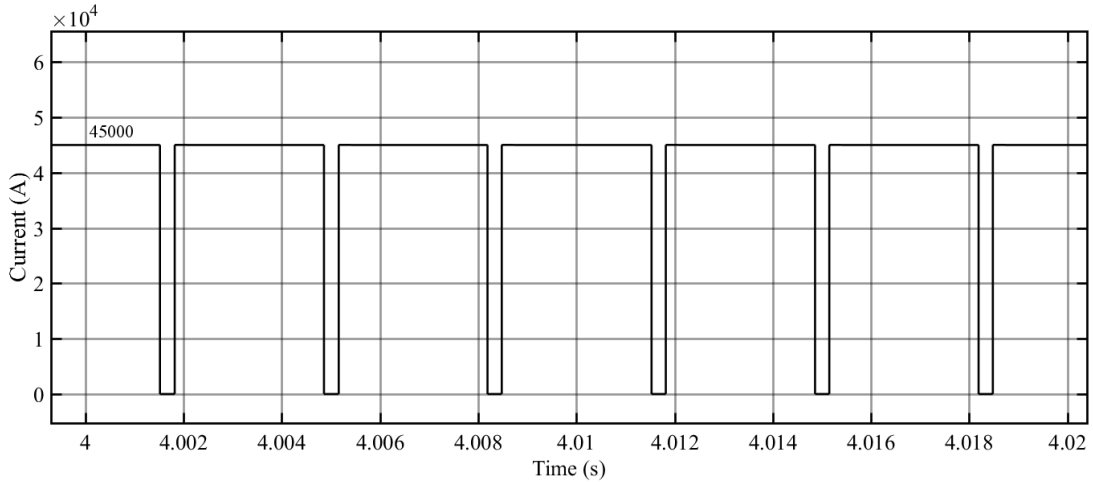

Figure 73 – Inverter IGCT current.

Table 26 shows that 68 IGCTs in parallel per valve are needed to satisfy the over-temperature limit. To compute the IGCT losses, the equations (4.38), (4.39), (4.40) and (4.41) have been used.

Table 26 – Conducting and switching losses and junction over-temperature of the load-side converter IGCTs

N_c	P_{CON} [W]	$P_{SW\ ON}$ [W]	$P_{SW\ OFF}$ [W]	P_{TOT} [W]	ΔT [K]
66	1648	200	2842	4690	77
67	1618	197	2800	4615	76
68	1590	194	2759	4542	74
69	1562	192	2719	4472	73
70	1535	189	2680	4404	72
71	1509	186	2642	4337	71

4.4 AFE Converter Model Simulations

As a trade-off between IGCTs and diodes losses and L-filter and capacitor bank sizes, a switching frequency of the ac/dc converter of 750 Hz seems reasonable. Table 27 and Table 28 show the number of static switches of a DEMO base converter rated for 8 kV and 45 kA.

Table 27 – Number of static switches of a DEMO ac/dc converter rated for 8 kV and 45 kA

IGCTs in parallel per valve	Diode in parallel per valve	Total IGCTs	Total diodes
74	15+15	888	360

Table 28 – Number of static switches of a DEMO load-side converter rated for 8 kV and 45 kA

IGCTs in parallel per valve	Diode in parallel per valve	Total IGCTs	Total diodes
68	19+19	544	304

In order to compare the reactive power requested by the CS3U thyristor-based converter and the reactive power requested by the CS3U AFE converter a simulation with CS3U plasma breakdown phase current and voltage has been performed (Figure 74).

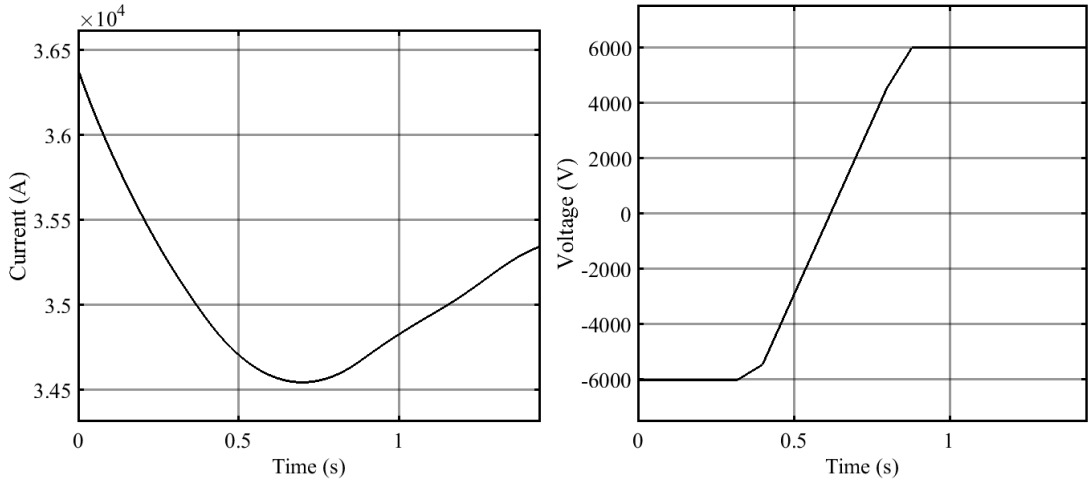

Figure 74 – CS3U plasma breakdown phase current and voltage.

As can be noted in Figure 75 the reactive power of the CS3U AFE converter remains close to zero (within +1.39 MVAR and -0.74 MVAR) while the reactive power of the CS3U thyristor-based converter is between +244.7 MVAR and +187.3 MVAR with sequential control and between +187.8 MVAR and +19.4 MVAR considering active bypass switches at the output of the converter units.

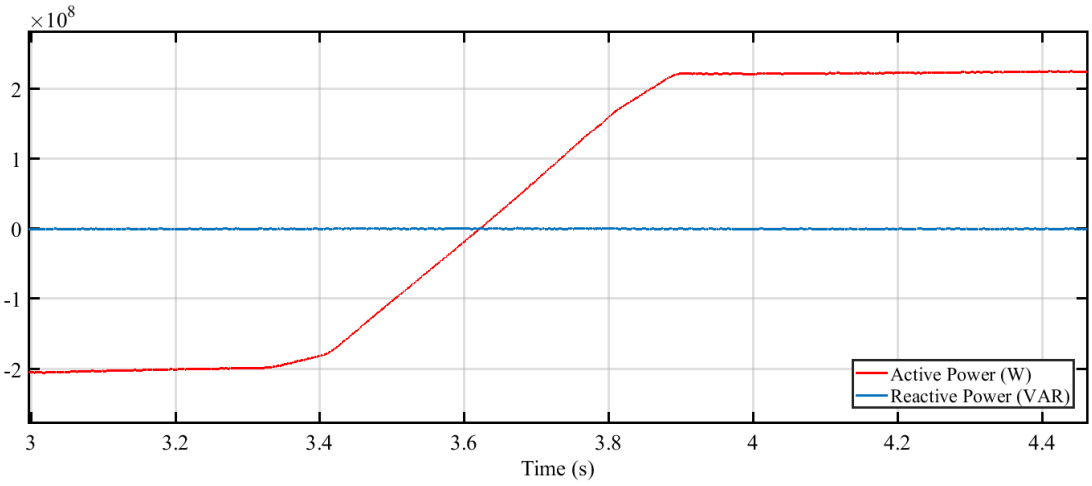

Figure 75 – Grid-side active and reactive power in CS3U plasma breakdown phase of AFE converter.

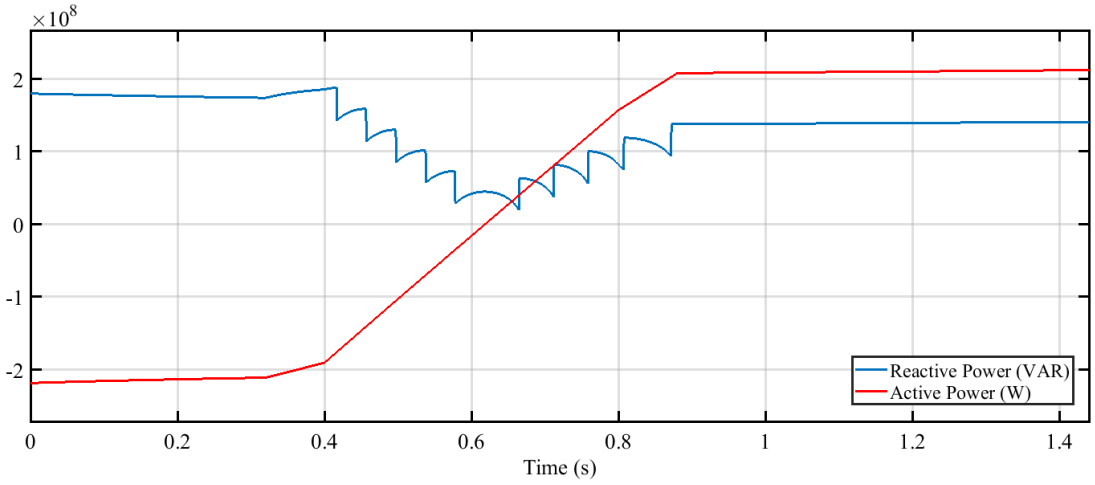

Figure 76 – Grid-side active and reactive power in CS3U plasma breakdown phase of thyristor-based converter with bypass control.

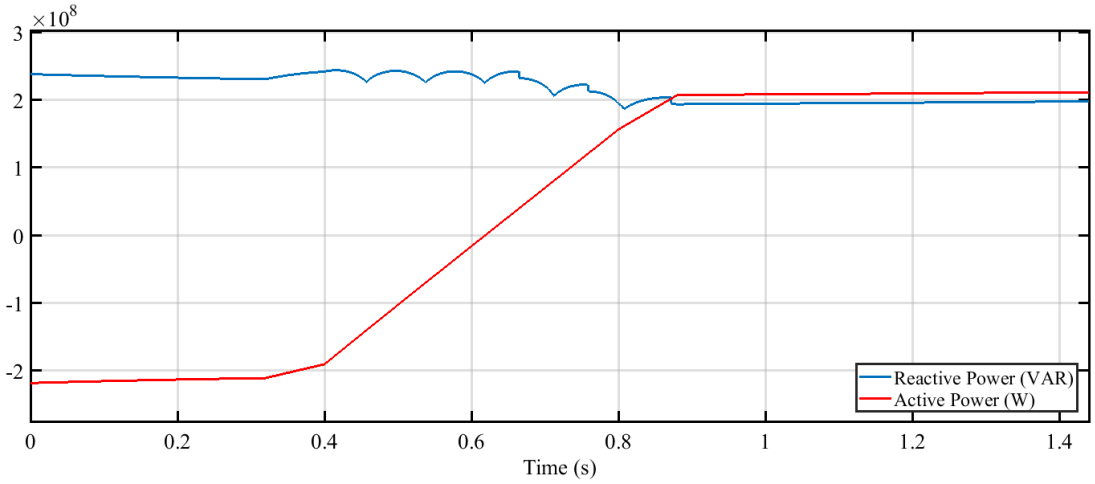

Figure 77 – Grid-side active and reactive power in CS3U plasma breakdown phase of thyristor-based converter with sequential control.

5 Base Converter Size Estimation and Comparison

5.1 AFE Converter

In this section an estimation of the AFE base converter size is attempted. As a starting point, the layout of Acceleration Grid Power Supply Conversion System (AGPS-CS) of ITER Neutral Beam Injectors (NBI) has been considered [33]. The AGPS-CS is made by thyristor bridges in 12-pulse configuration connected to the ITER grid, which supply five Neutral Point Clamped (NPC) IGCT-based inverters connected in parallel at the input side.

Each cubicle of AGPS-CS is 1 m × 1.4 m × 2.5 m [width × depth × height]. Half of it (footprint A_{AGPS} = 0.7 m^2) contains 3 modules, each module being an arm of the NPC inverter, made by 4 IGCTs, 4 freewheeling diodes and 2 clamp diodes. Therefore, each half-cubicle contains 30 components (N_{AGPS}) in total, with a rated power of 6 MVA and a switching frequency equal to 150 Hz.

The second half of the cubicle (footprint A_{AGPS} = 0.7 m^2) contains the capacitor banks, composed by 3 capacitive modules, each made by a pair of capacitor banks of 3 × 800 µF (oil-immersed film capacitors,

nominal dc-link voltage equal to 3250 V). Therefore, each half-cubicle has 76.05 kJ of stored energy ($E_{c\ AGPS}$).

Scaling the AGPS-CS size proportionally with the number of components of a DEMO AFE base converter rated for 8 kV and 45 kA (Table 27 and Table 28) we could tentatively estimate the area occupancy of its ac/dc converters, dc-link capacitor banks and load-side converters (assuming a switching frequency of the ac/dc converter of 750 Hz):

- Ac/dc converters. Its number of components ($N_{ac/dc}$) and area occupancy ($A_{ac/dc}$) can be estimated as:

$$N_{ac/dc} = 2 \times [74 \times 6 + 15 \times 2 \times 6] = 1248 \tag{5.1}$$

$$A_{ac/dc} = \frac{N_{ac/dc}}{N_{AGPS}} \times A_{AGPS} = \frac{1248}{30} \times 0.7 = 29.1\ m^2 \tag{5.2}$$

- Load-side converters. Its number of components (N_{ls}) and area occupancy (A_{ls}) can be estimated as:

$$N_{ls} = 2 \times [68 \times 4 + 19 \times 2 \times 4] = 848 \tag{5.3}$$

$$A_{ls} = \frac{N_{ls}}{N_{AGPS}} \times A_{AGPS} = \frac{848}{30} \times 0.7 = 19.8\ m^2 \tag{5.4}$$

- Dc-link capacitor bank. Its energy (E_c) and area occupancy (A_c) can be estimated as:

$$E_c = 2 \times 0.5 \times 0.1875 \times 4000^2 = 3\ MJ \tag{5.5}$$

$$A_c = \frac{E_c}{E_{c_{AGPS}}} \times A_{AGPS} = \frac{3000000}{76050} \times 0.7 = 27.6\ m^2 \tag{5.6}$$

- For the estimation of the footprint of the L-filter at the ac side of the ac/dc converter, the size of a three-phase output inductor of a 6 MVA inverter of the AGPS-CS of ITER NBI is taken as a reference. Each of these inductors has an inductance nominal value of 180 µH and it is rated for 850 Arms continuous duty (iron water-cooled reactor). When installed in its cubicle, it occupies a volume (including the free space in the cubicle of: 0.8 × 1.4 × 1 m [width × depth × height], therefore its footprint is 1.12 m^2. With some space optimisation, its footprint could be reduced maybe to 1 m^2, including all necessary auxiliaries.
  Considering each converter connected to a transformer with a percentage short-circuit impedance of 17% (same as ITER converter transformers short-circuit impedance [34]), short-circuit inductance (L_{sc}) and L-filter inductance (L) result:

$$L_{sc} = 0.17 \times \frac{V_2}{\sqrt{3} \times \mathrm{I}_2} \times \frac{1}{2\pi \times \mathrm{f}} = 0.17 \times \frac{2004}{\sqrt{3} \times 54500} \times \frac{1}{2\pi \times \mathrm{f}} = 11.5\ \mu H \tag{5.7}$$

$$L = L_f - L_{sc} = 21 - 11.5 = 9.5\ \mu H \tag{5.8}$$

  The rated current of a 9.5 µH L-filter of one cell of a DEMO base converter is 54.5 kA (measured through a simulation with a load equal to 8 kV x 45 kA). We could tentatively consider 64 reactor sets put in parallel to satisfy the rated current, each reactor having a reactance of 608 µH (made by 3 reactors in series rated 203 µH, similar to those of the AGPS-CS). Considering to stack these inductors in columns made by 3 elements, the total height of

each cubicle would be 3 m and the total footprint of the L-filters of the base converter would be:

$$A_L = 2 \times \frac{64 \times 3}{3} \times 1m^2 = 128\, m^2 \tag{5.9}$$

The total base converter area, including a margin of 20% to include auxiliaries, cooling systems and possible output decoupling inductors of the load-side converters, can be estimated as:

$$A_{AFE} = (A_{ac/dc} + A_{ls} + A_c + A_L) * 1.2 = (29.1 + 19.8 + 27.6 + 128) * 1.2 = 245\, m^2 \tag{5.10}$$

keeping a maximum height of 3 m. As it can be noted, most of the space occupancy is determined by the input L-filter inductors. Their dimensions could be overestimated, considering that bigger reactors rated for higher current with a better energy/volume ratio could adopted. A further reduction could be achieved by selecting a higher switching frequency or a different filter topology.

5.2 Thyristor-based Converter and RPC&HF System

In this chapter, the area occupancy of the DEMO base converters is tentatively estimated from that of the ITER base converters by scaling proportionally with the number of thyristors and assuming the same voltage margin. The sequential control of series-connected thyristor bridges is considered, thus the function of the external bypass is limited to protection only. In Table 29 are shown ITER and DEMO base-converter dimensions; those of ITER have been derived from the available CAD drawings. Bypass dimensions for ITER and DEMO are assumed to be the same because of same converter rated current (see Table 10). The area reserved for the step-down transformers is not considered.

Table 29 – ITER and DEMO base converter dimensions, considering the traditional thyristor bridge technology.

Base Converter	Units in series	Number of thyristors in parallel for each arm	Total number of thyristors	Area occupancy of a rectifier unit [m^2]	Total area occupancy of the thyristor bridges of a base converter [m^2]	Area occupancy of dc reactors, disconnectors and bypasses of a unit [m^2]	Total area occupancy of dc reactors, disconnectors and bypasses of a base converter [m^2]
ITER (2.1 kV x 45 kA)	2	12	576	6.6 × 4.1 = 27.1	2 × 27.1 = 54.2	7.3 × 3 = 22.0	2 × 22.0 = 44.0
DEMO (8 kV x 45 kA)	8	12	2304	6.6 × 4.1 = 27.1	8 × 27.1 = 217	7.3 × 3 = 22.0	8 × 22.0 = 176

Thyristor-based converters needs a large RPC&HF system. From the available CAD drawings, it has been calculated that the ITER RPC&HF system occupies an external area of 8408 m^2 and a building with an area 819 m^2, for a total area of 9227. m^2. Considering that ITER CPSS has a total installed power of 2.4 GVA (1.35 kV×45 kA×12 + 1.35 kV×55 kA×16 = 1.92 GVA considering the base converters for CS and PF coil only) and DEMO CPSS has an installed power equal in the order of 5 GVA (8 kV×45 kA×8 + 10 kV×45 kA×4 = 4.68 GVA considering the base converters for CS and PF

coil only), the scaled area of DEMO RPC&HF system is around 20000m^2. In this estimation, the installed power for VS power supplies and other converters pertaining to the DEMO PPEN are not included.

5.3 Size Comparison

A DEMO base converter rated for 8 kV and 45 kA has a rated power of 360 MVA, which is 7.2% of the total CPSS installed power. This percentage is used to account the respective area of the RPC&HF System in the thyristor-based solution (the converter area is multiplied by 1.2 to consider auxiliaries and cooling system).

Table 30 – Comparison between the area occupancy of a DEMO base converter (8 kV, 45 kA) based on the AFE solution and the traditional thyristor-based solution with RPC&HF system

Solution	Area occupancy [m^2]
AFE converters	245
Thyristor-based converters with sequential control + RPC&HF system	(217 + 176) × 1.2 + (20000 × 0.072) = 428 + 1868

In Table 30, for the converters, the area indicated is only that occupied by the cubicles/racks; the transformers and the space necessary around the cubicles/racks for installation and maintenance are not considered. However, the area occupied by the transformers should be similar for the two solutions and, from ITER experience, could be of the same order of the area necessary for the cubicles/racks. From Table 30, it can be noted that the area occupancy of AFE converters is lower to that necessary for thyristor-based converters and, for the latter, a significant area for RPC&HF system shall be added. In addition, it should be highlighted that, for AFE converters, the maximum height has been limited to 3 m, while the height of the ITER thyristor-based converters considered for this estimation is about 4.2 m (the highest element being the rack with dc reactors, disconnectors and bypasses).

The number of series-connected thyristor-based ac/dc converters could be reduced if a lower (but still safe, according to industrial standards) voltage margin is considered, with respect to that adopted in ITER. For example, assuming a voltage margin of 2.4 between the peak of the nominal ac input voltage and the V_{RRM} of the thyristors (5.2 kV), each thyristor bridge could produce a dc output voltage of 1.6 kV at the nominal current, therefore 5 units in series instead of 8 would be sufficient for a 8 kV base converter, giving a significant saving on the area occupancy, which would become 268 + 1868 m^2.

6 Conclusions

In the first part of this thesis the reactive power produced by DEMO CPSS with thyristor-based converters has been estimated. Firstly, DEMO CS and PF base converters are designed and the number of DEMO units in series has been scaled up to account for the higher voltages required in respect to those required in ITER. The first analytical model based on sequential logic control, similar to ITER converters control, shows a maximum requested reactive power over 2 GVA in all the phases of the plasma scenario considered, with a peak of about 2.41 GVA in breakdown and ramp-down phases. The second analytical model based on bypass logic control for series connected units shows a great reduction of DEMO reactive power in ramp-up and ramp-down phases of the plasma scenario, when the voltages required by the coils are low. In these two plasma phases the peak value of the reactive power remains under 500 MVAR. In plasma breakdown phase the reactive power reduction is proportionally lower, and its maximum value is 1.92 GVAR. This first part of the thesis shows that the requested reactive power values, with thyristor-based converters, remains high even adopting strategies for reactive power reduction. Therefore, it is justified the research and development of new and alternative solutions to supply DEMO coils and the investigation on their feasibility.

In the second part of this thesis, an Active-Front-End (AFE) topology for DEMO base converter is proposed, focusing on a tentative converter design and analysis. Possible issues in its integration in the circuit of DEMO CPSS and the protection strategies against faults are not considered in this thesis and can be the subject of future studies. Different switching frequencies have been considered in ac/dc converter design and thermal analysis, performed to compute the number of parallel static switches per valve. As a trade-off between IGCTs and diodes losses and L-filter and capacitor bank sizes, a switching frequency of 750 Hz has been selected to perform the final simulations. For the load-side converter design a switching frequency of 300 Hz has been considered, since it seems adequate for the requested dynamic performance, giving at the same time reasonable switches losses. The plasma breakdown phase simulation shows that the CS3U base converter reactive power remains within +1.39 MVAR and -0.74 MVAR, thanks to the current controller of the ac/dc converters that maintains the power factor close to one. The reactive power of the respective thyristor-based converter in plasma breakdown phase, with sequential control, is between +244.7 MVAR and +187.3 MVAR.

In the last section an estimation of the size of the considered AFE base converter is attempted, scaling from the size of an existing installation with similar technology, proportionally with the number of components, energy stored in the capacitor banks and inductance of the L-filter. The AFE base converter area occupancy would be around 245 m^2 in total, while that required for a thyristor base converter would be around 428 m^2, plus 1868 m^2 (mostly outdoor) for the RPC&HF system required in this solution. Assuming a lower (but still safe, according to industrial standards) voltage margin of 2.4, the number of series connected thyristor could be reduced and the area occupancy would become 268+1868 m^2. The thyristor base converter area occupancy would be similar to that of AFE base converter, but a large area would be needed for the RPC&HF system, which instead is not required in the AFE solution. It is to be underlined that the calculations performed in this thesis are based on the components available today. It is to be underlined that the calculations performed in this thesis are based on the components available today, and the actual industrial feasibility of AFE power converters rated for currents in the order of 50 kA and voltages around 8-10 kV is still to be demonstrated, being far beyond the present industrial standard. In addition, considering that the construction of DEMO is foreseen in the middle of the century, further evolution of the technology, especially that of power semiconductors, could allow different design approaches and a reduction of the number of components.

References

[1] ITER website, www.iter.org.

[2] S. Ciattaglia, G. Federici, L. Barucca, A. Lampasi, S. Minucci and I. Moscato, "The European DEMO fusion reactor: Design status and challenges from balance of plant point of view," 2017 IEEE International Conference on Environment and Electrical Engineering and 2017 IEEE Industrial and Commercial Power Systems Europe (EEEIC / I&CPS Europe), Milan, 2017, pp. 1-6.

[3] N. Mitchell et al., "The ITER Magnet System," in IEEE Transactions on Applied Superconductivity, vol. 18, no. 2, pp. 435-440, June 2008.

[4] P. Libeyre et al., "Status of design and manufacturing of the ITER Central Solenoid and Correction Coils," 2015 IEEE 26th Symposium on Fusion Engineering (SOFE), Austin, TX, 2015, pp. 1-8.

[5] N. Mitchell, A. Devred, P. Libeyre, B. Lim and F. Savary, "The ITER Magnets: Design and Construction Status," in IEEE Transactions on Applied Superconductivity, vol. 22, no. 3, pp. 4200809-4200809, June 2012.

[6] J. Hourtoule et al., "ITER electrical distribution system," 2013 IEEE 25th Symposium on Fusion Engineering (SOFE), San Francisco, CA, 2013, pp. 1-5.

[7] C. Neumeyer et al., "ITER power supply innovations and advances," 2013 IEEE 25th Symposium on Fusion Engineering (SOFE), San Francisco, CA, 2013, pp. 1-8.

[8] J. Tao et al., "ITER Coil Power Supply and Distribution System," 2011 IEEE/NPSS 24th Symposium on Fusion Engineering, Chicago, IL, 2011, pp. 1-8.

[9] Jong-Seok Oh,Jungwan Choi,Jae-Hak Suh,Jihyun Choi,Lacksang Lee,Changwoo Kim,Hyungjin Park,Seongman Jo,Seungyun Lee,Kwangcheol Hwang,Hyoyol Liu,Ki-Don Hong,Dong-Joon Sim,Jang-Soo Lee,Eui-Jae Lee,Yang-Hae Kwon,Dae-Yeol Lee,Ki-Won Ko,Jong-Min Kim et al., “Final design of the Korean AC/DC converters for the ITER coil power supply system”.

[10] A. D. Mankani et al., "The ITER reactive power compensation and harmonic filtering (RPC & HF) system: Stability & performance," 2011 IEEE/NPSS 24th Symposium on Fusion Engineering, Chicago, IL, 2011, pp. 1-6.

[11] Alberto Ferro and Elena Gaio, “DEMO electrical system configuration and circuits”.

[12] “ABB Phase Control Thyristor 5STP 52U5200”, https://library.e.abb.com/public/75c39bdddc9c4ab58397bbc46d062bef/5STP%2052U5200_5SYA1042-06%20Mar%2014.pdf.

[13] Zhiquan Song, Xing Zhang, Peng FU, Lin Dong, Min Wang and Tongzhen Fang, “Thyristor Selection Analysis for ITER Poloidal Field Converter”.

[14] E. Gaio, R. Piovan, V. Toigo and I. Benfatto, “The control system of the ITER vertical stabilization converter”

[15] N. Mohan, *Power Electronics (Third Edition)*, Hoepli.

[16] H. W. Yuan, L. S. Huang, P. Fu, G. Gao and Z. Q. Song, "Study on the four quadrants operation of ITER poloidal field converter system," 2014 International Power Electronics and Application Conference and Exposition, Shanghai, 2014, pp. 853-857.

[17] H. S. Heo et al., "Sequence control of small-scaled ITER Power Supply for reactive power compensation," 2010 IEEE International Conference on Industrial Technology, Vi a del Mar, 2010, pp. 813-817.

[18] Yuan Hongwen, Fu Peng, Gao Ge, Huang Liansheng, Song Zhiquan, He Shiying, Wu Yanan, Dong Lin, Wang Min and Fang Tongzhen. «On the Sequential Control of ITER Poloidal Field Converters for Reactive Power Reduction».

[19] Hongwen Yuan, Zhiquan Song, Peng Fu, Peng Wang, Ge Gao, Liansheng Huang, Lin Dong, Min Wang, Tongzhen Fang, “Analysis of Internal and External Bypass Circuit Design for ITER Poloidal Field Converter System”.

[20] E. Gaio, R. Piovan, V. Toigo and L. Benfatto, "Bypass operation of the ITER AC/DC converters for reactive power reduction," 17th IEEE/NPSS Symposium Fusion Engineering (Cat. No.97CH36131), San Diego, CA, 1997, pp. 1141-1144 vol.2.

[21] Bimal K. Bose, *Modern Power Electronics and AC Drives*, Pearson Education.

[22] Y. Ye, M. Kazerani and V. H. Quintana, "A novel modeling and control method for three-phase PWM converters," 2001 IEEE 32nd Annual Power Electronics Specialists Conference (IEEE Cat. No.01CH37230), Vancouver, BC, 2001, pp. 102-107 vol. 1.

[23] K. Qian, G. Gao and Z. Sheng, "A Maximum Current Control Method for Three-Phase PWM Rectifier for the ITER In-Vessel Vertical Stability Coil Power Supply," in IEEE Transactions on Plasma Science, vol. PP, no. 99, pp. 1-5.

[24] Pandit, Pankaj Prabhakar, "Modeling and Analysis of Active Front-End Induction Motor Drive for Reactive Power Compensation. "Master's Tesis, University of Tennessee, 2005.

[25] J. Rodriguez, S. Bernet, B. Wu, J. O. Pontt and S. Kouro, "Multilevel Voltage-Source-Converter Topologies for Industrial Medium-Voltage Drives," in IEEE Transactions on Industrial Electronics, vol. 54, no. 6, pp. 2930-2945, Dec. 2007.

[26] B. P. McGrath and D. G. Holmes, "Multicarrier PWM strategies for multilevel inverters," in IEEE Transactions on Industrial Electronics, vol. 49, no. 4, pp. 858-867, Aug 2002.

[27] “ABB Asymettric IGCTS 5SHY 42L6500”, http://search.abb.com/library/Download.aspx?DocumentID=5SYA1245-03&LanguageCode=en&DocumentPartId=&Action=Launch.

[28] “Infineon Diode d4600u45x172”, https://www.infineon.com/dgdl/Infineon-D4600U45X172-DS-v01_02-EN.pdf?fileId=5546d4625f96303e015fa5e43ef4397a.

[29] L. Malesani, L. Rossetto, P. Tenti and P. Tomasin, "AC/DC/AC PWM converter with reduced energy storage in the DC link," in IEEE Transactions on Industry Applications, vol. 31, no. 2, pp. 287-292, Mar/Apr 1995.

[30] S. Ponnaluri, V. Krishnamurthy and V. Kanetkar, "Generalized system design and analysis of PWM based power electronic converters," Conference Record of the 2000 IEEE Industry Applications Conference. Thirty-Fifth IAS Annual Meeting and World Conference on Industrial Applications of Electrical Energy (Cat. No.00CH37129), Rome, 2000, pp. 1972-1979 vol.3.

[31] Claudio Finotti, “Studies on the impact of the ITER Pulsed Load Power Supply System on the Pulsed Power Electrical Network”.

[32] Z. Song et al., "Prototype Design and Test of ITER PF Converter Unit," in IEEE Transactions on Plasma Science, vol. 44, no. 9, pp. 1677-1683, Sept. 2016.

[33] Zanotto L. et al., "Final design of the acceleration grid power supply conversion system of the MITICA Neutral Beam Injector", Fusion Engineering and Design 123, April 2017.

[34] J.S. Oh,J. Choi,J.H. Suh,H. Liu,K. Hwang,I. Chung,S. Lee,J. Kang,H. Park,W. Jung,S. Jo,H. Gweon,Y. Lee,W. Lee,J.B. Kim,S.H. Han,G.D. Hong,J.S. Lee,B.W. Lee,C.H. Yeo,H.G. Kim,E. Seo,P. Reynaud,J. Goff,H. Tan,J. Tao, “Preliminary design of the ITER AC/DC converters supplied by the Korean Domestic Agency”.

[35] M. Matteri, R. Ambrosino and R. Albanese, “Annex C to PMI-5.2.1-T016-D001 Final Report "EM investigations of dynamic phases in DEMO"”.

Appendix A

Table 31 – Central Solenoid Coils Breakdown Voltages

Time [s]	CS3U [V]	CS2U [V]	CS1 [V]	CS2L [V]	CS3L [V]
0.00	6000.00	-6000.00	12000.00	-6000.00	6000.00
0.01	6000.00	-5539.22	12000.00	-5698.72	6000.00
0.02	6000.00	-5078.44	12000.00	-5397.44	6000.00
0.02	6000.00	-4617.66	12000.00	-5096.16	6000.00
0.03	6000.00	-4156.88	12000.00	-4794.88	6000.00
0.04	6000.00	-3696.10	12000.00	-4493.60	6000.00
0.05	6000.00	-3235.32	12000.00	-4192.32	6000.00
0.06	6000.00	-2774.55	12000.00	-3891.04	6000.00
0.06	6000.00	-2313.77	12000.00	-3589.76	6000.00
0.07	6000.00	-1852.99	12000.00	-3288.48	6000.00
0.08	6000.00	-1392.21	12000.00	-2987.20	6000.00
0.09	6000.00	-1192.21	12000.00	-2787.20	6000.00
0.10	6000.00	-992.21	12000.00	-2587.20	6000.00
0.10	6000.00	-792.21	12000.00	-2387.20	6000.00
0.11	6000.00	-592.21	12000.00	-2187.20	6000.00
0.12	6000.00	-392.21	12000.00	-1987.20	6000.00
0.13	6000.00	-192.21	12000.00	-1787.20	6000.00
0.14	6000.00	7.79	12000.00	-1587.20	6000.00
0.14	6000.00	207.79	12000.00	-1387.20	6000.00
0.15	6000.00	407.79	12000.00	-1187.20	6000.00
0.16	6000.00	607.79	12000.00	-987.20	6000.00
0.17	6000.00	807.79	12000.00	-787.20	6000.00
0.18	6000.00	1007.79	12000.00	-587.20	6000.00
0.18	6000.00	1207.79	12000.00	-387.20	6000.00
0.19	6000.00	1407.79	12000.00	-187.20	6000.00
0.20	6000.00	1607.79	12000.00	12.80	6000.00
0.21	6000.00	1807.79	12000.00	212.80	6000.00
0.22	6000.00	2007.79	12000.00	412.80	6000.00
0.22	6000.00	2207.79	12000.00	612.80	6000.00
0.23	6000.00	2407.79	12000.00	812.80	6000.00
0.24	6000.00	2607.79	12000.00	1012.80	6000.00
0.25	6000.00	2807.79	12000.00	1212.80	6000.00
0.26	6000.00	3007.79	12000.00	1412.80	6000.00
0.26	6000.00	3207.79	12000.00	1612.80	6000.00
0.27	6000.00	3407.79	12000.00	1812.80	6000.00
0.28	6000.00	3607.79	12000.00	2012.80	6000.00

0.29	6000.00	3807.79	12000.00	2212.80	6000.00
0.30	6000.00	4007.79	12000.00	2412.80	6000.00
0.30	6000.00	4207.79	12000.00	2612.80	6000.00
0.31	6000.00	4407.79	12000.00	2812.80	6000.00
0.32	6000.00	4607.79	12000.00	3012.80	6000.00
0.33	5945.34	4547.01	12000.00	3212.80	6000.00
0.34	5890.68	4486.23	12000.00	3412.80	6000.00
0.34	5836.02	4425.45	12000.00	3612.80	6000.00
0.35	5781.36	4364.68	12000.00	3812.80	6000.00
0.36	5726.70	4303.90	12000.00	4012.80	6000.00
0.37	5672.04	4243.12	12000.00	4212.80	6000.00
0.38	5617.38	4182.34	12000.00	4412.80	6000.00
0.38	5562.72	4121.56	12000.00	4612.80	6000.00
0.39	5508.06	4060.78	12000.00	4812.80	6000.00
0.40	5453.40	4000.00	12000.00	5012.80	6000.00
0.41	5253.40	3800.00	11764.92	5086.60	6000.00
0.42	5053.40	3600.00	11529.84	5160.39	6000.00
0.42	4853.40	3400.00	11294.76	5234.18	6000.00
0.43	4653.40	3200.00	11059.69	5307.98	6000.00
0.44	4453.40	3000.00	10824.61	5381.77	6000.00
0.45	4253.40	2800.00	10589.53	5455.57	6000.00
0.46	4053.40	2600.00	10354.45	5529.36	6000.00
0.46	3853.40	2400.00	10119.37	5603.15	6000.00
0.47	3653.40	2200.00	9884.29	5676.95	6000.00
0.48	3453.40	2000.00	9649.22	5750.74	6000.00
0.49	3253.40	1800.00	9249.22	5550.74	6000.00
0.50	3053.40	1600.00	8849.22	5350.74	6000.00
0.50	2853.40	1400.00	8449.22	5150.74	6000.00
0.51	2653.40	1200.00	8049.22	4950.74	6000.00
0.52	2453.40	1000.00	7649.22	4750.74	6000.00
0.53	2253.40	800.00	7249.22	4550.74	6000.00
0.54	2053.40	600.00	6849.22	4350.74	6000.00
0.54	1853.40	400.00	6449.22	4150.74	6000.00
0.55	1653.40	200.00	6049.22	3950.74	6000.00
0.56	1453.40	0.00	5649.22	3750.74	6000.00
0.57	1253.40	-200.00	5249.22	3550.74	6000.00
0.58	1053.40	-400.00	4849.22	3350.74	6000.00
0.58	853.40	-600.00	4449.22	3150.74	6000.00
0.59	653.40	-800.00	4049.22	2950.74	6000.00
0.60	453.40	-1000.00	3649.22	2750.74	6000.00
0.61	253.40	-1200.00	3249.22	2550.74	6000.00

0.62	53.40	-1400.00	2849.22	2350.74	6000.00
0.62	-146.60	-1600.00	2449.22	2150.74	6000.00
0.63	-346.60	-1800.00	2049.22	1950.74	6000.00
0.64	-546.60	-2000.00	1649.22	1750.74	6000.00
0.65	-746.60	-2200.00	1249.22	1550.74	5800.00
0.66	-946.60	-2400.00	849.22	1350.74	5600.00
0.66	-1146.60	-2600.00	449.22	1150.74	5400.00
0.67	-1346.60	-2800.00	49.22	950.74	5200.00
0.68	-1546.60	-3000.00	-350.78	750.74	5000.00
0.69	-1746.60	-3200.00	-750.78	550.74	4800.00
0.70	-1946.60	-3400.00	-1150.78	350.74	4600.00
0.70	-2146.60	-3600.00	-1550.78	150.74	4400.00
0.71	-2346.60	-3800.00	-1950.78	-49.26	4200.00
0.72	-2546.60	-4000.00	-2350.78	-249.26	4000.00
0.73	-2746.60	-4200.00	-2750.78	-449.26	3800.00
0.74	-2946.60	-4400.00	-3150.78	-649.26	3600.00
0.74	-3146.60	-4600.00	-3550.78	-849.26	3400.00
0.75	-3346.60	-4800.00	-3950.78	-1049.26	3200.00
0.76	-3546.60	-5000.00	-4350.78	-1249.26	3000.00
0.77	-3746.60	-5200.00	-4750.78	-1449.26	2800.00
0.78	-3946.60	-5400.00	-5150.78	-1649.26	2600.00
0.78	-4146.60	-5600.00	-5550.78	-1849.26	2400.00
0.79	-4346.60	-5800.00	-5950.78	-2049.26	2200.00
0.80	-4546.60	-6000.00	-6350.78	-2249.26	2000.00
0.81	-4691.94	-6000.00	-6750.78	-2449.26	1800.00
0.82	-4837.28	-6000.00	-7150.78	-2649.26	1600.00
0.82	-4982.62	-6000.00	-7550.78	-2849.26	1400.00
0.83	-5127.96	-6000.00	-7950.78	-3049.26	1200.00
0.84	-5273.30	-6000.00	-8350.78	-3249.26	1000.00
0.85	-5418.64	-6000.00	-8750.78	-3449.26	800.00
0.86	-5563.98	-6000.00	-9150.78	-3649.26	600.00
0.86	-5709.32	-6000.00	-9550.78	-3849.26	400.00
0.87	-5854.66	-6000.00	-9950.78	-4049.26	200.00
0.88	-6000.00	-6000.00	-10350.78	-4249.26	0.00
0.89	-6000.00	-6000.00	-10501.57	-4424.33	-200.00
0.90	-6000.00	-6000.00	-10652.35	-4599.41	-400.00
0.90	-6000.00	-6000.00	-10803.13	-4774.48	-600.00
0.91	-6000.00	-6000.00	-10953.91	-4949.56	-800.00
0.92	-6000.00	-6000.00	-11104.69	-5124.63	-1000.00
0.93	-6000.00	-6000.00	-11255.47	-5299.70	-1200.00
0.94	-6000.00	-6000.00	-11406.25	-5474.78	-1400.00

0.94	-6000.00	-6000.00	-11557.03	-5649.85	-1600.00
0.95	-6000.00	-6000.00	-11707.81	-5824.93	-1800.00
0.96	-6000.00	-6000.00	-11858.60	-6000.00	-2000.00
0.97	-6000.00	-6000.00	-11458.60	-6000.00	-2200.00
0.98	-6000.00	-6000.00	-11058.60	-6000.00	-2400.00
0.98	-6000.00	-6000.00	-10658.60	-6000.00	-2600.00
0.99	-6000.00	-6000.00	-10258.60	-6000.00	-2800.00
1.00	-6000.00	-6000.00	-9858.60	-6000.00	-3000.00
1.01	-6000.00	-6000.00	-9458.60	-6000.00	-3200.00
1.02	-6000.00	-6000.00	-9058.60	-6000.00	-3400.00
1.02	-6000.00	-6000.00	-8658.60	-6000.00	-3600.00
1.03	-6000.00	-6000.00	-8258.60	-6000.00	-3800.00
1.04	-6000.00	-6000.00	-7858.60	-6000.00	-4000.00
1.05	-6000.00	-6000.00	-7458.60	-6000.00	-4200.00
1.06	-6000.00	-6000.00	-7058.60	-6000.00	-4400.00
1.06	-6000.00	-6000.00	-6658.60	-6000.00	-4600.00
1.07	-6000.00	-6000.00	-6258.60	-6000.00	-4800.00
1.08	-6000.00	-6000.00	-5858.60	-6000.00	-5000.00
1.09	-6000.00	-6000.00	-5458.60	-6000.00	-5200.00
1.10	-6000.00	-6000.00	-5058.60	-6000.00	-5400.00
1.10	-6000.00	-6000.00	-4658.60	-6000.00	-5600.00
1.11	-6000.00	-6000.00	-4258.60	-6000.00	-5800.00
1.12	-6000.00	-6000.00	-3858.60	-6000.00	-6000.00
1.13	-6000.00	-6000.00	-4149.18	-6000.00	-6000.00
1.14	-6000.00	-6000.00	-4439.77	-6000.00	-6000.00
1.14	-6000.00	-6000.00	-4730.36	-6000.00	-6000.00
1.15	-6000.00	-6000.00	-5020.94	-6000.00	-6000.00
1.16	-6000.00	-6000.00	-5311.53	-6000.00	-6000.00
1.17	-6000.00	-6000.00	-5602.12	-6000.00	-6000.00
1.18	-6000.00	-6000.00	-5892.70	-6000.00	-6000.00
1.18	-6000.00	-6000.00	-6183.29	-6000.00	-6000.00
1.19	-6000.00	-6000.00	-6473.88	-6000.00	-6000.00
1.20	-6000.00	-6000.00	-6764.46	-6000.00	-6000.00
1.21	-6000.00	-6000.00	-6796.52	-6000.00	-6000.00
1.22	-6000.00	-6000.00	-6828.58	-6000.00	-6000.00
1.22	-6000.00	-6000.00	-6860.64	-6000.00	-6000.00
1.23	-6000.00	-6000.00	-6892.70	-6000.00	-6000.00
1.24	-6000.00	-6000.00	-6924.76	-6000.00	-6000.00
1.25	-6000.00	-6000.00	-6956.82	-6000.00	-6000.00
1.26	-6000.00	-6000.00	-6988.89	-6000.00	-6000.00
1.26	-6000.00	-6000.00	-7020.95	-6000.00	-6000.00

1.27	-6000.00	-6000.00	-7053.01	-6000.00	-6000.00
1.28	-6000.00	-6000.00	-7085.07	-6000.00	-6000.00
1.29	-6000.00	-6000.00	-7398.32	-6000.00	-6000.00
1.30	-6000.00	-6000.00	-7711.58	-6000.00	-6000.00
1.30	-6000.00	-6000.00	-8024.84	-6000.00	-6000.00
1.31	-6000.00	-6000.00	-8338.10	-6000.00	-6000.00
1.32	-6000.00	-6000.00	-8651.36	-6000.00	-6000.00
1.33	-6000.00	-6000.00	-8964.61	-6000.00	-6000.00
1.34	-6000.00	-6000.00	-9277.87	-6000.00	-6000.00
1.34	-6000.00	-6000.00	-9591.13	-6000.00	-6000.00
1.35	-6000.00	-6000.00	-9904.39	-6000.00	-6000.00
1.36	-6000.00	-6000.00	-10217.65	-6000.00	-6000.00
1.37	-6000.00	-6000.00	-7995.88	-6000.00	-6000.00
1.38	-6000.00	-6000.00	-5774.12	-6000.00	-6000.00
1.38	-6000.00	-6000.00	-3552.35	-6000.00	-6000.00
1.39	-6000.00	-6000.00	-1330.59	-6000.00	-6000.00
1.40	-6000.00	-6000.00	891.18	-6000.00	-6000.00
1.41	-6000.00	-6000.00	3112.94	-6000.00	-6000.00
1.42	-6000.00	-6000.00	5334.71	-6000.00	-6000.00
1.42	-6000.00	-6000.00	7556.47	-6000.00	-6000.00
1.43	-6000.00	-6000.00	9778.24	-6000.00	-6000.00
1.44	-6000.00	-6000.00	12000.00	-6000.00	-6000.00

Table 32 – Central Solenoid Coils Breakdown Currents

Time	CS3U	CS2U	CS1	CS2L	CS3L
0.00	36381.95	45000.45	40000.00	45000.45	45000.45
0.01	36339.27	44980.42	39946.92	44996.59	44933.34
0.02	36297.57	44958.67	39895.45	44991.68	44867.02
0.02	36256.80	44935.10	39845.40	44985.66	44801.44
0.03	36216.92	44909.66	39796.61	44978.48	44736.57
0.04	36177.90	44882.29	39748.98	44970.10	44672.38
0.05	36139.72	44852.96	39702.45	44960.48	44608.85
0.06	36102.37	44821.64	39656.93	44949.62	44545.97
0.06	36065.83	44788.33	39612.40	44937.47	44483.71
0.07	36030.08	44753.02	39568.81	44924.03	44422.08
0.08	35995.14	44715.70	39526.13	44909.28	44361.05
0.09	35960.80	44677.08	39484.24	44893.51	44300.55
0.10	35926.90	44637.88	39443.02	44877.00	44240.51
0.10	35893.43	44598.07	39402.44	44859.73	44180.91
0.11	35860.39	44557.64	39362.50	44841.69	44121.76
0.12	35827.76	44516.57	39323.17	44822.88	44063.04

0.13	35795.55	44474.86	39284.45	44803.29	44004.76
0.14	35763.74	44432.50	39246.31	44782.90	43946.91
0.14	35732.35	44389.48	39208.76	44761.71	43889.47
0.15	35701.35	44345.78	39171.77	44739.73	43832.46
0.16	35670.75	44301.41	39135.33	44716.93	43775.87
0.17	35640.55	44256.36	39099.44	44693.32	43719.69
0.18	35610.74	44210.61	39064.08	44668.90	43663.92
0.18	35581.32	44164.17	39029.25	44643.66	43608.55
0.19	35552.28	44117.03	38994.93	44617.60	43553.60
0.20	35523.63	44069.19	38961.13	44590.71	43499.04
0.21	35495.35	44020.63	38927.82	44562.99	43444.88
0.22	35467.46	43971.36	38895.01	44534.44	43391.12
0.22	35439.93	43921.37	38862.68	44505.06	43337.76
0.23	35412.77	43870.65	38830.83	44474.84	43284.78
0.24	35385.99	43819.21	38799.45	44443.79	43232.20
0.25	35359.56	43767.03	38768.53	44411.90	43180.00
0.26	35333.51	43714.12	38738.06	44379.16	43128.20
0.26	35307.81	43660.47	38708.05	44345.58	43076.77
0.27	35282.47	43606.08	38678.48	44311.16	43025.73
0.28	35257.48	43550.94	38649.35	44275.89	42975.06
0.29	35232.85	43495.05	38620.65	44239.77	42924.78
0.30	35208.56	43438.41	38592.38	44202.80	42874.87
0.30	35184.63	43381.02	38564.53	44164.99	42825.34
0.31	35161.04	43322.87	38537.09	44126.32	42776.17
0.32	35137.80	43263.96	38510.07	44086.79	42727.38
0.33	35114.86	43204.97	38483.38	44046.44	42678.96
0.34	35092.18	43146.55	38456.96	44005.25	42630.90
0.34	35069.76	43088.70	38430.79	43963.25	42583.20
0.35	35047.60	43031.38	38404.88	43920.42	42535.86
0.36	35025.69	42974.59	38379.21	43876.77	42488.88
0.37	35004.02	42918.32	38353.79	43832.30	42442.25
0.38	34982.60	42862.53	38328.61	43787.00	42395.98
0.38	34961.42	42807.24	38303.67	43740.88	42350.06
0.39	34940.49	42752.42	38278.95	43693.94	42304.49
0.40	34919.79	42698.06	38254.47	43646.17	42259.28
0.41	34899.52	42644.40	38230.40	43597.87	42214.33
0.42	34879.85	42591.65	38206.93	43549.31	42169.59
0.42	34860.79	42539.80	38184.04	43500.49	42125.05
0.43	34842.32	42488.83	38161.73	43451.41	42080.70
0.44	34824.44	42438.71	38139.98	43402.04	42036.55
0.45	34807.15	42389.44	38118.79	43352.40	41992.59

0.46	34790.44	42341.01	38098.14	43302.46	41948.83
0.46	34774.31	42293.40	38078.02	43252.23	41905.25
0.47	34758.75	42246.59	38058.44	43201.70	41861.86
0.48	34743.75	42200.58	38039.37	43150.87	41818.66
0.49	34729.33	42155.33	38020.92	43100.44	41775.48
0.50	34715.48	42110.80	38003.20	43051.10	41732.13
0.50	34702.19	42066.99	37986.17	43002.81	41688.63
0.51	34689.47	42023.87	37969.83	42955.56	41644.97
0.52	34677.30	41981.45	37954.18	42909.34	41601.14
0.53	34665.70	41939.71	37939.19	42864.12	41557.15
0.54	34654.64	41898.65	37924.86	42819.90	41512.98
0.54	34644.14	41858.26	37911.18	42776.65	41468.65
0.55	34634.19	41818.52	37898.14	42734.36	41424.15
0.56	34624.78	41779.44	37885.73	42693.03	41379.47
0.57	34615.91	41741.01	37873.94	42652.64	41334.62
0.58	34607.59	41703.22	37862.77	42613.19	41289.60
0.58	34599.80	41666.05	37852.20	42574.65	41244.40
0.59	34592.54	41629.52	37842.24	42537.03	41199.01
0.60	34585.82	41593.60	37832.87	42500.32	41153.45
0.61	34579.62	41558.29	37824.08	42464.50	41107.71
0.62	34573.96	41523.59	37815.88	42429.57	41061.79
0.62	34568.81	41489.50	37808.24	42395.52	41015.68
0.63	34564.20	41456.00	37801.18	42362.35	40969.39
0.64	34560.10	41423.09	37794.67	42330.05	40922.91
0.65	34556.52	41390.76	37788.73	42298.48	40876.72
0.66	34553.46	41359.00	37783.36	42267.50	40831.28
0.66	34550.91	41327.82	37778.55	42237.11	40786.59
0.67	34548.88	41297.21	37774.29	42207.31	40742.63
0.68	34547.35	41267.15	37770.58	42178.08	40699.42
0.69	34546.34	41237.65	37767.42	42149.43	40656.94
0.70	34545.83	41208.70	37764.80	42121.33	40615.19
0.70	34545.83	41180.30	37762.72	42093.80	40574.16
0.71	34546.33	41152.45	37761.17	42066.82	40533.86
0.72	34547.34	41125.13	37760.14	42040.39	40494.29
0.73	34548.84	41098.34	37759.65	42014.51	40455.43
0.74	34550.85	41072.09	37759.67	41989.16	40417.28
0.74	34553.35	41046.36	37760.20	41964.35	40379.85
0.75	34556.35	41021.15	37761.25	41940.07	40343.13
0.76	34559.84	40996.47	37762.80	41916.32	40307.12
0.77	34563.82	40972.30	37764.86	41893.09	40271.81
0.78	34568.30	40948.64	37767.42	41870.38	40237.21

0.78	34573.26	40925.49	37770.48	41848.19	40203.31
0.79	34578.72	40902.85	37774.03	41826.50	40170.11
0.80	34584.66	40880.70	37778.07	41805.33	40137.60
0.81	34591.08	40858.55	37782.65	41784.65	40105.80
0.82	34597.99	40835.86	37787.80	41764.44	40074.69
0.82	34605.37	40812.66	37793.51	41744.70	40044.27
0.83	34613.24	40788.93	37799.76	41725.42	40014.54
0.84	34621.58	40764.69	37806.55	41706.59	39985.51
0.85	34630.40	40739.95	37813.87	41688.22	39957.16
0.86	34639.69	40714.69	37821.72	41670.28	39929.50
0.86	34649.46	40688.93	37830.08	41652.79	39902.51
0.87	34659.70	40662.68	37838.97	41635.74	39876.21
0.88	34670.42	40635.93	37848.37	41619.11	39850.59
0.89	34681.33	40608.85	37858.02	41602.92	39825.66
0.90	34692.15	40581.59	37867.64	41587.16	39801.40
0.90	34702.89	40554.16	37877.25	41571.84	39777.84
0.91	34713.55	40526.56	37886.86	41556.94	39754.96
0.92	34724.13	40498.80	37896.47	41542.48	39732.76
0.93	34734.64	40470.89	37906.10	41528.45	39711.25
0.94	34745.07	40442.83	37915.74	41514.85	39690.41
0.94	34755.44	40414.62	37925.41	41501.68	39670.26
0.95	34765.73	40386.27	37935.10	41488.95	39650.79
0.96	34775.96	40357.78	37944.82	41476.64	39631.99
0.97	34786.10	40329.29	37954.01	41464.44	39613.96
0.98	34796.14	40300.94	37962.14	41452.02	39596.78
0.98	34806.06	40272.75	37969.23	41439.39	39580.46
0.99	34815.88	40244.71	37975.30	41426.57	39565.00
1.00	34825.60	40216.84	37980.37	41413.56	39550.40
1.01	34835.22	40189.12	37984.47	41400.39	39536.64
1.02	34844.74	40161.57	37987.60	41387.05	39523.75
1.02	34854.16	40134.20	37989.78	41373.55	39511.70
1.03	34863.48	40106.99	37991.02	41359.90	39500.51
1.04	34872.70	40079.96	37991.35	41346.11	39490.17
1.05	34881.85	40053.11	37990.75	41332.18	39480.69
1.06	34890.95	40026.44	37989.26	41318.12	39472.06
1.06	34900.01	39999.95	37986.88	41303.92	39464.27
1.07	34909.02	39973.64	37983.62	41289.61	39457.34
1.08	34917.99	39947.52	37979.50	41275.18	39451.26
1.09	34926.92	39921.60	37974.51	41260.64	39446.03
1.10	34935.80	39895.87	37968.68	41245.98	39441.64
1.10	34944.65	39870.33	37962.00	41231.22	39438.11

1.11	34953.46	39845.00	37954.48	41216.37	39435.43
1.12	34962.23	39819.86	37946.14	41201.41	39433.59
1.13	34971.05	39794.74	37937.74	41186.30	39432.16
1.14	34980.00	39769.45	37930.02	41170.98	39430.69
1.14	34989.10	39743.98	37922.96	41155.46	39429.19
1.15	34998.34	39718.33	37916.54	41139.73	39427.67
1.16	35007.72	39692.52	37910.75	41123.81	39426.12
1.17	35017.24	39666.53	37905.58	41107.68	39424.55
1.18	35026.92	39640.38	37901.02	41091.36	39422.96
1.18	35036.74	39614.06	37897.05	41074.85	39421.36
1.19	35046.71	39587.58	37893.68	41058.15	39419.74
1.20	35056.83	39560.93	37890.90	41041.25	39418.11
1.21	35067.07	39534.19	37888.40	41024.24	39416.45
1.22	35077.41	39507.43	37885.91	41007.18	39414.77
1.22	35087.84	39480.66	37883.44	40990.08	39413.05
1.23	35098.37	39453.88	37880.98	40972.94	39411.31
1.24	35108.99	39427.09	37878.54	40955.75	39409.53
1.25	35119.71	39400.28	37876.12	40938.53	39407.73
1.26	35130.52	39373.47	37873.72	40921.28	39405.91
1.26	35141.44	39346.65	37871.34	40903.99	39404.06
1.27	35152.45	39319.83	37868.99	40886.66	39402.18
1.28	35163.56	39293.00	37866.67	40869.31	39400.28
1.29	35174.64	39266.10	37864.68	40851.85	39398.37
1.30	35185.56	39239.07	37863.33	40834.20	39396.47
1.30	35196.32	39211.91	37862.61	40816.37	39394.56
1.31	35206.92	39184.63	37862.51	40798.36	39392.66
1.32	35217.35	39157.21	37863.02	40780.17	39390.76
1.33	35227.62	39129.66	37864.14	40761.80	39388.87
1.34	35237.72	39101.98	37865.85	40743.25	39386.98
1.34	35247.66	39074.17	37868.17	40724.52	39385.10
1.35	35257.43	39046.22	37871.07	40705.62	39383.22
1.36	35267.03	39018.15	37874.56	40686.53	39381.35
1.37	35276.35	38990.63	37875.82	40667.96	39379.38
1.38	35285.28	38964.37	37872.13	40650.59	39377.21
1.38	35293.80	38939.36	37863.57	40634.44	39374.84
1.39	35301.93	38915.62	37850.23	40619.50	39372.26
1.40	35309.66	38893.14	37832.18	40605.79	39369.48
1.41	35316.99	38871.93	37809.48	40593.30	39366.49
1.42	35323.91	38851.99	37782.18	40582.05	39363.30
1.42	35330.43	38833.32	37750.34	40572.03	39359.90
1.43	35336.55	38815.93	37713.99	40563.25	39356.30

1.44	35342.26	38799.81	37673.19	40555.71	39352.50

Table 33 – Poloidal Field Coils Breakdown Voltages

Time	P1	P2	P3	P4	P5	P6
0.00	6000.00	9000.00	9000.00	9000.00	9000.00	6000.00
0.01	6000.00	9000.00	9000.00	9000.00	9000.00	6000.00
0.02	6000.00	9000.00	9000.00	9000.00	9000.00	6000.00
0.02	6000.00	9000.00	9000.00	9000.00	9000.00	6000.00
0.03	6000.00	9000.00	9000.00	9000.00	9000.00	6000.00
0.04	6000.00	9000.00	9000.00	9000.00	9000.00	6000.00
0.05	6000.00	9000.00	9000.00	9000.00	9000.00	6000.00
0.06	6000.00	9000.00	9000.00	9000.00	9000.00	6000.00
0.06	6000.00	9000.00	9000.00	9000.00	9000.00	6000.00
0.07	6000.00	9000.00	9000.00	9000.00	9000.00	6000.00
0.08	6000.00	9000.00	9000.00	9000.00	9000.00	6000.00
0.09	6000.00	9000.00	9000.00	9000.00	9000.00	6000.00
0.10	6000.00	9000.00	9000.00	9000.00	9000.00	6000.00
0.10	6000.00	9000.00	9000.00	9000.00	9000.00	6000.00
0.11	6000.00	9000.00	9000.00	9000.00	9000.00	6000.00
0.12	6000.00	9000.00	9000.00	9000.00	9000.00	6000.00
0.13	6000.00	9000.00	9000.00	9000.00	9000.00	6000.00
0.14	6000.00	9000.00	9000.00	9000.00	9000.00	6000.00
0.14	6000.00	9000.00	9000.00	9000.00	9000.00	6000.00
0.15	6000.00	9000.00	9000.00	9000.00	9000.00	6000.00
0.16	6000.00	9000.00	9000.00	9000.00	9000.00	6000.00
0.17	6000.00	9000.00	9000.00	9000.00	9000.00	6000.00
0.18	6000.00	9000.00	9000.00	9000.00	9000.00	6000.00
0.18	6000.00	9000.00	9000.00	9000.00	9000.00	6000.00
0.19	6000.00	9000.00	9000.00	9000.00	9000.00	6000.00
0.20	6000.00	9000.00	9000.00	9000.00	9000.00	6000.00
0.21	6000.00	9000.00	9000.00	9000.00	9000.00	6000.00
0.22	6000.00	9000.00	9000.00	9000.00	9000.00	6000.00
0.22	6000.00	9000.00	9000.00	9000.00	9000.00	6000.00
0.23	6000.00	9000.00	9000.00	9000.00	9000.00	6000.00
0.24	6000.00	9000.00	9000.00	9000.00	9000.00	6000.00
0.25	6000.00	9000.00	9000.00	9000.00	9000.00	6000.00
0.26	6000.00	9000.00	9000.00	9000.00	9000.00	6000.00
0.26	6000.00	9000.00	9000.00	9000.00	9000.00	6000.00
0.27	6000.00	9000.00	9000.00	9000.00	9000.00	6000.00
0.28	6000.00	9000.00	9000.00	9000.00	9000.00	6000.00
0.29	6000.00	9000.00	9000.00	9000.00	9000.00	6000.00

0.30	6000.00	9000.00	9000.00	9000.00	9000.00	6000.00
0.30	6000.00	9000.00	9000.00	9000.00	9000.00	6000.00
0.31	6000.00	9000.00	9000.00	9000.00	9000.00	6000.00
0.32	6000.00	9000.00	9000.00	9000.00	9000.00	6000.00
0.33	6000.00	9000.00	9000.00	9000.00	9000.00	6000.00
0.34	6000.00	9000.00	9000.00	9000.00	9000.00	6000.00
0.34	6000.00	9000.00	9000.00	9000.00	9000.00	6000.00
0.35	6000.00	9000.00	9000.00	9000.00	9000.00	6000.00
0.36	6000.00	9000.00	9000.00	9000.00	9000.00	6000.00
0.37	6000.00	9000.00	9000.00	9000.00	9000.00	6000.00
0.38	6000.00	9000.00	9000.00	9000.00	9000.00	6000.00
0.38	6000.00	9000.00	9000.00	9000.00	9000.00	6000.00
0.39	6000.00	9000.00	9000.00	9000.00	9000.00	6000.00
0.40	6000.00	9000.00	9000.00	9000.00	9000.00	6000.00
0.41	5800.00	9000.00	8728.99	9000.00	9000.00	6000.00
0.42	5600.00	9000.00	8457.97	9000.00	9000.00	6000.00
0.42	5400.00	9000.00	8186.96	9000.00	9000.00	6000.00
0.43	5200.00	9000.00	7915.95	9000.00	9000.00	6000.00
0.44	5000.00	9000.00	7644.93	9000.00	9000.00	6000.00
0.45	4800.00	9000.00	7373.92	9000.00	9000.00	6000.00
0.46	4600.00	9000.00	7102.91	9000.00	9000.00	6000.00
0.46	4400.00	9000.00	6831.90	9000.00	9000.00	6000.00
0.47	4200.00	9000.00	6560.88	9000.00	9000.00	6000.00
0.48	4000.00	9000.00	6289.87	9000.00	9000.00	6000.00
0.49	3800.00	9000.00	5989.87	9000.00	9000.00	6000.00
0.50	3600.00	9000.00	5689.87	9000.00	9000.00	6000.00
0.50	3400.00	9000.00	5389.87	9000.00	9000.00	6000.00
0.51	3200.00	9000.00	5089.87	9000.00	9000.00	6000.00
0.52	3000.00	9000.00	4789.87	9000.00	9000.00	6000.00
0.53	2800.00	9000.00	4489.87	9000.00	9000.00	6000.00
0.54	2600.00	9000.00	4189.87	9000.00	9000.00	6000.00
0.54	2400.00	9000.00	3889.87	9000.00	9000.00	6000.00
0.55	2200.00	9000.00	3589.87	9000.00	9000.00	6000.00
0.56	2000.00	9000.00	3289.87	9000.00	9000.00	6000.00
0.57	1800.00	8909.43	2989.87	9000.00	9000.00	6000.00
0.58	1600.00	8818.86	2689.87	9000.00	9000.00	6000.00
0.58	1400.00	8728.29	2389.87	9000.00	9000.00	6000.00
0.59	1200.00	8637.72	2089.87	9000.00	9000.00	6000.00
0.60	1000.00	8547.15	1789.87	9000.00	9000.00	6000.00
0.61	800.00	8456.58	1489.87	9000.00	9000.00	6000.00
0.62	600.00	8366.01	1189.87	9000.00	9000.00	6000.00

0.62	400.00	8275.44	889.87	9000.00	9000.00	6000.00
0.63	200.00	8184.87	589.87	9000.00	9000.00	6000.00
0.64	0.00	8094.30	289.87	9000.00	9000.00	6000.00
0.65	-200.00	7794.30	-10.13	9000.00	9000.00	6000.00
0.66	-400.00	7494.30	-310.13	9000.00	9000.00	6000.00
0.66	-600.00	7194.30	-610.13	9000.00	9000.00	6000.00
0.67	-800.00	6894.30	-910.13	9000.00	9000.00	6000.00
0.68	-1000.00	6594.30	-1210.13	9000.00	9000.00	6000.00
0.69	-1200.00	6294.30	-1510.13	9000.00	9000.00	6000.00
0.70	-1400.00	5994.30	-1810.13	9000.00	9000.00	6000.00
0.70	-1600.00	5694.30	-2110.13	9000.00	9000.00	6000.00
0.71	-1800.00	5394.30	-2410.13	9000.00	9000.00	6000.00
0.72	-2000.00	5094.30	-2710.13	9000.00	9000.00	6000.00
0.73	-2200.00	4794.30	-3010.13	8700.00	9000.00	6000.00
0.74	-2400.00	4494.30	-3310.13	8400.00	9000.00	6000.00
0.74	-2600.00	4194.30	-3610.13	8100.00	9000.00	6000.00
0.75	-2800.00	3894.30	-3910.13	7800.00	9000.00	6000.00
0.76	-3000.00	3594.30	-4210.13	7500.00	9000.00	6000.00
0.77	-3200.00	3294.30	-4510.13	7200.00	9000.00	6000.00
0.78	-3400.00	2994.30	-4810.13	6900.00	9000.00	6000.00
0.78	-3600.00	2694.30	-5110.13	6600.00	9000.00	6000.00
0.79	-3800.00	2394.30	-5410.13	6300.00	9000.00	6000.00
0.80	-4000.00	2094.30	-5710.13	6000.00	9000.00	6000.00
0.81	-4200.00	1862.44	-5490.32	6092.82	9000.00	6000.00
0.82	-4400.00	1630.57	-5270.50	6185.64	9000.00	6000.00
0.82	-4600.00	1398.71	-5050.69	6278.45	9000.00	6000.00
0.83	-4800.00	1166.84	-4830.88	6371.27	9000.00	6000.00
0.84	-5000.00	934.98	-4611.06	6464.09	9000.00	6000.00
0.85	-5200.00	703.11	-4391.25	6556.91	9000.00	6000.00
0.86	-5400.00	471.24	-4171.44	6649.72	9000.00	6000.00
0.86	-5600.00	239.38	-3951.62	6742.54	9000.00	6000.00
0.87	-5800.00	7.51	-3731.81	6835.36	9000.00	6000.00
0.88	-6000.00	-224.35	-3511.99	6928.18	9000.00	6000.00
0.89	-6000.00	75.65	-3211.99	6628.18	9000.00	6000.00
0.90	-6000.00	375.65	-2911.99	6328.18	9000.00	6000.00
0.90	-6000.00	675.65	-2611.99	6028.18	9000.00	6000.00
0.91	-6000.00	975.65	-2311.99	5728.18	9000.00	6000.00
0.92	-6000.00	1275.65	-2011.99	5428.18	9000.00	6000.00
0.93	-6000.00	1575.65	-1711.99	5128.18	9000.00	6000.00
0.94	-6000.00	1875.65	-1411.99	4828.18	9000.00	6000.00
0.94	-6000.00	2175.65	-1111.99	4528.18	9000.00	6000.00

0.95	-6000.00	2475.65	-811.99	4228.18	9000.00	6000.00
0.96	-6000.00	2775.65	-511.99	3928.18	9000.00	6000.00
0.97	-6000.00	2948.21	-211.99	3770.54	9000.00	6000.00
0.98	-6000.00	3120.76	88.01	3612.89	9000.00	6000.00
0.98	-6000.00	3293.32	388.01	3455.25	9000.00	6000.00
0.99	-6000.00	3465.88	688.01	3297.61	9000.00	6000.00
1.00	-6000.00	3638.44	988.01	3139.97	9000.00	6000.00
1.01	-6000.00	3811.00	1288.01	2982.33	9000.00	6000.00
1.02	-6000.00	3983.56	1588.01	2824.69	9000.00	6000.00
1.02	-6000.00	4156.12	1888.01	2667.05	9000.00	6000.00
1.03	-6000.00	4328.68	2188.01	2509.41	9000.00	6000.00
1.04	-6000.00	4501.24	2488.01	2351.77	9000.00	6000.00
1.05	-5940.93	4201.24	2788.01	2651.77	9000.00	6000.00
1.06	-5881.86	3901.24	3088.01	2951.77	9000.00	6000.00
1.06	-5822.79	3601.24	3388.01	3251.77	9000.00	6000.00
1.07	-5763.72	3301.24	3688.01	3551.77	9000.00	6000.00
1.08	-5704.65	3001.24	3988.01	3851.77	9000.00	6000.00
1.09	-5645.58	2701.24	4288.01	4151.77	9000.00	6000.00
1.10	-5586.51	2401.24	4588.01	4451.77	9000.00	6000.00
1.10	-5527.43	2101.24	4888.01	4751.77	9000.00	6000.00
1.11	-5468.36	1801.24	5188.01	5051.77	9000.00	6000.00
1.12	-5409.29	1501.24	5488.01	5351.77	9000.00	6000.00
1.13	-5209.29	1796.41	5188.01	5336.03	9000.00	6000.00
1.14	-5009.29	2091.58	4888.01	5320.29	9000.00	6000.00
1.14	-4809.29	2386.75	4588.01	5304.55	9000.00	6000.00
1.15	-4609.29	2681.92	4288.01	5288.81	9000.00	6000.00
1.16	-4409.29	2977.09	3988.01	5273.07	9000.00	6000.00
1.17	-4209.29	3272.27	3688.01	5257.33	9000.00	6000.00
1.18	-4009.29	3567.44	3388.01	5241.59	9000.00	6000.00
1.18	-3809.29	3862.61	3088.01	5225.85	9000.00	6000.00
1.19	-3609.29	4157.78	2788.01	5210.11	9000.00	6000.00
1.20	-3409.29	4452.95	2488.01	5194.37	9000.00	6000.00
1.21	-3254.27	4189.51	2273.97	5067.95	9000.00	6000.00
1.22	-3099.26	3926.08	2059.94	4941.54	9000.00	6000.00
1.22	-2944.24	3662.64	1845.91	4815.12	9000.00	6000.00
1.23	-2789.22	3399.20	1631.88	4688.71	9000.00	6000.00
1.24	-2634.20	3135.76	1417.84	4562.29	9000.00	6000.00
1.25	-2479.18	2872.32	1203.81	4435.87	9000.00	6000.00
1.26	-2324.16	2608.88	989.78	4309.46	9000.00	6000.00
1.26	-2169.14	2345.44	775.75	4183.04	9000.00	6000.00
1.27	-2014.13	2082.01	561.71	4056.63	9000.00	6000.00

1.28	-1859.11	1818.57	347.68	3930.21	9000.00	6000.00
1.29	-2059.11	2062.86	647.68	4082.76	9000.00	6000.00
1.30	-2259.11	2307.16	947.68	4235.31	9000.00	6000.00
1.30	-2459.11	2551.46	1247.68	4387.86	9000.00	6000.00
1.31	-2659.11	2795.75	1547.68	4540.41	9000.00	6000.00
1.32	-2859.11	3040.05	1847.68	4692.96	9000.00	6000.00
1.33	-3059.11	3284.35	2147.68	4845.51	9000.00	6000.00
1.34	-3259.11	3528.64	2447.68	4998.07	9000.00	6000.00
1.34	-3459.11	3772.94	2747.68	5150.62	9000.00	6000.00
1.35	-3659.11	4017.24	3047.68	5303.17	9000.00	6000.00
1.36	-3859.11	4261.53	3347.68	5455.72	9000.00	6000.00
1.37	-4073.20	2935.38	3912.91	4010.14	9000.00	6000.00
1.38	-4287.29	1609.23	4478.15	2564.57	9000.00	6000.00
1.38	-4501.38	283.07	5043.38	1119.00	9000.00	6000.00
1.39	-4715.46	-1043.08	5608.61	-326.57	9000.00	6000.00
1.40	-4929.55	-2369.23	6173.84	-1772.14	9000.00	6000.00
1.41	-5143.64	-3695.39	6739.07	-3217.71	9000.00	6000.00
1.42	-5357.73	-5021.54	7304.30	-4663.29	9000.00	6000.00
1.42	-5571.82	-6347.69	7869.54	-6108.86	9000.00	6000.00
1.43	-5785.91	-7673.85	8434.77	-7554.43	9000.00	6000.00
1.44	-6000.00	-9000.00	9000.00	-9000.00	9000.00	6000.00

Table 34 – Poloidal Field Coils Breakdown Currents

Time	P1	P2	P3	P4	P5	P6
0.00	37484.40	9038.05	411.34	2755.34	1340.68	8897.81
0.01	37440.64	9002.31	399.68	2741.91	1336.27	8896.71
0.02	37397.41	8967.21	388.31	2728.73	1331.97	8895.72
0.02	37354.63	8932.66	377.21	2715.76	1327.75	8894.81
0.03	37312.24	8898.61	366.35	2703.00	1323.62	8893.99
0.04	37270.21	8865.01	355.71	2690.42	1319.56	8893.23
0.05	37228.49	8831.81	345.27	2678.01	1315.58	8892.53
0.06	37187.07	8798.98	335.03	2665.77	1311.67	8891.89
0.06	37145.92	8766.51	324.96	2653.68	1307.83	8891.31
0.07	37105.04	8734.37	315.06	2641.73	1304.04	8890.78
0.08	37064.41	8702.55	305.32	2629.91	1300.32	8890.31
0.09	37024.03	8671.02	295.74	2618.23	1296.65	8889.88
0.10	36983.90	8639.78	286.30	2606.66	1293.03	8889.50
0.10	36944.02	8608.81	277.00	2595.22	1289.47	8889.18
0.11	36904.37	8578.11	267.83	2583.88	1285.96	8888.89
0.12	36864.96	8547.68	258.80	2572.66	1282.49	8888.66
0.13	36825.78	8517.50	249.89	2561.55	1279.07	8888.47

0.14	36786.82	8487.56	241.11	2550.54	1275.70	8888.32
0.14	36748.07	8457.87	232.45	2539.62	1272.38	8888.22
0.15	36709.54	8428.41	223.90	2528.81	1269.10	8888.16
0.16	36671.23	8399.18	215.47	2518.10	1265.86	8888.15
0.17	36633.11	8370.18	207.16	2507.48	1262.67	8888.17
0.18	36595.20	8341.41	198.95	2496.95	1259.52	8888.24
0.18	36557.49	8312.86	190.86	2486.51	1256.41	8888.35
0.19	36519.97	8284.52	182.86	2476.16	1253.34	8888.50
0.20	36482.65	8256.39	174.98	2465.90	1250.32	8888.69
0.21	36445.51	8228.47	167.20	2455.73	1247.33	8888.92
0.22	36408.56	8200.76	159.51	2445.64	1244.38	8889.19
0.22	36371.79	8173.25	151.93	2435.63	1241.48	8889.50
0.23	36335.21	8145.93	144.45	2425.71	1238.61	8889.84
0.24	36298.79	8118.82	137.06	2415.87	1235.78	8890.22
0.25	36262.56	8091.89	129.77	2406.11	1232.99	8890.64
0.26	36226.49	8065.16	122.57	2396.44	1230.24	8891.10
0.26	36190.59	8038.61	115.46	2386.83	1227.53	8891.59
0.27	36154.85	8012.25	108.44	2377.31	1224.85	8892.12
0.28	36119.28	7986.07	101.52	2367.86	1222.21	8892.68
0.29	36083.87	7960.07	94.68	2358.49	1219.61	8893.28
0.30	36048.61	7934.24	87.93	2349.20	1217.04	8893.92
0.30	36013.51	7908.59	81.26	2339.97	1214.51	8894.58
0.31	35978.56	7883.11	74.68	2330.82	1212.02	8895.28
0.32	35943.77	7857.80	68.18	2321.75	1209.56	8896.02
0.33	35909.10	7832.65	61.76	2312.74	1207.14	8896.79
0.34	35874.56	7807.66	55.42	2303.80	1204.75	8897.58
0.34	35840.14	7782.84	49.16	2294.94	1202.40	8898.42
0.35	35805.83	7758.18	42.98	2286.14	1200.08	8899.28
0.36	35771.63	7733.67	36.88	2277.41	1197.80	8900.17
0.37	35737.54	7709.31	30.85	2268.74	1195.55	8901.10
0.38	35703.56	7685.11	24.90	2260.15	1193.33	8902.05
0.38	35669.68	7661.06	19.02	2251.61	1191.15	8903.04
0.39	35635.90	7637.15	13.21	2243.14	1189.00	8904.05
0.40	35602.21	7613.39	7.48	2234.74	1186.89	8905.10
0.41	35568.95	7589.71	2.08	2226.36	1184.80	8906.17
0.42	35536.44	7566.07	-2.73	2217.96	1182.74	8907.28
0.42	35504.65	7542.45	-6.94	2209.54	1180.70	8908.41
0.43	35473.60	7518.85	-10.57	2201.10	1178.69	8909.57
0.44	35443.26	7495.27	-13.63	2192.63	1176.71	8910.76
0.45	35413.63	7471.70	-16.10	2184.14	1174.75	8911.98
0.46	35384.71	7448.14	-18.01	2175.61	1172.81	8913.22

0.46	35356.48	7424.58	-19.35	2167.06	1170.90	8914.49
0.47	35328.95	7401.02	-20.13	2158.48	1169.01	8915.79
0.48	35302.10	7377.45	-20.35	2149.86	1167.14	8917.11
0.49	35275.93	7353.88	-19.98	2141.20	1165.30	8918.47
0.50	35250.44	7330.27	-19.00	2132.50	1163.48	8919.85
0.50	35225.61	7306.65	-17.42	2123.75	1161.68	8921.26
0.51	35201.45	7282.99	-15.23	2114.95	1159.90	8922.69
0.52	35177.95	7259.29	-12.44	2106.10	1158.14	8924.16
0.53	35155.10	7235.56	-9.06	2097.20	1156.40	8925.65
0.54	35132.89	7211.79	-5.08	2088.25	1154.68	8927.16
0.54	35111.33	7187.97	-0.51	2079.24	1152.98	8928.71
0.55	35090.41	7164.10	4.65	2070.17	1151.30	8930.27
0.56	35070.13	7140.17	10.40	2061.05	1149.64	8931.87
0.57	35050.46	7116.40	16.71	2051.86	1147.99	8933.48
0.58	35031.42	7092.97	23.58	2042.61	1146.37	8935.12
0.58	35012.99	7069.87	30.99	2033.29	1144.76	8936.78
0.59	34995.16	7047.10	38.95	2023.90	1143.16	8938.46
0.60	34977.94	7024.66	47.45	2014.44	1141.58	8940.17
0.61	34961.31	7002.52	56.50	2004.91	1140.02	8941.89
0.62	34945.28	6980.70	66.07	1995.31	1138.47	8943.64
0.62	34929.84	6959.18	76.19	1985.64	1136.93	8945.40
0.63	34914.99	6937.95	86.83	1975.88	1135.41	8947.18
0.64	34900.72	6917.02	98.01	1966.05	1133.90	8948.98
0.65	34887.02	6896.84	109.67	1956.14	1132.41	8950.79
0.66	34873.87	6877.88	121.79	1946.14	1130.92	8952.58
0.66	34861.27	6860.12	134.37	1936.05	1129.45	8954.36
0.67	34849.22	6843.55	147.38	1925.86	1127.98	8956.12
0.68	34837.71	6828.15	160.85	1915.58	1126.52	8957.86
0.69	34826.74	6813.91	174.75	1905.21	1125.07	8959.59
0.70	34816.30	6800.83	189.09	1894.73	1123.63	8961.30
0.70	34806.39	6788.88	203.86	1884.16	1122.20	8962.99
0.71	34797.00	6778.06	219.06	1873.49	1120.77	8964.66
0.72	34788.14	6768.36	234.69	1862.72	1119.35	8966.31
0.73	34779.80	6759.76	250.70	1852.14	1117.92	8967.93
0.74	34771.96	6752.26	267.04	1842.04	1116.46	8969.54
0.74	34764.64	6745.83	283.71	1832.42	1114.96	8971.11
0.75	34757.82	6740.47	300.70	1823.26	1113.43	8972.66
0.76	34751.51	6736.18	318.01	1814.57	1111.86	8974.19
0.77	34745.70	6732.94	335.64	1806.33	1110.26	8975.69
0.78	34740.38	6730.74	353.58	1798.54	1108.61	8977.16
0.78	34735.55	6729.59	371.83	1791.21	1106.93	8978.60

0.79	34731.21	6729.47	390.38	1784.31	1105.21	8980.01
0.80	34727.36	6730.38	409.24	1777.86	1103.45	8981.39
0.81	34724.01	6732.24	427.95	1771.53	1101.67	8982.74
0.82	34721.18	6734.99	446.07	1765.02	1099.91	8984.06
0.82	34718.87	6738.63	463.61	1758.32	1098.16	8985.35
0.83	34717.06	6743.13	480.56	1751.43	1096.43	8986.60
0.84	34715.75	6748.51	496.92	1744.35	1094.70	8987.82
0.85	34714.94	6754.75	512.70	1737.08	1092.99	8989.01
0.86	34714.64	6761.85	527.90	1729.63	1091.28	8990.16
0.86	34714.82	6769.81	542.52	1721.98	1089.58	8991.28
0.87	34715.50	6778.62	556.56	1714.15	1087.89	8992.35
0.88	34716.67	6788.28	570.03	1706.13	1086.21	8993.39
0.89	34718.02	6797.61	582.87	1698.34	1084.50	8994.39
0.90	34719.27	6805.44	595.05	1691.17	1082.76	8995.34
0.90	34720.42	6811.80	606.58	1684.63	1080.99	8996.26
0.91	34721.48	6816.71	617.45	1678.72	1079.17	8997.13
0.92	34722.44	6820.19	627.69	1673.43	1077.31	8997.96
0.93	34723.33	6822.27	637.28	1668.76	1075.41	8998.75
0.94	34724.13	6822.96	646.25	1664.71	1073.46	8999.49
0.94	34724.86	6822.28	654.58	1661.28	1071.48	9000.18
0.95	34725.52	6820.23	662.30	1658.47	1069.45	9000.83
0.96	34726.10	6816.85	669.39	1656.27	1067.37	9001.44
0.97	34726.62	6812.42	675.87	1654.54	1065.26	9002.00
0.98	34727.06	6807.25	681.75	1653.14	1063.11	9002.51
0.98	34727.44	6801.35	687.01	1652.08	1060.94	9002.97
0.99	34727.75	6794.72	691.68	1651.35	1058.74	9003.39
1.00	34727.99	6787.36	695.75	1650.97	1056.51	9003.75
1.01	34728.18	6779.29	699.23	1650.92	1054.25	9004.07
1.02	34728.31	6770.51	702.11	1651.22	1051.96	9004.34
1.02	34728.38	6761.02	704.42	1651.86	1049.64	9004.56
1.03	34728.40	6750.84	706.13	1652.84	1047.29	9004.73
1.04	34728.36	6739.96	707.27	1654.17	1044.91	9004.84
1.05	34728.15	6729.47	707.83	1655.39	1042.53	9004.91
1.06	34727.61	6720.45	707.78	1656.05	1040.17	9004.94
1.06	34726.77	6712.86	707.15	1656.16	1037.83	9004.91
1.07	34725.61	6706.71	705.92	1655.72	1035.52	9004.84
1.08	34724.15	6701.96	704.10	1654.74	1033.23	9004.71
1.09	34722.38	6698.62	701.70	1653.23	1030.98	9004.54
1.10	34720.30	6696.68	698.70	1651.19	1028.75	9004.32
1.10	34717.92	6696.12	695.13	1648.63	1026.55	9004.05
1.11	34715.24	6696.94	690.97	1645.57	1024.38	9003.74

1.12	34712.26	6699.13	686.23	1641.99	1022.24	9003.37
1.13	34708.73	6701.25	681.55	1638.14	1020.11	9002.97
1.14	34704.42	6701.86	677.57	1634.26	1017.96	9002.55
1.14	34699.33	6700.99	674.27	1630.34	1015.80	9002.10
1.15	34693.46	6698.66	671.67	1626.38	1013.62	9001.64
1.16	34686.83	6694.87	669.74	1622.38	1011.43	9001.16
1.17	34679.44	6689.65	668.50	1618.33	1009.22	9000.66
1.18	34671.29	6683.01	667.93	1614.23	1007.00	9000.14
1.18	34662.39	6674.96	668.03	1610.08	1004.76	8999.60
1.19	34652.74	6665.50	668.80	1605.87	1002.51	8999.04
1.20	34642.36	6654.65	670.24	1601.62	1000.24	8998.47
1.21	34631.29	6643.68	672.15	1597.41	997.95	8997.88
1.22	34619.62	6633.85	674.35	1593.37	995.62	8997.27
1.22	34607.33	6625.15	676.81	1589.48	993.27	8996.64
1.23	34594.43	6617.55	679.54	1585.75	990.88	8996.00
1.24	34580.92	6611.04	682.54	1582.16	988.46	8995.34
1.25	34566.80	6605.60	685.80	1578.73	986.00	8994.66
1.26	34552.07	6601.23	689.31	1575.45	983.51	8993.97
1.26	34536.74	6597.91	693.08	1572.30	980.99	8993.27
1.27	34520.80	6595.64	697.10	1569.30	978.43	8992.54
1.28	34504.26	6594.39	701.36	1566.45	975.85	8991.81
1.29	34487.83	6593.11	705.49	1563.54	973.25	8991.06
1.30	34472.20	6590.72	709.10	1560.40	970.66	8990.29
1.30	34457.37	6587.25	712.21	1557.03	968.10	8989.52
1.31	34443.33	6582.72	714.83	1553.43	965.55	8988.74
1.32	34430.09	6577.14	716.97	1549.62	963.01	8987.94
1.33	34417.63	6570.53	718.63	1545.60	960.50	8987.13
1.34	34405.96	6562.90	719.83	1541.37	958.01	8986.32
1.34	34395.06	6554.26	720.57	1536.94	955.53	8985.49
1.35	34384.94	6544.63	720.85	1532.31	953.08	8984.65
1.36	34375.60	6534.02	720.69	1527.47	950.64	8983.81
1.37	34366.99	6525.98	719.33	1524.02	948.13	8982.95
1.38	34359.06	6524.02	716.04	1523.51	945.43	8982.08
1.38	34351.80	6528.06	710.78	1525.90	942.54	8981.19
1.39	34345.21	6538.06	703.56	1531.19	939.46	8980.28
1.40	34339.28	6553.95	694.36	1539.34	936.18	8979.37
1.41	34334.01	6575.68	683.18	1550.35	932.70	8978.43
1.42	34329.38	6603.21	670.00	1564.20	929.03	8977.49
1.42	34325.39	6636.51	654.82	1580.86	925.14	8976.52
1.43	34322.03	6675.53	637.62	1600.34	921.06	8975.55
1.44	34319.31	6720.25	618.41	1622.62	916.76	8974.56

Table 35 – Central Solenoid Coils Ramp-up Voltages [35]

time	CS3U [V]	CS2U [V]	CS1 [V]	CS2L [V]	CS3L [V]
0	-415,51	-925,25	-2174,16	-1063,21	-586,54
25	-128,72	-345,91	-821,85	-339,39	-151,02
50	-116,45	-279,96	-687,13	-261,38	-137,77
75	-65,85	-182,03	-443,95	-153,36	-68,33
100	-44,76	-141,15	-399,59	-145,62	-64,51
125	-41,41	-113,66	-317,01	-119,74	-58,49
146					

Table 36 – Central Solenoid Coils Ramp-up Currents [35]

Time [s]	ICS3U [kA]	ICS2U [kA]	ICS1 [kA]	ICS2L [kA]	ICS3L [kA]
0	28,79	27,63	23,98	26,40	38,15
25	28,23	20,15	16,46	17,66	34,52
50	28,48	14,19	10,35	12,19	33,10
75	28,27	7,39	2,65	6,65	31,01
100	28,53	1,20	-4,16	2,37	30,10
125	29,24	-4,36	-11,91	-2,86	29,05
146	29,53	-9,47	-18,98	-7,83	27,68

Table 37 – Poloidal Field Coils Ramp-up Voltages [35]

time	P1 [V]	P2 [V]	P3 [V]	P4 [V]	P5 [V]	P6 [V]
0	-493,36	-766,67	-681,09	-902,02	-2420,76	-255,91
25	-176,51	-264,46	-251,18	-529,86	-854,54	-1,30
50	-147,66	-187,39	-229,92	-405,71	-395,58	-250,94
75	-87,22	-120,44	-157,75	-296,33	-200,02	-154,84
100	-67,57	-132,94	-145,60	-200,15	-210,96	-147,75
125	-58,59	-105,92	-114,50	-144,68	-160,46	-140,14
146						

Table 38 – Poloidal Field Coils Ramp-up Currents [35]

Time [s]	IP1 [kA]	IP2 [kA]	IP3 [kA]	IP4 [kA]	IP5 [kA]	IP6 [kA]
0	25,82	-4,65	4,86	-1,76	-7,52	11,38
25	23,00	-10,77	4,69	-3,35	-10,79	12,39
50	20,70	-15,02	4,96	-6,82	-12,85	13,26
75	17,85	-19,03	4,54	-11,13	-13,60	13,20
100	15,53	-22,58	4,05	-15,76	-13,79	13,06
125	13,47	-28,01	3,23	-18,91	-14,48	12,90
146	11,38	-32,98	2,44	-21,36	-15,05	12,61

Table 39 – Central Solenoid Coils Ramp-down Voltages [35]

Time	CS3U [V]	CS2U [V]	CS1 [V]	CS2L [V]	CS3L [V]
0	579,49	-619,67	-1297,12	215,99	-83,12
21	-1118,23	304,67	474,24	446,32	-716,72
46	-192,23	297,29	620,81	258,56	-464,35
71	-636,10	304,84	921,68	269,36	-187,52
96	470,93	669,86	973,23	176,05	-4,65
121	-549,08	840,48	1169,50	458,08	73,04
146					

Table 40 – Central Solenoid Coils Ramp-down Currents [35]

time	ICS3U [kA]	ICS2U [kA]	ICS1 [kA]	ICS2L [kA]	ICS3L [kA]
0	-3,71	-37,61	-40,11	-39,30	-16,71
21	7,44	-45,00	-45,00	-34,05	-17,73
46	-11,10	-35,43	-44,05	-24,43	-29,74
71	-14,67	-30,79	-41,61	-19,31	-37,31
96	-25,83	-24,73	-37,71	-15,96	-40,73
121	-17,86	-18,54	-33,73	-14,95	-41,21
146	-27,57	-5,43	-30,03	-10,28	-41,71

Table 41 – Poloidal Field Coils Ramp-down Voltages [35]

Time	P1 [V]	P2 [V]	P3 [V]	P4 [V]	P5 [V]	P6 [V]
0	-539,46	387,75	2177,61	1709,97	725,60	-1755,96
21	81,77	292,29	531,07	326,61	812,87	-628,15
46	-160,83	312,49	337,45	782,79	353,23	-381,62
71	93,96	323,37	451,75	711,82	693,60	-526,87
96	-1142,40	786,26	73,38	1343,04	787,08	-358,88
121	-743,39	850,71	234,96	961,92	1518,31	-599,99
146						

Table 42 – Poloidal Field Coils Ramp-down Currents [35]

time	IP1 [kA]	IP2 [kA]	IP3 [kA]	IP4 [kA]	IP5 [kA]	IP6 [kA]
0	-11,02	-38,22	-1,53	-32,93	-13,41	7,63
21	-17,81	-37,21	6,18	-27,88	-13,03	5,68
46	-13,29	-34,38	8,25	-27,24	-11,59	5,20
71	-14,60	-30,88	8,58	-23,53	-11,38	4,94
96	-11,68	-27,81	9,53	-20,65	-10,51	4,20
121	-27,05	-17,86	6,46	-14,07	-10,01	3,45
146	-34,76	-7,88	4,58	-10,33	-7,88	2,17